Earth-based Uranus Stellar Occultations User Guide V1.0

Richard G. French* and Colleen A. McGhee-French
Astronomy Department, Wellesley College, Wellesley, MA 02481
Mitchell K. Gordon
Carl Sagan Center, SETI Institute, Mountain View, CA 94043

* *rfrench@wellesley.edu*

December 8, 2020

Contents

1 Introduction **1**

2 The structure and contents of an observation bundle **2**

2.1 readme.txt 4

2.2 The document/ directory 4

2.3 The browse/ directory 4

2.3.1 browse/global/ 4

2.3.2 browse/atmosphere/ 12

2.3.3 browse/rings/ 13

2.3.4 browse/ring_models/ 17

2.4 The data/ directory 18

2.4.1 data/global/ 19

2.4.2 data/atmosphere/ 22

2.4.3 data/rings/ 24

2.4.4 data/ring_models/ 26

2.5 The context/ directory 37

2.6 The xml_schema/ directory 37

3 The structure and contents of the uranus_occ_support bundle **38**

3.1 readme.txt 38

3.2 The document/ directory 39

3.2.1 The document/supplemental_docs/ directory 39

3.2.2 The document/user_guide/ directory. 40

3.3 The data/ directory 40

3.3.1 Ring orbit fit `rfrench_20201201` results 40
3.3.2 Input files for ring orbit fit `rfrench_20201201` 44
3.4 The `spice_kernels/` directory 45
3.4.1 The `spice_kernels/fk/` directory 46
3.4.2 The `spice_kernels/spk/` directory 47
3.5 The `context/` directory 47
3.6 The `xml_schema/` directory 47

4 Summary information about observation bundles **47**

Acknowledgements **48**

A Selected output from the RINGFIT orbital fit to the rings **49**

B Using frame kernels to compute ring geometry **54**

B.1 Determining the pole direction of a ring plane at a given time 55
B.2 Confirming the definition of the origin of inertial longitude 59
B.3 Computing the skyplane view of the epsilon ring 61
B.4 Computing the ring longitude as a broken angle 69
B.5 Computing the ring intercept point for a stellar occultation 72

C Custom spk kernel for the KAO **74**

List of Figures

1 Directory structure of observation bundle uranus_occ_u17b_saao_188cm. . . 3

2 Earth-based view of the occultation of Uranus star u17b observed from SAAO. The periapse of each ring is marked by a black dot. The occultation chord begins with the green dot and terminates with the red dot, at times shown in the lower left of the figure. The atmosphere occultation is marked in green, where the star disappears behind the geometric limb of the planet. (u17b_saao_188cm_2220nm_obs_geom.pdf) 5

3 View of Earth from Uranus at the midpoint of recorded observations of the 24-25 March 1983 occultation of star u17b from SAAO. The + symbol marks the sub-Uranus point; the large black dot marks the location of SAAO. The antisolar point (when visible) is marked by the ⊙ symbol. The gray region is in darkness. The observations were halted just at sunrise. 6

4 Altitude of Uranus (black curve) as a function of Earth observed time for the u17b occultation observed from SAAO. Selected predicted ring event times are labeled by the name of the ring, although not all of them may be visible in the observations. The planet occulted the star, resulting in an atmospheric occultation, marked in this plot as a green line. For this event, sunrise occurred near the end of the occultation (see the solar altitude plotted in red), affecting the quality of the egress ring occultations. (u17b_saao_188cm_2220nm_alt.pdf) 7

5 Unnormalized lightcurve of the occultation of Uranus star u17b observed from SAAO on March 24/25, 1983, plotted as observed signal vs observation time. (u17b_saao_188cm_2220nm_counts-v-time_occult.pdf) 8

6 Lightcurve of the occultation of Uranus star u17b observed from SAAO. The upper panel shows the observed signal as a function of Earth received time, and the lower panel shows the normalized signal over the same interval, with ring events marked in blue, the atmosphere ingress and egress occultation marked in green, and sky level checks marked in red. (The sky level checks dip below the zero level because during these intervals, the telescope nodded away from the star as well as the rings, which contributed a few percent to the full signal when the star was centered in the aperture of the high-speed photometer.) Notice that the normalization procedure has nearly eliminated the undulations and abrupt changes in the raw data. (first page of u17b_saao_188cm_2220nm_counts-v-time_normalization.pdf) 10

7 Lightcurve of the atmospheric occultation of Uranus star u17b observed from SAAO. As in Fig. 6, the upper panel shows the observed signal as a function of Earth received time, and the lower panel shows the normalized signal over the same interval. (second page of u17b_saao_188cm_2220nm_counts-v-time_normalization.pdf) 1

8 Observed ingress atmosphere lightcurve of the occultation of Uranus star u17b observed from SAAO, plotted as observed counts vs. time. (u17b_saao_188cm_2220nm_counts-v-t

9 Egress atmosphere lightcurve of the occultation of Uranus star u17b observed from SAAO. Note the brief sky checks that interrupt both the ingress and egress atmosphere lightcurves. (u17b_saao_188cm_2220nm_counts-v-time_atmos_egress.pdf) 1

10 Observed ingress ring lightcurve of the occultation of Uranus star u17b observed from SAAO, plotted as observed signal vs time, with predicted locations of individual ring events shown by labeled vertical dotted lines. (u17b_saao_188cm_2220nm_counts

11 Egress ring lightcurve of the occultation of Uranus star u17b observed from SAAO, plotted as observed signal vs time, with predicted locations of individual ring events shown by labeled vertical dotted lines. (u17b_saao_188cm_2220nm_counts-v-time_

12 Normalized ingress ring lightcurve of the occultation of Uranus star u17b observed from SAAO, plotted as a function of equatorial radius. Individual ring events are shown in red and sky checks are shown in blue. Predicted ring event radii are indicated by labeled dashed lines. (u17b_saao_188cm_2220nm_radius_equator_ingress_1

13 Normalized egress ring lightcurve of the occultation of Uranus star u17b observed from SAAO, plotted as a function of equatorial radius. Individual ring events are shown in red and sky checks are shown in blue. Predicted ring event radii are indicated by labeled dashed lines. (u17b_saao_188cm_2220nm_radius_equator_egress_10

14 Gallery of individual unnormalized ring occultations as a function of time (lower axis) and ring plane radius (upper axis) for the occultation of Uranus star u17b observed from SAAO. There is no detection of the λ ring at the predicted orbital radius for this incomplete ring. The ring 6 egress occultation was lost in the strongly-varying background signal, and is not shown. The rising slopes for the egress α and β rings result from sunrise encroaching on the observations. (u17b_saao_188cm_2220nm_counts-v-time_rings_indiv.pdf) 17

15 Gallery of individual normalized ring profiles and the corresponding best-fitting square-well models. The intrinsic square well is shown in red, and the blue curve is the model profile computed from the diffraction pattern produced the by square well, appropriately accounting for the wavelength range of the filter used during the observations, the finite projected size of the occulted star, and any instrumental time constant. (u17b_saao_188cm_2220nm_ring_sqw_gallery.pdf) 18

16 Screen shot of a part of the u17b_saao_188cm_2220nm_counts-v-time_occult.xml label file, showing the description of the file contents and the definition of the Observed Event Time column for the associated *.tab file. 20

17 Directory structure and representative contents of the data/ring_models/ directory. 27

18 Square-well model fit to the egress ring 4 profile of the occultation of Uranus star u17b observed from SAAO. See text for details. (u17b_saao_188cm_2220nm_ring_four_egress

19 Square-well model fit to the egress α ring profile of the occultation of Uranus star u137 observed from the IRTF on March 16, 1966. See text for details. . 33

20 Examples of ring profiles with QI of 3 (right) and 4 (left), from the 1990 June 21 occultation of U65 observed from the IRTF. The γ egress profile at right shows a clear but noisy detection, warranting a QI of 3. The η ring profile at left is marginal, and earns a QI of only 4, although its fitted midpoint is very close to the expected location based our our comprehensive ring orbit model. 36

21 Directory structure of uranus_occ_support bundle. 38

22 Contents of the document/ directory of the uranus_occ_support bundle. . . 39

23 Contents of the data/directory of the uranus_occ_support bundle. 40

24 Directory structure of the spice_kernels/ directory of the uranus_occ_support bundle. 46

25 Table II of Gresh et al. 1989. 57

26 Sky plane view of Uranus and the ϵ ring as observed from Earth on 2020 Jan 25 12:00 UTC. The visible Uranus pole is marked by a diamond and the + symbol marks the location of the periapse of the ϵ ring at the time of observation. 64

27 Sky plane view of Uranus (blue circle) and the ϵ ring (green ellipse) as observed from Earth on 2020 Jan 25 12:00 UTC. The visible Uranus pole is marked by the orange dot and the + symbol marks the location of the periapse of the ϵ ring at the time of observation. 67

28 Sky plane view of Uranus and the ten classical rings as observed from Earth on 2020 Jan 25 12:00 UTC. The periapse of the ϵ ring at the time of observation is marked by a black dot on the outer ring, at the same position angle as in Figs. 26 and 27. 68

29 Flight path of the KAO during the 1977 March 10 discovery observations of the Uranian rings, beginning a the filled circle and ending at the open circle. The large dark circle marks the antisolar point on Earth, and the + symbol marks the sub-Uranus point on Earth at mid-occultation time. 75

List of Tables

1 Uranus Ring Occultation Data Bundles 2

2 Uranus Gravity Parameters and Pole 41

3 Star Catalog Positions and Corrections 42

4 Geocentric Telescope Coordinates 43

5 Observatory Time Offsets 43

6 Spice Kernels 44

7 Uranus Ring Orbital Elements 45

8 Uranus Ring Normal Modes 46

9 Occultation Bundle Quality Indices and Rank 48

1 Introduction

This *User Guide* provides a detailed description of the organization and contents of the Earth-based Uranus ring occultation observations archived at NASA's Planetary Data System Ring-Moon Systems Node under NASA PDART grant NNX15AJ60G: "Restoration and Submission of Uranus Ring Occultation Observations to the Planetary Data System." The archive contains a comprehensive set of high-SNR digitally-recorded Earth-based Uranus occultations and individual high-resolution ring profiles registered on an accurate radius scale based on a least-squares fit to the occultation data for the orbits of the ten classical Uranian rings and the Uranus pole direction.

The archive includes browse products to provide a quick overview of each occultation, normalized and geometrically registered lightcurves of the entire recorded event (including atmospheric occultations, when present), and detailed model fits to individual ring profiles for the ten classical narrow Uranian rings (6, 5, 4, α, β, η, γ, δ, λ, and ϵ). Each occultation set contains a digital table listing details of each observed ring event, such as fitted values of the ring width and optical depth, the geometry of each individual profile, a quality index to provide a shorthand assessment of the quality of each profile, and predicted ring event times for rings that were not detected in the observations.[1]

The PDS Uranus ring occultation archive is contained in a set of *bundles* of two types: *observation bundles* that each contain detailed information about a single occultation observation, and a single *support bundle* that contains information applicable to all observation bundles, including this *User Guide*, the global ring orbit fit used to determine the geometry for each occultation, and NAIF *frame kernels*[2] to compute the Uranus ring geometry at any given time, based on this orbit fit.

The *User Guide* is organized as follows. Section 2 provides a detailed description of the directory structure and contents of a typical observation bundle. Section 3 contains similar information for the single support bundle for the entire ring archive, and Section 4 contains summary information about the observation bundles in the archive. The Appendices contain selected output from the IDL[3] program used to perform the orbital fit to the rings, detailed examples in both Python and IDL to illustrate the use of the frame kernels included in the support bundle, and a description of any specialized ephemeris files used for the orbit fit that are not otherwise available.

First-time users are encouraged to read or skim the entire *User Guide* before making use of

[1] This is likely to be of most use to those interested in investigating the incomplete azimuthal structure of the λ ring.

[2] NASA's Navigation and Ancillary Information Facility (NAIF) uses *frames* to enable users to compute the geometry of an observation in a variety of reference frames. In this instance, the individual ring planes of the ten classical Uranian rings are defined in special-purpose *frame kernel* files. See https://naif.jpl.nasa.gov/pub/naif/toolkit_docs/C/req/frames.html.

[3] IDL – Interactive Data Language – is a widely-used commercial scientific programming language currently available from https://www.harrisgeospatial.com/Software-Technology/IDL.

the archived results. Those primarily interested in useful tables of ring-by-ring results for specific occultations are directed to Sections 2.4.4.3 and 4. For a comprehensive review of the Uranian rings, see Nicholson et al. 2018.

2 The structure and contents of an observation bundle

Each observation bundle in the Uranus ring occultation archive corresponds to a single occultation of the Uranus system from a specific observatory and telescope at a given wavelength or set of wavelengths. The current list of observation bundles to be archived in the PDS is shown in Table 1.

Table 1: Uranus Ring Occultation Data Bundles

Bundle ID[a]	Date (UTC)	Star ID	Observatory Name	Telescope Diameter (cm)	Wavelength (nm)
u0_kao_91cm	1977 Mar 10	U0	Kuiper Airborne Observatory	91	734
u2_teide_155cm	1977 Dec 23	U2	Observatorio del Teide	155	880
u5_lco_250cm	1978 Apr 10	U5	Las Campanas Observatory	250	2200
u9_lco_250cm	1979 Jun 10	U9	Las Campanas Observatory	250	2200
u11_ctio_400cm	1980 Mar 20	U11	Cerro Tololo Inter-American Observatory	400	2200
u12_ctio_400cm	1980 Aug 15	U12	Cerro Tololo Inter-American Observatory	400	2200
u12_eso_360cm	1980 Aug 15	U12	European Southern Observatory	360	2200
u12_lco_250cm	1980 Aug 15	U12	Las Campanas Observatory	250	2200
u13_sso_390cm	1981 Apr 26	U13	Siding Spring Observatory	390	2200
u14_lco_100cm	1982 Apr 22	U14	Las Campanas Observatory	100	880
u14_teide_155cm	1982 Apr 22	U14	Observatorio del Teide	155	880
u14_ctio_400cm	1982 Apr 22	U14	Cerro Tololo Inter-American Observatory	400	880
u14_ctio_150cm	1982 Apr 22	U14	Cerro Tololo Inter-American Observatory	150	2200
u14_lco_250cm	1982 Apr 22	U14	Las Campanas Observatory	250	2200
u14_opmt_200cm	1982 Apr 22	U14	Observatoire du Pic du Midi et de Toulouse	200	2200
u14_eso_104cm	1982 Apr 22	U14	European Southern Observatory	104	2200
u14_opmt_106cm	1982 Apr 22	U14	Observatoire du Pic du Midi et de Toulouse	106	880
u15_mso_190cm	1982 May 01	U15	Mount Stromlo Observatory	190	2200
u16_palomar_508cm	1982 Jun 04	U16	Palomar Observatory	508	2200
u17b_saao_188cm	1983 Mar 24	U17b	South African Astronomical Observatory	188	2220
u23_ctio_400cm	1985 May 04	U23	Cerro Tololo Inter-American Observatory	400	2200
u23_teide_155cm	1985 May 04	U23	Observatorio del Teide	155	2200
u23_mcdonald_270cm	1985 May 04	U23	McDonald Observatory	270	2200
u25_palomar_508cm	1985 May 24	U25	Palomar Observatory	508	2200
u25_mcdonald_270cm	1985 May 24	U25	McDonald Observatory	270	2200
u25_ctio_400cm	1985 May 24	U25	Cerro Tololo Inter-American Observatory	400	2200
u28_irtf_320cm	1986 Apr 26	U28	IRTF	320	2200
u34_irtf_320cm	1987 Feb 26	U34	IRTF	320	2200
u36_irtf_320cm	1987 Mar 30	U36	United Kingdom Infrared Telescope	320	2200
u36_maunakea_380cm	1987 Mar 30	U36	United Kingdom Infrared Telescope	380	2200
u36_ctio_400cm	1987 Apr 02	U36	Cerro Tololo Inter-American Observatory	400	2200
u36_sso_390cm	1987 Apr 02	U36	Siding Spring Observatory	390	2200
u36_sso_230cm	1987 Apr 02	U36	Siding Spring Observatory	230	2200
u1052_irtf_320cm	1988 May 12	u1052	IRTF	320	2200
u65_irtf_320cm	1990 Jun 21	U65	IRTF	320	2200
u83_irtf_320cm	1991 Jun 25	U83	IRTF	320	2200
u84_irtf_320cm	1991 Jun 28	U84	IRTF	320	2200
u102a_irtf_320cm	1992 Jul 08	u102a	IRTF	320	2200
u102b_irtf_320cm	1992 Jul 08	u102b	IRTF	320	2200
u103_palomar_508cm	1992 Jul 11	U103	Palomar Observatory	508	2200
u103_eso_220cm	1992 Jul 11	U103	European Southern Observatory	220	2200
u9539_ctio_400cm	1993 Jun 30	U9539	Cerro Tololo Inter-American Observatory	400	2200
u134_saao_188cm	1995 Sep 09	U134	South African Astronomical Observatory	188	2220
u137_irtf_320cm	1996 Mar 16	U137	IRTF	320	2200
u137_hst_fos	1996 Mar 16	U137	Hubble Space Telescope	FOS[b]	540
u138_hst_fos	1996 Apr 10	U138	Hubble Space Telescope	FOS[b]	540
u138_palomar_508cm	1996 Apr 10	U138	Palomar Observatory	508	2200
u144_saao_188cm	1997 Sep 30	U144	South African Astronomical Observatory	188	2220
u144_caha_123cm	1997 Sep 30	U144	Centro Astronomico Hispano-Aleman	123	2220
u149_lowell_180cm	1998 Nov 06	U149	Lowell Observatory	180	890
u149_irtf_320cm	1998 Nov 06	U149	IRTF	320	2200
u0201_palomar_508cm	2002 Jul 29	u0201	Palomar Observatory	508	2200

[a] The full PDS bundle ID has a prefix of uranus_occ_. For example, uranus_occ_u0_kao_91cm. As of the date of the version of the *User Guide*, all but the U36 occultation data sets are included in the archive set. The U36 data will be added to the PDS once a satisfactory geometric solution has been obtained for this multi-day, multi-star occultation.

[b] Faint Object Spectrograph (FOS) of the Hubble Space Telescope

In this *User Guide*, we will use the `uranus_occ_u17b_saao_188cm` bundle as our primary example: the 1983 March 24-25 occultation of Uranus occultation star U17b observed from the the South African Astronomical Observatory (SAAO) using the 188 cm telescope in the infrared at a wavelength of 2220 nm (Elliot et al. 1987). We recommend that users navigate their way through this bundle as they read this *User Guide*.

The directory structure of a typical observation bundle is shown below in Fig. 1:

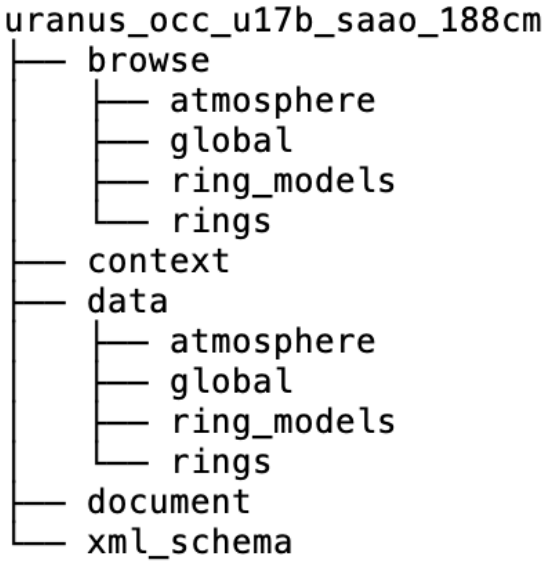

Fig. 1: Directory structure of observation bundle `uranus_occ_u17b_saao_188cm`.

Briefly, the top-level directories contain:

- `browse/` Overview plots of the occultation lightcurve and event geometry.
- `context/` Used internally by PDS.
- `data/` Tabular data of occultation observations and individual ring events.
- `document/` PDS documentation of the observation bundle.
- `readme.txt` A text file directing the user to this *User Guide*.
- `xml_schema/` Used internally by PDS.

We describe each of these directories below, following a logical sequence for the user, rather than a strictly alphabetical order.

2.1 `readme.txt`

The documentation for every observation bundle is consolidated into this *User Guide*, rather than residing in the `document/` directory of each individual bundle. This single source of information will be updated as needed, and we hope that users will benefit from the introductory material in the guide that is applicable to every occultation bundle. The `readme.txt` file provides users with information about how to locate the current edition of this *User Guide* on the PDS.

2.2 The `document/` directory

As noted above, all documentation about a specific observation bundle is consolidated in this *User Guide*, rather than being contained in the `document/` directory of the specific bundle, because users are likely to require general information applicable to all observation bundles in order to make best use of the archive. The important message is that *users should consult the User Guide to find information specific to any given occultation bundle* – see Section 4.

2.3 The `browse/` directory

2.3.1 `browse/global/`

We recommend that users begin with the `browse/global/` directory to get an overview of an entire occultation event. Every observation bundle has an earth-based view of the occultation track, such as the u17b occultation shown in Fig. 2. The beginning and end of the archived occultation chord are marked by green and red dots, respectively. The green dashed line along the occultation chord marks the grazing atmospheric occultation for this event, and individual ring periapses are marked with a black dot.

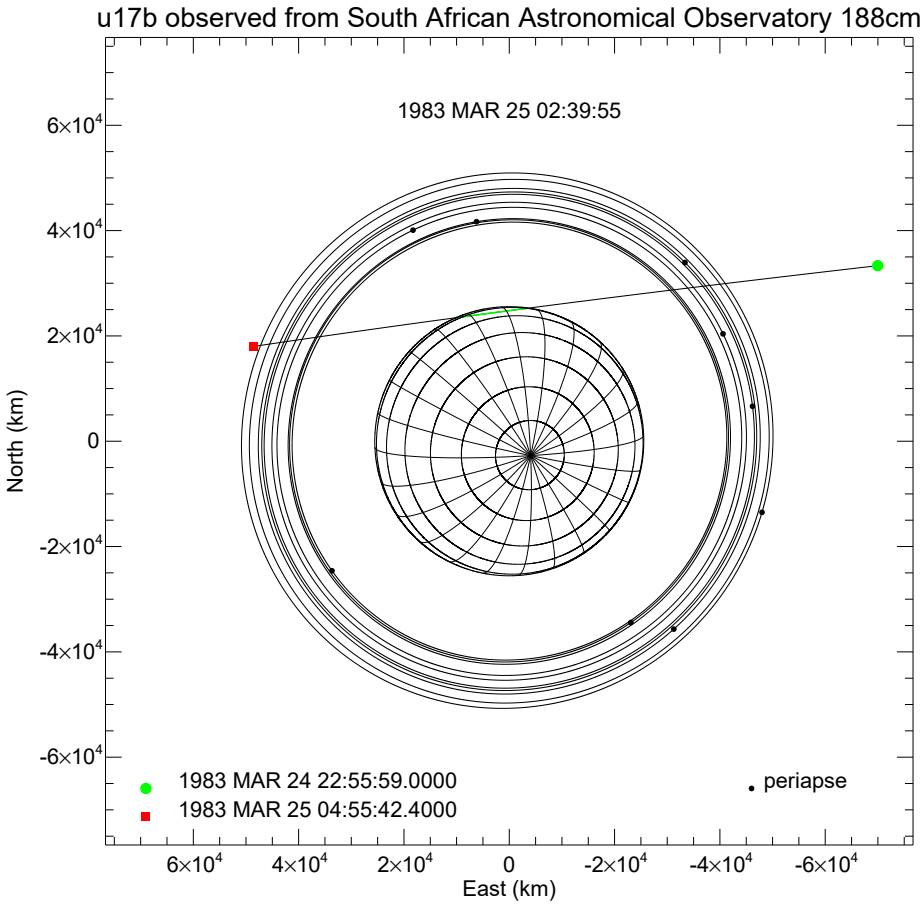

Fig. 2: Earth-based view of the occultation of Uranus star u17b observed from SAAO. The periapse of each ring is marked by a black dot. The occultation chord begins with the green dot and terminates with the red dot, at times shown in the lower left of the figure. The atmosphere occultation is marked in green, where the star disappears behind the geometric limb of the planet. (`u17b_saao_188cm_2220nm_obs_geom.pdf`)

The view of Earth from Uranus at mid-occultation is shown in Fig. 3. The sky plane coordinates of the occultation chord as a function of observation time are among the geometric quantities included in the time-series data files.

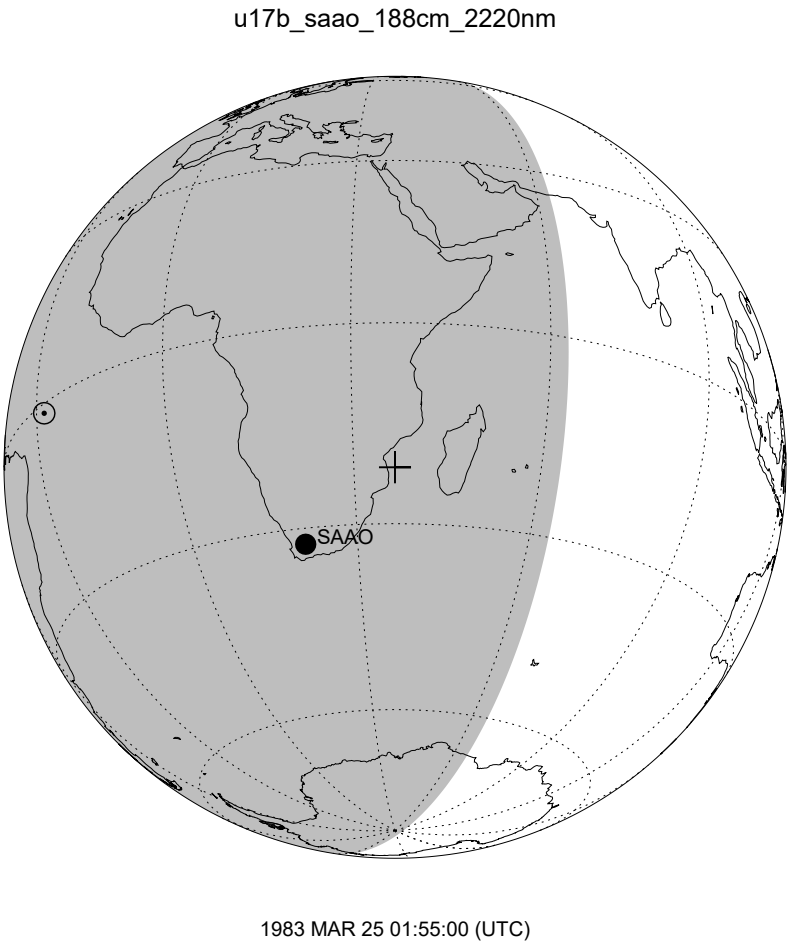

Fig. 3: View of Earth from Uranus at the midpoint of recorded observations of the 24-25 March 1983 occultation of star u17b from SAAO. The + symbol marks the sub-Uranus point; the large black dot marks the location of SAAO. The antisolar point (when visible) is marked by the ⊙ symbol. The gray region is in darkness. The observations were halted just at sunrise.

The altitude of Uranus above the horizon throughout the observation period for this occultation is shown in Fig. 4, with individual ring events marked for ingress and egress. In this case, the atmospheric occultation occurred with Uranus nearly overhead, and the egress ring events occurred during sunrise, as shown by the curve showing the altitude of the sun (in red).

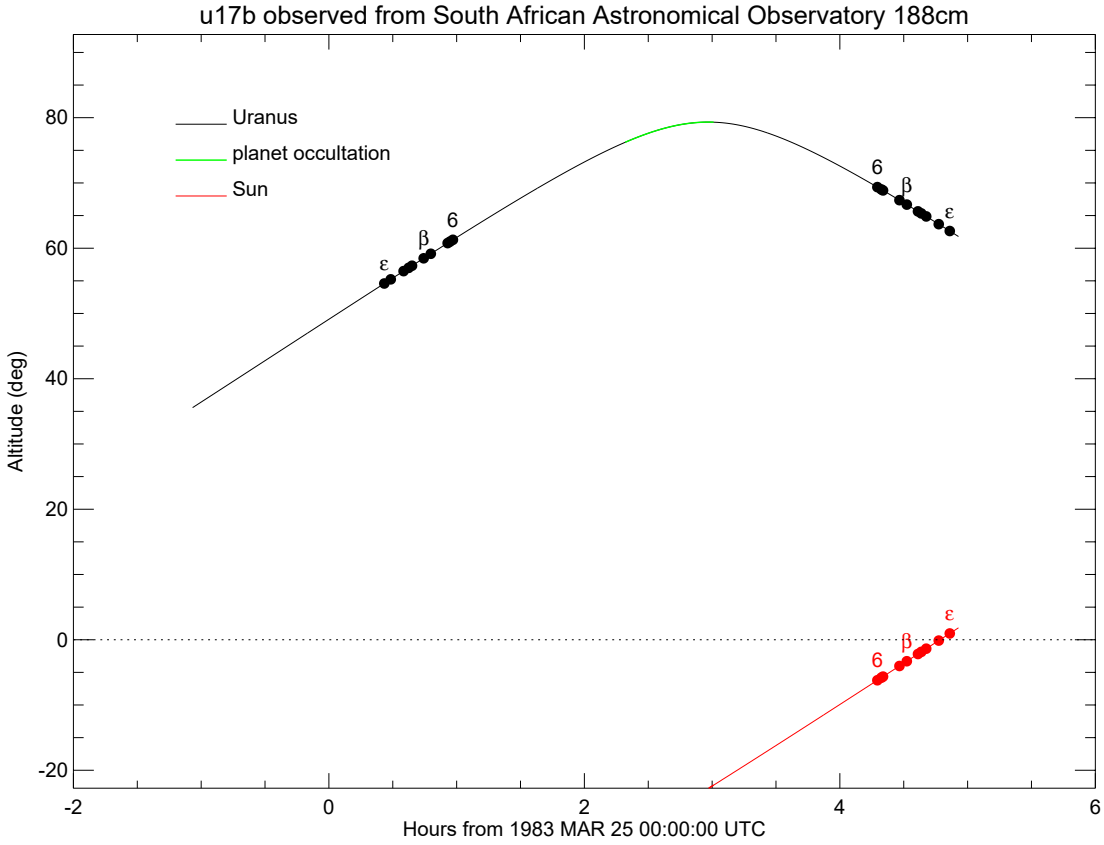

Fig. 4: Altitude of Uranus (black curve) as a function of Earth observed time for the u17b occultation observed from SAAO. Selected predicted ring event times are labeled by the name of the ring, although not all of them may be visible in the observations. The planet occulted the star, resulting in an atmospheric occultation, marked in this plot as a green line. For this event, sunrise occurred near the end of the occultation (see the solar altitude plotted in red), affecting the quality of the egress ring occultations. (`u17b_saao_188cm_2220nm_alt.pdf`)

The `browse/global/` directory also contains a plot of the raw lightcurve of the entire occultation (Fig. 5.) The u17b occultation was recorded at a wavelength of 2220 nm in the 'direct' mode, without a chopping secondary to compensate for the strong background IR flux, and there are obvious sudden jumps in the count level over the course of the occultation to keep the signal in range. Sunrise occurred during the egress ring events.

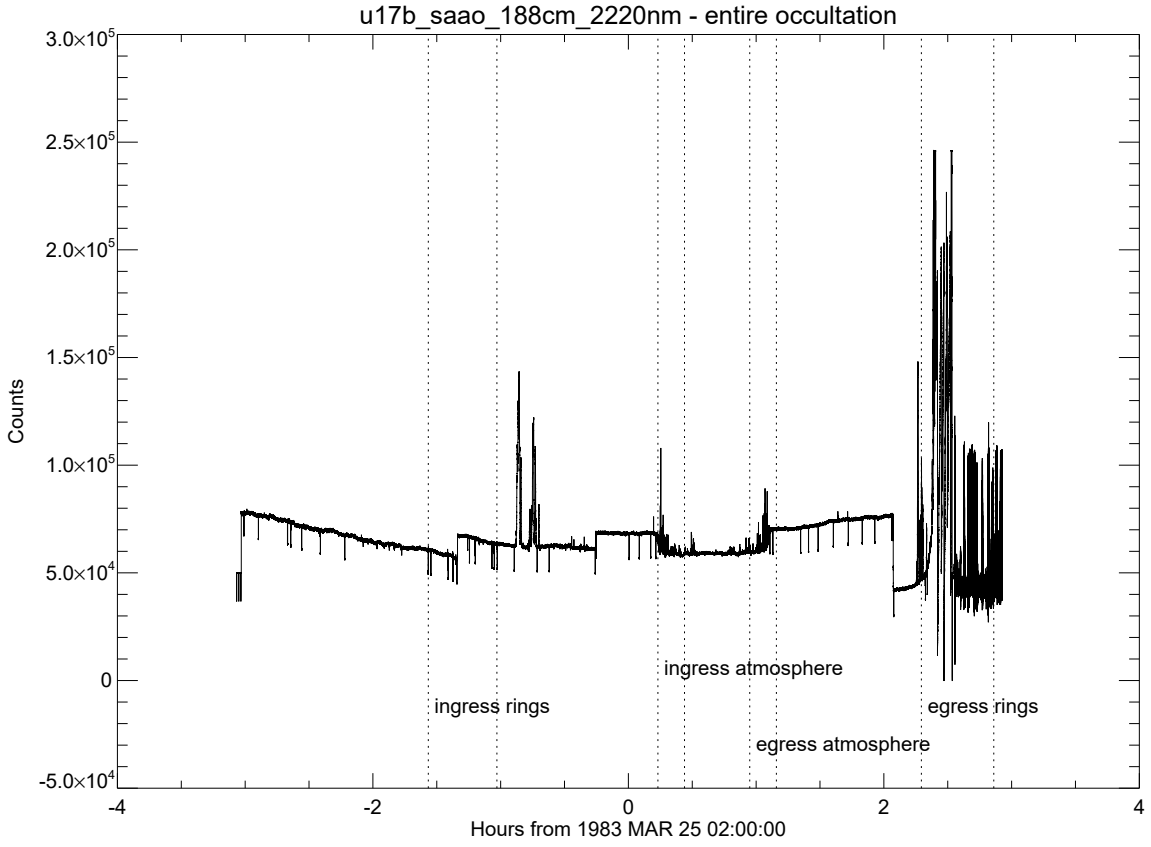

Fig. 5: Unnormalized lightcurve of the occultation of Uranus star u17b observed from SAAO on March 24/25, 1983, plotted as observed signal vs observation time. (`u17b_saao_188cm_2220nm_counts-v-time_occult.pdf`)

Every archived occultation observation is normalized in units of the unocculted stellar flux and flagged to identify regions of the recorded signal corresponding to the injection of time signals, sky background level checks, clouds, suspected ring events, intermittent noise, or periods of rapid background variation due to sunrise or sunset. The archived data files include digital flags for every data point to document these identifications, described in more detail below.

The normalization procedures can vary considerably from data set to data set. For the u17b occultation, the initial processing fitted thirteen separate polynomials to the regions of the data where the full unocculted star signal was recorded. Then, using measurements of the sky level checks, the time-variable full stellar signal intensity was estimated, accounting for the approximate contribution of reflected sunlight from the rings to the total signal. Finally,

a running mean average of the observations was used to reduce the remaining undulations in the signal – a procedure that was followed for many of the observation bundles.

The final normalized lightcurve for the u17b event is shown in Fig. 6, plotted as a function of time. The upper panel shows the raw lightcurve as a function of time, and the lower panel shows the normalized lightcurve, with individual sky background sky level checks marked in red, ring events marked in blue, and the atmospheric occultation shown in green.

While the detailed process of normalization and calibration will differ from observation to observation, every observation bundle contains both raw and normalized lightcurves of the entire occultation.

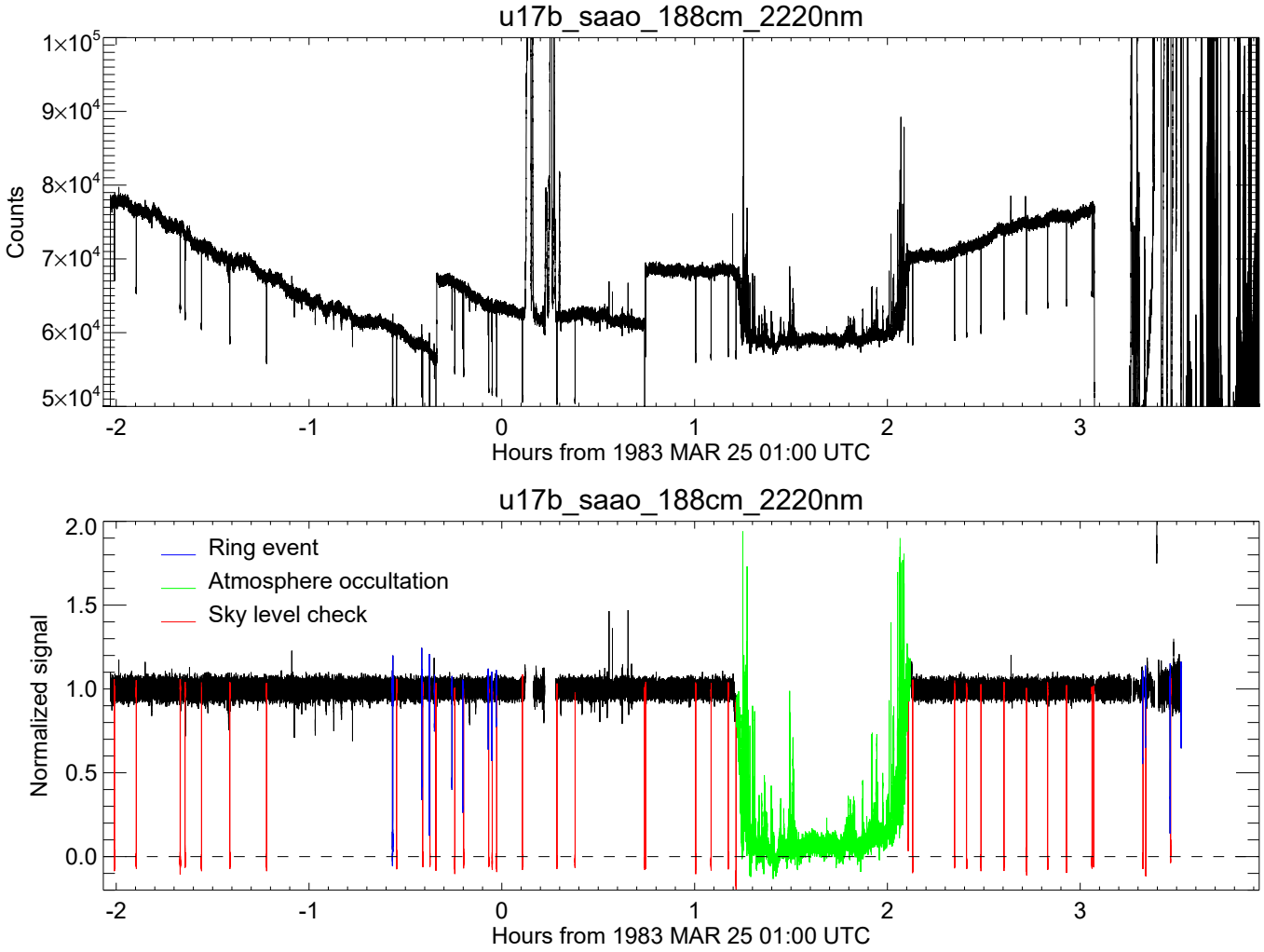

Fig. 6: Lightcurve of the occultation of Uranus star u17b observed from SAAO. The upper panel shows the observed signal as a function of Earth received time, and the lower panel shows the normalized signal over the same interval, with ring events marked in blue, the atmosphere ingress and egress occultation marked in green, and sky level checks marked in red. (The sky level checks dip below the zero level because during these intervals, the telescope nodded away from the star as well as the rings, which contributed a few percent to the full signal when the star was centered in the aperture of the high-speed photometer.) Notice that the normalization procedure has nearly eliminated the undulations and abrupt changes in the raw data. (first page of `u17b_saao_188cm_2220nm_counts-v-time_normalization.pdf`)

The u17b observations included an atmosphere occultation, and the corresponding raw and normalized lightcurves for the atmospheric component of Fig. 6 are shown in Fig. 7. *Users are cautioned that the normalization of atmospheric occultations is only approximate, and for detailed studies we strongly recommend that users perform their own independent estimates of proper normalization of the observations.*

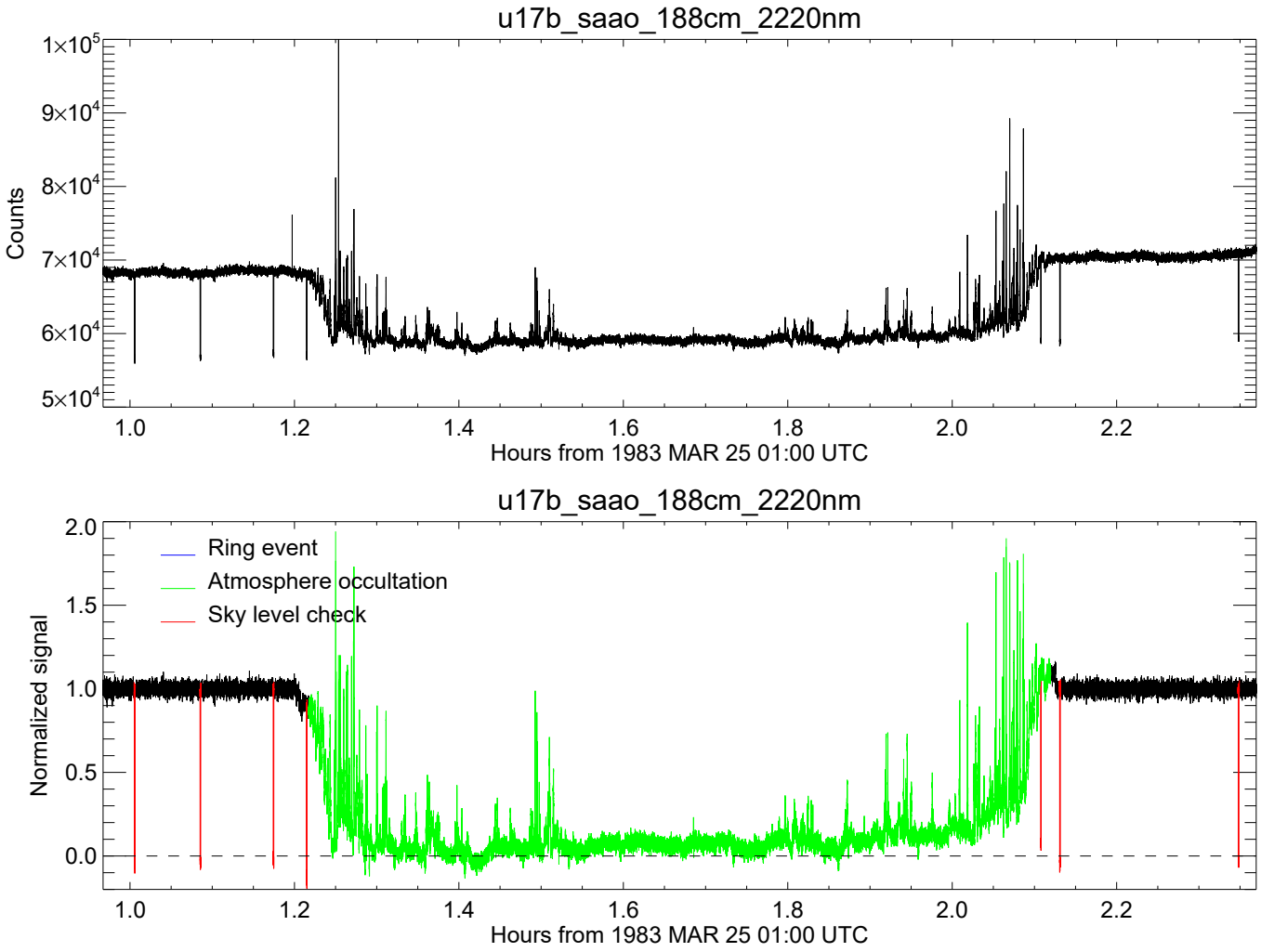

Fig. 7: Lightcurve of the atmospheric occultation of Uranus star u17b observed from SAAO. As in Fig. 6, the upper panel shows the observed signal as a function of Earth received time, and the lower panel shows the normalized signal over the same interval. (second page of `u17b_saao_188cm_2220nm_counts-v-time_normalization.pdf`)

2.3.2 `browse/atmosphere/`

For observations that include an atmospheric occultation, the `browse/atmosphere/` directory contains plots of the raw ingress and/or egress atmosphere occultation lightcurves as a function of time. The results for the u17b occultation are shown in Figs. 8 and 9.

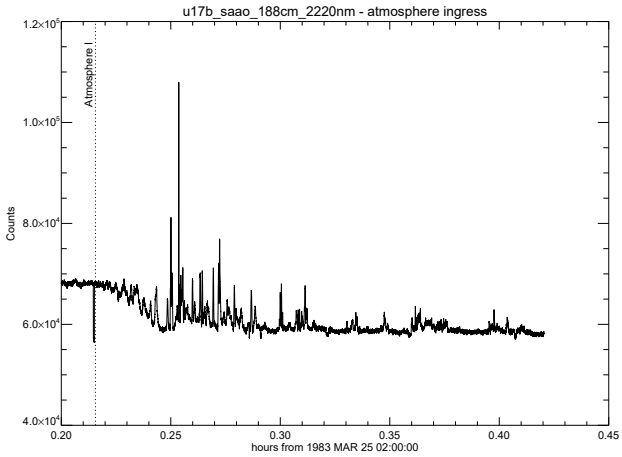

Fig. 8: Observed ingress atmosphere lightcurve of the occultation of Uranus star u17b observed from SAAO, plotted as observed counts vs. time.
(`u17b_saao_188cm_2220nm_counts-v-time_atmos_ingress.pdf`)

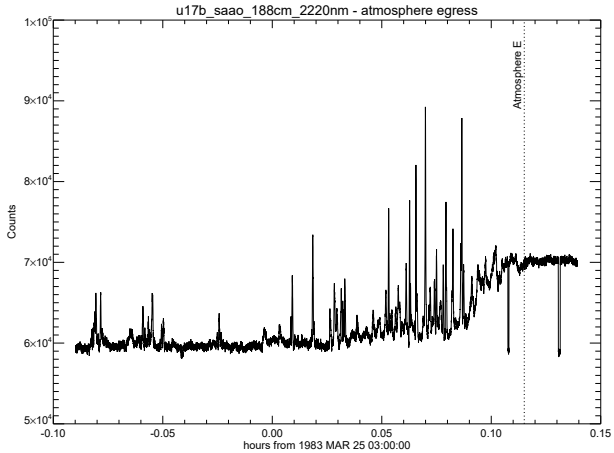

Fig. 9: Egress atmosphere lightcurve of the occultation of Uranus star u17b observed from SAAO. Note the brief sky checks that interrupt both the ingress and egress atmosphere lightcurves. (`u17b_saao_188cm_2220nm_counts-v-time_atmos_egress.pdf`)

2.3.3 `browse/rings/`

The `browse/rings/` directory contains higher-resolution plots of the raw ingress and egress ring occultation lightcurves, with individual ring events labeled (Figs. 10 and 11). Notice in this case that the dips in the lightcurve immediately following several ring events are sky level checks. The overall signal level was manually adjusted shortly after the η ring ingress event. Sunrise rapidly encroached on the egress ring occultations, requiring multiple manual changes in the signal level, and eventual saturation by sunlight.

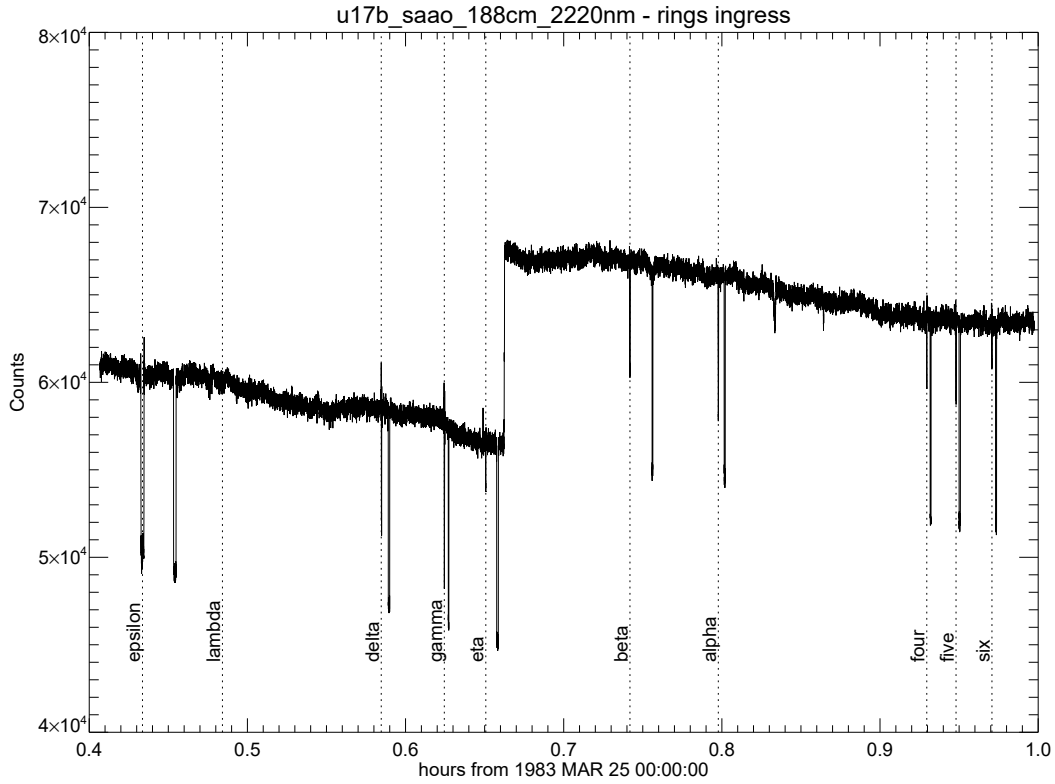

Fig. 10: Observed ingress ring lightcurve of the occultation of Uranus star u17b observed from SAAO, plotted as observed signal vs time, with predicted locations of individual ring events shown by labeled vertical dotted lines. (`u17b_saao_188cm_2220nm_counts-v-time_rings_ingress.pdf`)

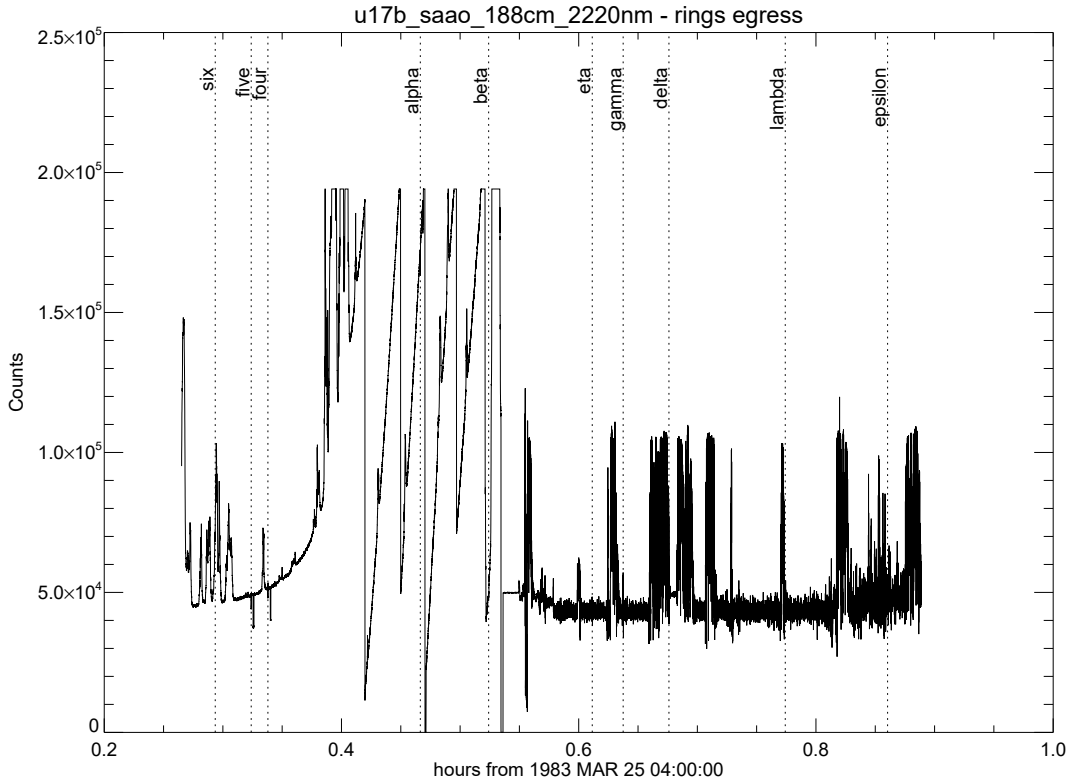

Fig. 11: Egress ring lightcurve of the occultation of Uranus star u17b observed from SAAO, plotted as observed signal vs time, with predicted locations of individual ring events shown by labeled vertical dotted lines. (`u17b_saao_188cm_2220nm_counts-v-time_rings_egress.pdf`)

Based on a ring orbit fit described below, the radial scale of the occultation can be calculated. The `browse/rings/` directory includes normalized 1000m-resolution plots of the ring as a function of equatorial distance from the center of the planet (Figs. 12 and 13). Individual ring events are shown in red and sky level checks are shown in blue.

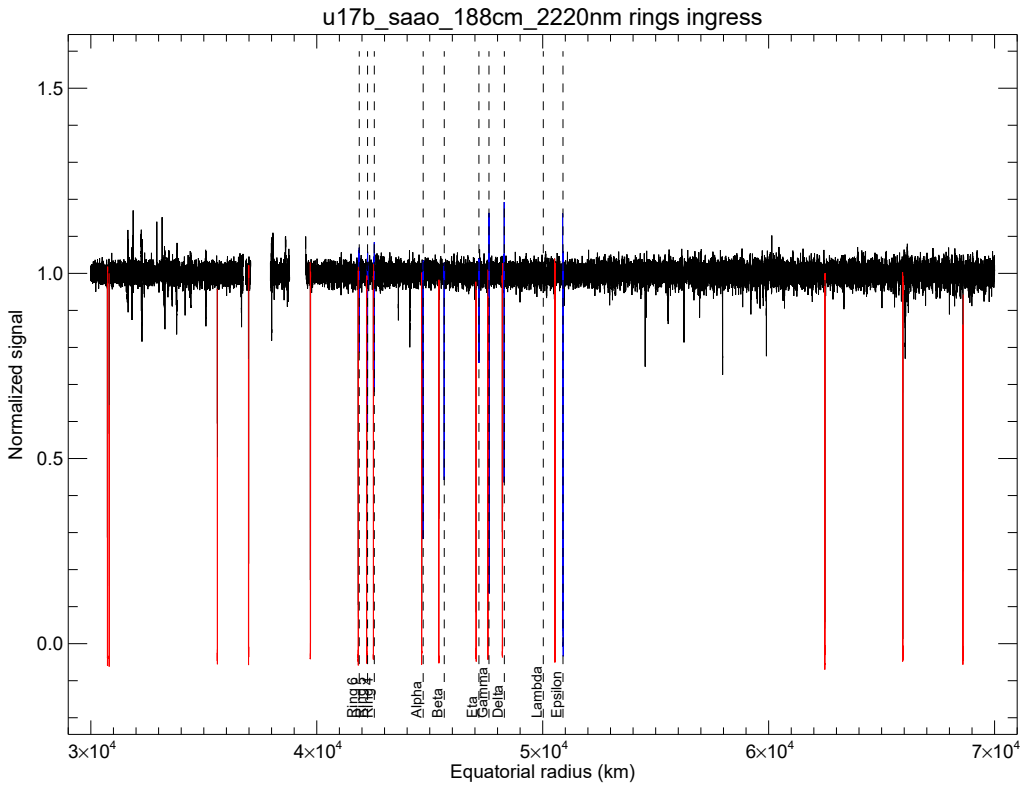

Fig. 12: Normalized ingress ring lightcurve of the occultation of Uranus star u17b observed from SAAO, plotted as a function of equatorial radius. Individual ring events are shown in red and sky checks are shown in blue. Predicted ring event radii are indicated by labeled dashed lines. (`u17b_saao_188cm_2220nm_radius_equator_ingress_1000m.pdf`)

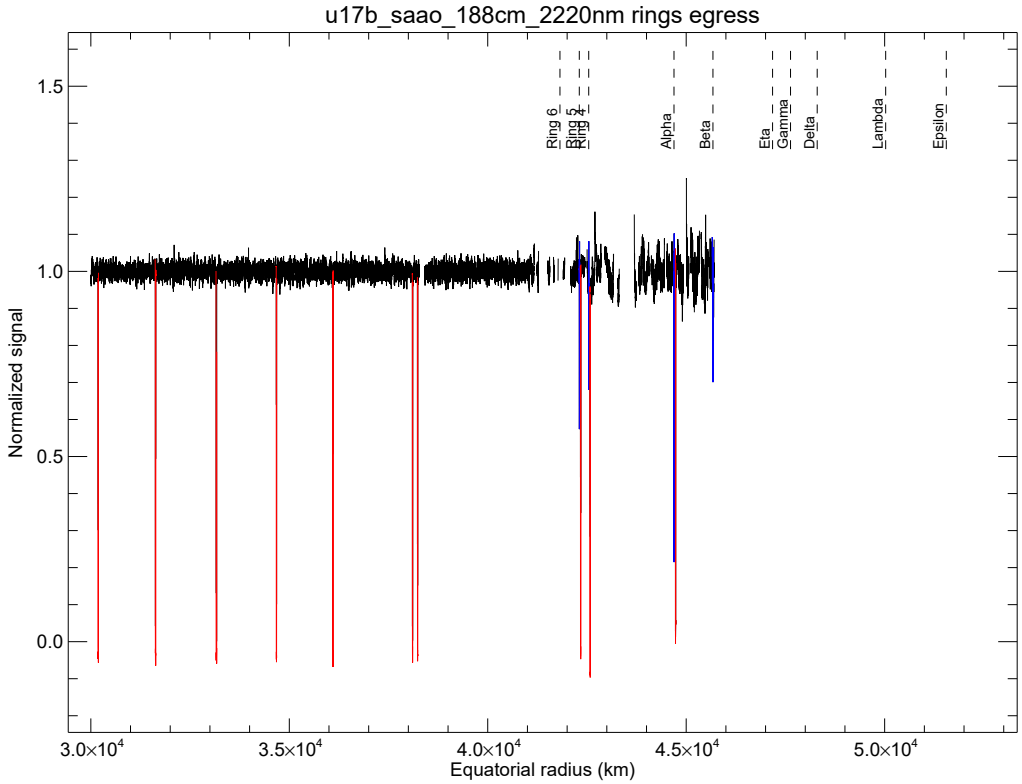

Fig. 13: Normalized egress ring lightcurve of the occultation of Uranus star u17b observed from SAAO, plotted as a function of equatorial radius. Individual ring events are shown in red and sky checks are shown in blue. Predicted ring event radii are indicated by labeled dashed lines. (`u17b_saao_188cm_2220nm_radius_equator_egress_1000m.pdf`)

The `browse/rings/` directory includes a gallery plot of selected individual unnormalized observations centered on the predicted radial location for selected rings (Fig. 14). The panels are arranged in a checkerboard panel that is identical for all observation bundles, to aid in the comparison of results from event to event. The top two rows of five panels each show, from left to right, rings 6, 5, 4, α, and β, with ingress in the top row and egress immediately below, to make it easy to compare two profiles of the same ring, when possible. The bottom two rows show rings η, γ, δ, λ, and ϵ, once again first in ingress and then directly below in the last row for egress. (For the u17b occultation, the bottom row is missing because those ring events occurred during sunrise and are not visible in the data.)

For the λ ring, which is known to be azimuthally clumpy and arc-like, the observed ingress lightcurve over the radial region near the orbit of the ring is included in this figure, even though no ring occultation is evident, to provide users with a sense of the data quality in

the vicinity of this non-detection. Individual ring occultations that are badly contaminated by noise are not shown. The arrival of sunrise is evident in the egress lightcurves, and this gallery plot provides a quick view of the varying quality of individual ring events over the course of an occultation.

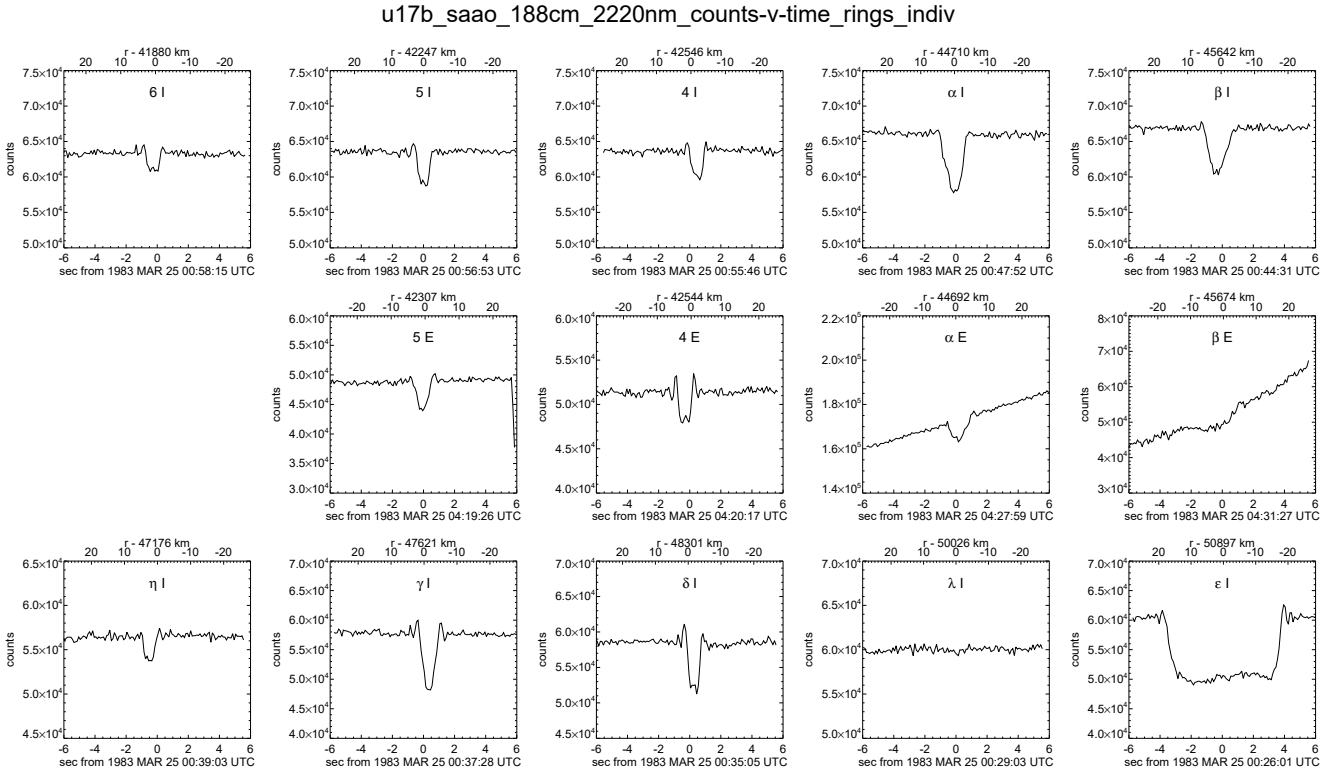

Fig. 14: Gallery of individual unnormalized ring occultations as a function of time (lower axis) and ring plane radius (upper axis) for the occultation of Uranus star u17b observed from SAAO. There is no detection of the λ ring at the predicted orbital radius for this incomplete ring. The ring 6 egress occultation was lost in the strongly-varying background signal, and is not shown. The rising slopes for the egress α and β rings result from sunrise encroaching on the observations. (`u17b_saao_188cm_2220nm_counts-v-time_rings_indiv.pdf`)

2.3.4 `browse/ring_models/`

The `browse/ring_models/` directory contains a gallery of individual ring profiles and the best-fitting model, using a square-well diffraction model described below in Section 2.4.4. Figure 15 shows the gallery for the u17b occultation, laid out in the same checkerboard pattern as in Fig. 14, with the top row showing, from left to right, ingress profiles of rings 6 through β, and the second row showing the egress profiles for the same rings. The third row shows ingress profiles for η through ϵ, with the fourth row showing the corresponding egress

profiles (for u17b, this final row is absent because the ring events occurred during sunrise). Each panel includes a quality index in parentheses, ranging from 1 for the best profiles to 4 for marginal detections. (See Section 2.4.4 for more details about the quality index.)

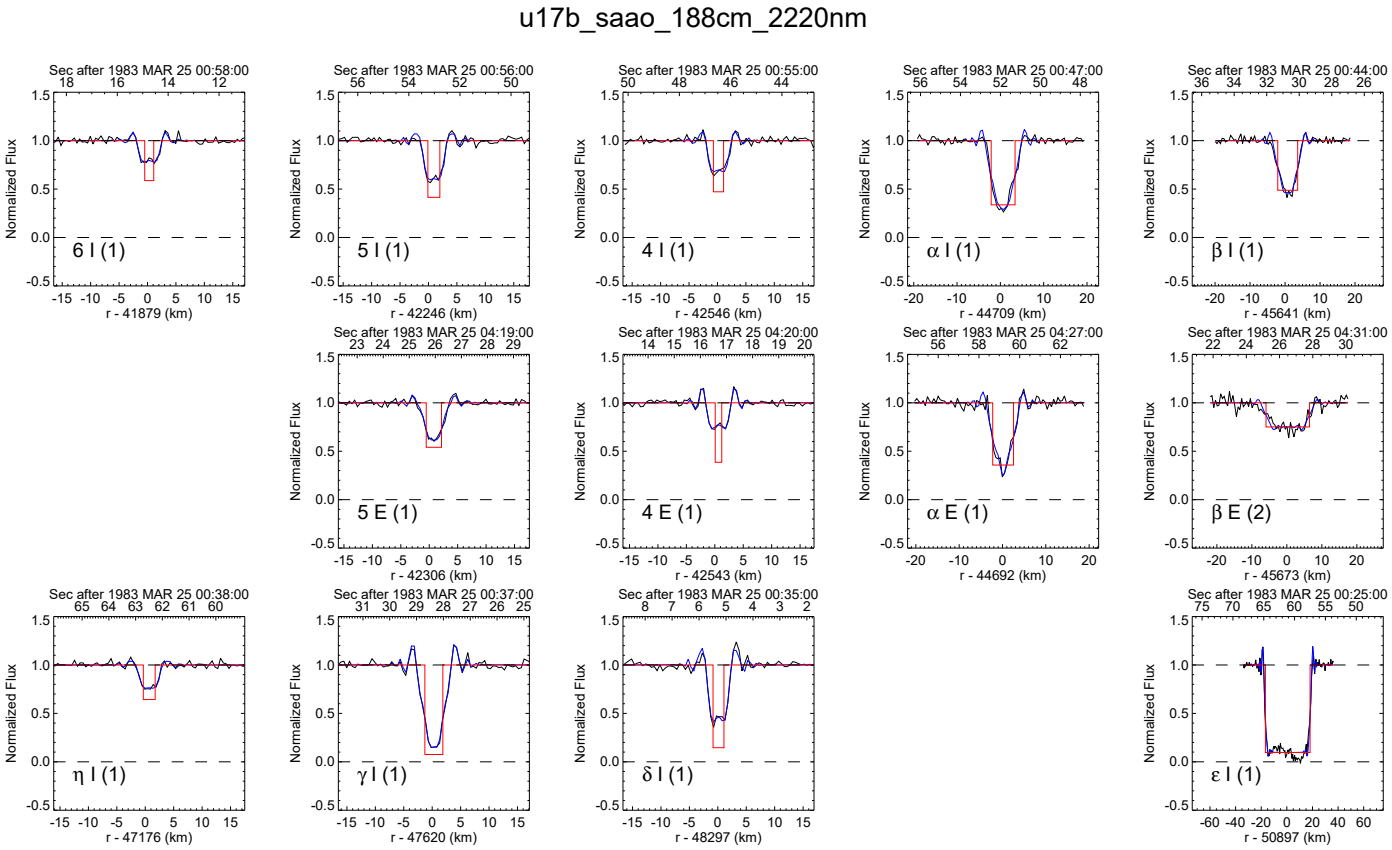

Fig. 15: Gallery of individual normalized ring profiles and the corresponding best-fitting square-well models. The intrinsic square well is shown in red, and the blue curve is the model profile computed from the diffraction pattern produced the by square well, appropriately accounting for the wavelength range of the filter used during the observations, the finite projected size of the occulted star, and any instrumental time constant. (`u17b_saao_188cm_2220nm_ring_sqw_gallery.pdf`)

2.4 The `data/` directory

The `data/` directory contains `*.tab` tables of the occultation data, both as raw counts vs time and as normalized signal vs orbital radius. (For users interested in the details of diffraction model fits to individual ring profiles, used to determine the ring event times used in our global ring orbit model, see the `data/ring_models/` directory described in Section 2.4.4.) The accompanying `*.xml` label files contain column definitions and other useful

auxiliary information. Examples of these files are described below. Of particular interest to many users will be the ring-by-ring summary table that provides detailed information about the derived ring profile width, optical depth, and orbital geometry for all ring events (both observed and those predicted but not seen in the data) – see Section 2.4.4.3.

2.4.1 `data/global/`

Th `data/global/` directory contains a single multi-column comma-separated-value (csv) `*.tab` file of the entire occultation lightcurve, and an accompanying `*.xml` label file that defines the columns in the table and provides additional information. In this instance, the files are `u17b_saao_188cm_2220nm_counts-v-time_occult.tab` and `u17b_saao_188cm_2220nm_counts-v-time_occult.xml`, respectively. The `*.xml` file can be viewed directly using a web browser or other xml reader. Figure 16 shows a screenshot of part of this file, displayed using Xcode on a Macintosh computer.

```
</File>
<Header>
    <offset unit="byte">0</offset>
    <object_length unit="byte">264</object_length>
    <parsing_standard_id>UTF-8 Text</parsing_standard_id>
    <description>Provides the column headers, separated by commas, for the data table.</description>
</Header>
<Table_Character>
    <offset unit="byte">264</offset>
    <records>215834</records>
    <description>This is a calibrated time series of an occultation by the Uranus system
          generated from an earth-based stellar occultation. The data are uniformly spaced in time, and
          normalized in units of stellar intensity. The data may include occultations by both the rings
          and the planet, or just the planet. The occultation by the rings, if present, is based on
          the equatorial ring plane radius sampled at each time point, computed from an orbit
          model for the ring system.
    </description>
    <record_delimiter>Carriage-Return Line-Feed</record_delimiter>
    <Record_Character>
        <fields>15</fields>
        <groups>0</groups>
        <record_length unit="byte">212</record_length>
        <Field_Character>
            <name>Observed Event Time</name>
            <field_number>1</field_number>
            <field_location unit="byte">1</field_location>
            <data_type>ASCII_Real</data_type>
            <field_length unit="byte">16</field_length>
            <unit>second</unit>
            <description>The instant at which photons were received at the observer location. It is
                represented in the Universal Coordinated Time system, as a number of elapsed
                seconds since the time given by the reference_time_utc attribute specified in this file.
                It refers to the middle of the bin.
            </description>
```

Fig. 16: Screen shot of a part of the `u17b_saao_188cm_2220nm_counts-v-time_occult.xml` label file, showing the description of the file contents and the definition of the `Observed Event Time` column for the associated `*.tab` file.

More sophisticated XML readers can render this in more useful form, but for easier readability, we have extracted the file and column descriptions to illustrate the contents of the `*.tab` file. It contains a calibrated time series of the observations with both raw and normalized star signal as a function of time. The geometry of the ring plane intercept point is recorded as well. The `Note Flag` in the final column flags the characteristics of every data point, using an additive scheme such that individual flag values are summed, enabling multiple flags to be applied to an individual data point.

```
Description: This is a calibrated time series of an occultation by the rings
     and atmosphere of Uranus generated from an earth-based stellar
     occultation. The data are uniformly spaced in time, normalized in units
     of stellar intensity, and include the equatorial ring plane radius
     sampled at each time point, computed from an orbit model for the ring
     system.
Observed Event Time (column 1):
     The instant at which photons were received at the observer location. It
     is represented in the Universal Coordinated Time system, as a
     number of elapsed seconds since the time given by the
     reference_time_utc attribute specified in this file. It refers to the
     middle of the bin.
Observed Event TDB (column 2):
     The instant at which photons were received at the observer location. It
     is represented in the 'Barycentric Dynamical Time' system, as a
     number of elapsed seconds since the J2000 epoch.
Mean_Signal (column 3):
     Mean counts received by the instrument during this time bin. The
     background signal has not been subtracted. Refer to NOTE FLAG for
     guidance on validity of data.
Normalized Signal (column 4):
     Normalized signal during this time bin, in units of the unocculted
     stellar signal, such that 1.0 corresponds to the full unocculted star
     signal and 0.0 corresponds to no counts from the star (a completely
     opaque ring). NORMALIZED SIGNAL = (MEAN_SIGNAL -
     BACKGROUND_MODEL)/(UNOCCULTED STAR MODEL).
     This is an approximate normalization, computed using regional
     polynomial fits. For high-precision photometry of ring events, use
     locally computed normalization.
Sky-plane F (column 5):
     The east/west component of r sky (positive in the east direction),
     in km.
Sky-plane G (column 6):
     The north/south component of r sky (positive in the north direction),
     in km.
Sky-plane Radius (column 7):
     The length of the radius vector in the plane of the sky measured from the
     center of the occulting object to the position of the occulted star or
     spacecraft, in km.
Ring Radius (column 8):
     Radial distance of the occultation intercept point (middle of the bin)
     from the center of the planet, in km. Distances are measured along
     the equator plane.
Ring Longitude (column 9):
     Inertial longitude on the ring plane corresponding to the midpoint of
     the bin (in degrees).
Observed Ring Azimuth (column 10):
     Angle measured at a point in the ring plane, starting from the direction
     of a photon heading to the observer, and ending at the direction of a
     local radial vector. This angle is projected into the ring plane and
     measured in the prograde direction (in degrees).
Ring Event TDB (column 11):
     The time at which photons left the ring plane. This time is earlier than
     the associated Observed Event TDB by an amount equal to the light
     travel time. It is represented in the 'Barycentric Dynamical Time'
     system, as a number of elapsed seconds since the J2000 epoch.
Unocculted Star Model (column 12):
     Model of the unocculted star signal as a function of ring plane radius.
     This is necessary because of variations in atmospheric transparency
```

```
     and other time-dependent effects.
Background Star Model (column 13):
     Model of the background signal which varies over the course of the
     occultation due to sky brightness and contributions from reflected
     sunlight from the rings and planet.
Number Of Samples Per Bin (column 14):
     The number of raw data points per bin.
Note Flag (column 15):
     A numerical flag that associates specific comments with individual
     data bins. When more than one comment applies, the values are
     summed. The values and their associated comments are:
      0: radius and longitude are based on Uranus equatorial plane.
      1: radius and longitude are based inclined ring plane model
         referred to in metadata associated with file.
      2: observed ring occultation event
      4: telescope pointed to nearby sky for background level check
      8: input signal from time source, not from photometer on telescope
     16: line of sight intersects planet
     32: dawn/dusk - rapid background level change; no background or
         star intensity estimate.
     64: unreliable data (e.g., clouds, telescope guiding error, or instrument
         adjustment); no background or star intensity estimate.
```

A subset of the additional header keywords includes:

```
rings:occultation_type               stellar
rings:occultation_direction          both
riings:planetary_occultation_flag    Y
rings:star_name                      Hipparcos 80841
rings:minimum_wavelength unit="nm"   2040.0
rings:maximum_wavelength unit="nm"   2400.0
```

For additional details, refer to `u17b_saao_188cm_2220nm_counts-v-time_occult.xml`.

2.4.2 `data/atmosphere/`

For observation bundles containing an atmosphere occultation, the `data/atmosphere/` directory contains separate multi-column comma-separated-value (csv) `*.tab` files for the atmospheric ingress and/or egress lightcurves, and accompanying `*.xml` label files. In this instance, the ingress table and label files are
`u17b_saao_188cm_2220nm_counts-v-time_atmos_ingress.tab` and
`u17b_saao_188cm_2220nm_counts-v-time_atmos_ingress.xml`, with corresponding files for egress. For easy readability, we extract the file and column descriptions below to illustrate the contents of the ingress file.

```
Description: Derived normalized signal vs. time from the ingress atmospheric
     occultation of star u17b (Hipparcos 80841) observed by the SAAO 188cm
     Telescope.
Observed Event Time (column 1):
```

```
     The instant at which photons were received at the observer location. It
     is represented in the Universal Coordinated Time system, as a
     number of elapsed seconds since the time given by the
     reference_time_utc attribute specified in this file. It refers to the
     middle of the bin.
Observed Event TDB (column 2):
     The instant at which photons were received at the observer location. It
     is represented in the 'Barycentric Dynamical Time' system, as a
     number of elapsed seconds since the J2000 epoch.
Mean_Signal (column 3):
     Mean counts received by the instrument during this time bin. The
     background signal has not been subtracted. Refer to NOTE FLAG for
     guidance on validity of data.
Normalized Signal (column 4):
     Normalized signal during this time bin, in units of the unocculted
     stellar signal, such that 1.0 corresponds to the full unocculted star
     signal and 0.0 corresponds to no counts from the star (a
     completely opaque ring). NORMALIZED SIGNAL =
     (MEAN_SIGNAL - BACKGROUND_MODEL)/(UNOCCULTED
     STAR MODEL). This is an approximate normalization, computed
     using regional polynomial fits. For high-precision photometry of
     ring events, use locally computed normalization.
Sky-plane F (column 5):
     The east/west component of r sky (positive in the east direction), in km.
Sky-plane G (column 6):
     The north/south component of r sky (positive in the north direction), in km.
Sky-plane Radius (column 7):
     The length of the radius vector in the plane of the sky measured from the
     center of the occulting object to the position of the occulted star or
     spacecraft, in km.
Unocculted Star Model (column 8):
     Model of the unocculted star signal as a function of ring plane radius.
     This is necessary because of variations in atmospheric transparency
     and other time-dependent effects.
Background Star Model (column 9):
     Model of the background signal which varies over the course of the
     occultation due to sky brightness and contributions from reflected
     sunlight from the rings and planet.
Number Of Samples Per Bin (column 10):
     The number of raw data points per bin.
Note Flag (column 11):
     A numerical flag that associates specific comments with individual
     data bins. When more than one comment applies, the values are
     summed. The values and their associated comments are:
      0: radius and longitude are based on Uranus equatorial plane.
      1: radius and longitude are based inclined ring plane model
         referred to in metadata associated with file.
      2: observed ring occultation event
      4: telescope pointed to nearby sky for background level check
      8: input signal from time source, not from photometer on telescope
     16: line of sight intersects planet
     32: dawn/dusk - rapid background level change; no background or
         star intensity estimate.
     64: unreliable data (e.g., clouds, telescope guiding error, or instrument
         adjustment); no background or star intensity estimate.
```

For additional details, refer to `u17b_saao_188cm_2220nm_counts-v-time_atmos_ingress.xml`.

2.4.3 `data/rings/`

The `data/rings/` directory contains ring occultation observations interpolated or averaged to three uniform radial resolutions: 1000m, 500m, and 100m. Separate data files are included for the entire ingress and egress regions, registered in radius to the equatorial plane, and individual ring event files registered to the corresponding ring plane, taking account of the time-variable pole of the inclined rings.

2.4.3.1 Ring data files spanning ingress or egress

The following files span the ring ingress region at three resolutions:

```
u17b_saao_188cm_2220nm_radius_equator_ingress_1000m.tab
u17b_saao_188cm_2220nm_radius_equator_ingress_500m.tab
u17b_saao_188cm_2220nm_radius_equator_ingress_100m.tab
```

A similar set of files span ring egress:

```
u17b_saao_188cm_2220nm_radius_equator_egress_1000m.tab
u17b_saao_188cm_2220nm_radius_equator_egress_500m.tab
u17b_saao_188cm_2220nm_radius_equator_egress_100m.tab
```

Corresponding files with the suffix `.xml` contain the following description and column definitions:

```
Description: Derived radial profile of the Uranus ring system from the
     occultation of star u17b (Hipparcos 80841). This profile is based
     on the equatorial plane.
Ring Radius (column 1):
     Radial distance of the occultation intercept point (middle of the
     bin) from the center of the planet, in km. Distances are measured
     along the equatorial plane. The radius scale is only approximate
     for inclined rings.
Ring Longitude (column 2):
     Inertial longitude on the ring plane corresponding to the midpoint
     of the bin.
Observed Ring Azimuth (column 3):
     Angle measured at a point in the ring plane, starting from the
     direction of a photon heading to the observer, and ending at the
     direction of a local radial vector. This angle is projected into the
     ring plane and measured in the prograde direction.
Normalized Signal (column 4):
     Normalized signal during this radius bin, in units of the unocculted
     stellar signal, such that 1.0 corresponds to the full unocculted star
     signal and 0.0 corresponds to no counts from the star (a completely
     opaque ring). Normalized Signal = (Mean Signal - Background
     Model)/(Unocculted Star Model)
```

```
     This is an approximate normalization, based when possible on
     regional polynomial fits. For high-precision photometry of ring events,
     use locally computed normalization.
Mean Signal (column 5):
     Mean counts received by the instrument during this radius bin. The
     background signal has not been subtracted. Refer to Note Flag for
     guidance on validity of data.
Mean_Signal_Uncertainty (column 6):
     The uncertainty in the mean signal level expressed as the standard
     deviation per radial bin, computed when possible from the adjacent
     mean signal level over a span of (typically) N=50 free-space radial
     samples on each side for which the Note Flag is 0 or 1,
     or at least N total nearby samples for which the Note Flag is 0 or 1.
     For cases with fewer than N total nearby samples available, and the
     Note Flag is 0, or for all cases when the Note Flag indicates a ring
     occultation event, the uncertainty is estimated by interpolation from
     nearby free-space values. Otherwise, the value is set to -1.
Observed Event Time (column 7):
     The instant at which photons were received at the observer location. It
     is represented in the Universal Coordinated Time system, as a
     number of elapsed seconds since the time given by the
     reference_time_utc attribute specified in this file.
     It refers to the middle of the bin.
Observed Event TDB (column 8):
     The instant at which photons were received at the observer location. It
     is represented in the 'Barycentric Dynamical Time' system, as a
     number of elapsed seconds since the J2000 epoch. It refers to the
     middle of the bin.
Ring Event Time (column 9):
     The time at which photons left the ring plane. This time is earlier than
     the associated observed event time by an amount equal to the light
     travel time. It is given as a number of elapsed seconds since the
     time given by the reference_time_utc attribute specified in this file.
     It refers to the middle of the bin.
Ring Event TDB (column 10):
     The time at which photons left the ring plane. This time is earlier than
     the associated Observed Event TDB by an amount equal to the light
     travel time. It is represented in the 'Barycentric Dynamical Time'
     system, as a number of elapsed seconds since the J2000 epoch.
Background Model (column 11):
     Model of the background signal, which may vary over the course of
     the occultation due to variations in sky brightness and contributions
     from reflected sunlight from the rings and planet.
Unocculted Star Model (column 12):
     Model of the unocculted star signal as a function of ring plane radius.
     This may be affected by variations in atmospheric transparency and
     other time-dependent effects. Note that sky level checks in the data,
     often just after an individual ring occultation event, compare the
     background sky level to the measured intensity not only of the
     occultation star but also the contribution of the brightness of the
     planet and rings in the photometric aperture, which can contribute
     several percent of the unocculted stellar flux to the total counts
     observed when the aperture is centered on the occultation star.
     When possible, this effect has been included when computing the
     model of the unocculted star signal listed here.
Number Of Samples Per Bin (column 13):
     Number of raw time bins contributing to this radius bin. When the
     radially interpolated signal subsamples the raw data, this
     value will be 1.
```

```
Note Flag (column 14):
     A numerical flag that associates specific comments with individual
     data bins. When more than one comment applies, the values are
     summed. The values and their associated comments are:
      0: radius and longitude are based on Uranus equatorial plane.
      1: radius and longitude are based inclined ring plane model
         referred to in metadata associated with file.
      2: observed ring occultation event
      4: telescope pointed to nearby sky for background level check
      8: input signal from time source, not from photometer on telescope
     16: line of sight intersects planet
     32: dawn/dusk - rapid background level change; no background or
         star intensity estimate.
     64: unreliable data (e.g., clouds, telescope guiding error, or instrument
         adjustment); no background or star intensity estimate.
```

2.4.3.2 Individual ring data files

The `data/ring/` directory also contains individual ring data files, spanning the local region centered on each ring and taking into account the instantaneous orientation of the possibly-inclined ring plane. For example, ring 6 ingress has the following table files:

```
u17b_saao_188cm_2220nm_radius_six_ingress_1000m.tab
u17b_saao_188cm_2220nm_radius_six_ingress_500m.tab
u17b_saao_188cm_2220nm_radius_six_ingress_100m.tab
```

Descriptions and column definitions in the associated `*.xml` files are similar to those for the equatorial files, except in reference to the individual ring plane instead of the equatorial plane.

2.4.4 `data/ring_models/`

The `data/ring_models/` directory contains summary files of all observed or predicted ring events during a given occultation, and detailed results of diffraction square-well model fits to individual ring profiles. Figure 17 shows the directory structure and representative contents for a single ring.

```
data/ring_models
├── u17b_saao_188cm_2220nm_predicted_ring_event_times.pdf
├── u17b_saao_188cm_2220nm_predicted_ring_event_times.tab
├── u17b_saao_188cm_2220nm_predicted_ring_event_times.txt
├── u17b_saao_188cm_2220nm_predicted_ring_event_times.xml
...
├── u17b_saao_188cm_2220nm_ring_alpha_egress_sqw.pdf
├── u17b_saao_188cm_2220nm_ring_alpha_egress_sqw.txt
├── u17b_saao_188cm_2220nm_ring_alpha_egress_sqw.xml
├── u17b_saao_188cm_2220nm_ring_alpha_egress_sqw_c.tab
├── u17b_saao_188cm_2220nm_ring_alpha_egress_sqw_h.tab
├── u17b_saao_188cm_2220nm_ring_alpha_egress_sqw_i.tab
├── u17b_saao_188cm_2220nm_ring_alpha_egress_sqw_p.tab
├── u17b_saao_188cm_2220nm_ring_alpha_egress_sqw_s.tab
├── u17b_saao_188cm_2220nm_ring_alpha_ingress_sqw.pdf
...
├── u17b_saao_188cm_2220nm_fitted_ring_event_times.tab
├── u17b_saao_188cm_2220nm_fitted_ring_event_times.xml
```

Fig. 17: Directory structure and representative contents of the `data/ring_models/` directory.

2.4.4.1 Predicted ring event times

Files `u17b_saao_188cm_2220nm_predicted_ring_event_times.{tab,pdf,txt}` (and the accompanying `*.xml` label file) contain useful summaries of the detailed input used to compute the occultation geometry and a ring-by-ring list of predicted event times (both Earth-received times and times at the ring plane) and ring plane geometry (radius, true anomaly, and inertial longitude) for an occultation bundle. The altitude of the occulted star and the Sun relative to the horizon as seen by the ground-based observer are listed as well, along with the equatorial plane opening angle, the position angle of the pole and the observer-planet distance. For occultations with atmosphere occultations, the predicted atmospheric occultation time is listed as well. The `*.tab` file contains a machine-readable version of the predicted ring events time. The `*.pdf` file is a printable version of the `*.txt` file, which is reproduced below:

```
u17b_saao_188cm_2220nm_predicted_ring_event_times.txt produced Fri Dec  4 10:06:37 2020 using
rfrench@maxwell.fios-router.home:/Volumes/PromisePegasus48TBb/dione_raid2/Research/uranus/PDART2014/programs/pro_occinfo2geom_plots_pds4_v7.pro

Bundle ID: uranus_occ_u17b_saao_188cm

Event:                                  u17b
Planet:                                 Uranus
Reference:                              Elliot et al. Icarus 71, 91-102 (1987)
Title:                                  The Occultation of KME 17 by Uranus and its Rings
Computations from:                      1983-03-24T22:55:59.0000Z to 1983-03-25T04:55:42.4000Z
Observatory name:                       South African Astronomical Observatory
Observatory code file directory:        /Volumes/dione_raid2/Research/kernels/
Observatory code file:                  ObsCodes_pck00010_20200709_Elon+ocobs_v9BJ.obs
Observatory code:                       SAA
Observatory abbreviation:               saao
Entry from observatory code file:
    SAA G +020 48 38.52  -32 22 46.3        1768 SAAO SUTHERLAND 74"                                ocobs_v9BJ.tx
Telescope:                              188cm
Instrument:                             Generic InSb High Speed Photometer
```

```
Mean wavelength (nm)                     2220nm
Observatory latitude (deg):                -32.379527778
Observatory E longitude (deg):              20.810700000
Observatory altitude (km):                   1.768000000
Ellipsoid source:                        /Volumes/dione_raid2/Research/kernels/pck00010.tpc
Observatory reference frame:             ITRF93
Earth equatorial radius (km):               6378.136600000
Earth 1/flattening:                          298.257006177
Topocentric position vector:                5041.279432685    1916.079799298   -3396.994745721
Leapsecond kernel file:                  /Volumes/dione_raid2/Research/kernels/naif0012.tls
Star catalog directory:                  /Volumes/dione_raid2/Research/RINGFIT/stars/data/
Star catalog file:                       ustarsALLd.v3.merged.sortedA.csv
Star catalog ID:                         80841
Star number:                                75
Star name:                               U17
Star source catalog:                     Hipparcos
Star RA (deg):                             247.630359900
Star Dec (deg):                            -21.741990010
Star epoch:                              1991-04-02T13:30:00.0000Z
Star parallax (mas):                         5.120000000
Star pm RA (mas/yr):                        -3.360000000
Star pm Dec (mas/yr):                        5.480000000
Star catalog positions in frame:         J2000
Star frame for calculations:             J2000
Heliocentric frame for calculations:     J2000
Ringfit savefile directory:              /Volumes/dione_raid2/Research/RINGFIT/tests/Uranus/Ur017L/savefiles/
Ringfit savefile for star/time offsets:  ringfit_v1.8.Ur017L-RF-V0204.sav
Ringfit output file directory:           /Volumes/dione_raid2/Research/RINGFIT/tests/Uranus/Ur017L/outfiles/
Ringfit output file:                     ringfit_v1.8.Ur017L-RF-V0204.out
Star offsets dRA,dDec (mas):               -35.888294013       4.293142371
Time offset for this obstr./event (sec):     0.000000000
Kernel directory:                        /Volumes/dione_raid2/Research/kernels/
   ../../../../kernels/ura111.bsp
   ../../../../kernels/vgr2.ura111.bsp
   ../../../../kernels/earthstns_itrf93_040916.bsp
   ../../../../kernels/earth_720101_031229.bpc
   ../../../../kernels/pg3f0000r.bsp
   ../../../../kernels/pg490000r.bsp
   ../../../../kernels/naif0012.tls
   /Volumes/dione_raid2/Research/RINGFIT/tests/Uranus/Ur017L/savefiles/../kernels/RAJobs_U111+rgf9.spk
   /Volumes/dione_raid2/Research/RINGFIT/tests/Uranus/Ur017L/savefiles/../kernels/URKALLv1.spk
   /Volumes/dione_raid2/Research/kernels/uranus_ringframes_rfrench20201201_v1.tf
   /Volumes/dione_raid2/Research/kernels/pck00010.tpc
```

Predicted Ring/Atmosphere Occultation Events

Ring	I/E	UTC(Earth)	UTC(@ring)	R(model)	R-dot	Anomaly	Sin B	Ulon	Alt(deg)	Sun(deg)
epsilon	I	1983-03-25T00:26:01.18Z	1983-03-24T21:52:11.72Z	50897.35	-4.814	51.962	-0.98067	32.701	54.592	-50.772
lambda	I	1983-03-25T00:29:02.59Z	1983-03-24T21:55:13.15Z	50026.01	-4.791	264.808	-0.98067	33.267	55.226	-50.330
delta	I	1983-03-25T00:35:04.56Z	1983-03-24T22:01:15.15Z	48300.53	-4.741	106.883	-0.98067	34.458	56.488	-49.427
gamma	I	1983-03-25T00:37:28.17Z	1983-03-24T22:03:38.78Z	47621.17	-4.719	356.368	-0.98067	34.955	56.987	-49.061
eta	I	1983-03-25T00:39:02.62Z	1983-03-24T22:05:13.23Z	47176.09	-4.704	31.309	-0.98067	35.289	57.315	-48.817
beta	I	1983-03-25T00:44:30.73Z	1983-03-24T22:10:41.38Z	45641.66	-4.648	13.497	-0.98067	36.502	58.453	-47.958
alpha	I	1983-03-25T00:47:51.88Z	1983-03-24T22:14:02.54Z	44709.56	-4.610	285.514	-0.98069	37.291	59.148	-47.421
four	I	1983-03-25T00:55:46.44Z	1983-03-24T22:21:57.15Z	42546.34	-4.511	303.392	-0.98064	39.270	60.781	-46.124
five	I	1983-03-25T00:56:52.99Z	1983-03-24T22:23:03.70Z	42247.08	-4.495	98.712	-0.98074	39.563	61.009	-45.939
six	I	1983-03-25T00:58:14.70Z	1983-03-24T22:24:25.42Z	41879.50	-4.475	187.481	-0.98046	39.938	61.288	-45.711
Atmosphere	I	1983-03-25T02:12:56.12Z							75.308	-31.931
Atmosphere	E	1983-03-25T03:06:54.27Z							79.152	-20.997
six	E	1983-03-25T04:17:36.77Z	1983-03-25T01:43:48.59Z	41819.31	4.556	294.993	-0.98046	147.843	69.363	-6.212
five	E	1983-03-25T04:19:25.88Z	1983-03-25T01:45:37.71Z	42306.52	4.583	207.105	-0.98074	148.347	69.017	-5.828
four	E	1983-03-25T04:20:16.68Z	1983-03-25T01:46:28.51Z	42543.58	4.597	52.331	-0.98064	148.577	68.855	-5.650
alpha	E	1983-03-25T04:27:59.17Z	1983-03-25T01:54:11.04Z	44692.06	4.704	38.450	-0.98069	150.561	67.362	-4.024
beta	E	1983-03-25T04:31:26.58Z	1983-03-25T01:57:38.47Z	45673.66	4.748	128.054	-0.98067	151.389	66.683	-3.294
eta	E	1983-03-25T04:36:40.99Z	1983-03-25T02:02:52.92Z	47176.37	4.809	148.295	-0.98067	152.581	65.645	-2.188
gamma	E	1983-03-25T04:38:14.88Z	1983-03-25T02:04:26.81Z	47628.66	4.826	114.042	-0.98067	152.922	65.333	-1.858
delta	E	1983-03-25T04:40:33.80Z	1983-03-25T02:06:45.75Z	48300.65	4.850	225.541	-0.98067	153.415	64.869	-1.370
lambda	E	1983-03-25T04:46:27.44Z	1983-03-25T02:12:39.42Z	50026.01	4.907	25.886	-0.98067	154.611	63.682	-0.126
epsilon	E	1983-03-25T04:51:37.32Z	1983-03-25T02:17:49.32Z	51553.48	4.952	174.604	-0.98067	155.594	62.633	0.963

```
Event geometry at 1983-03-25T02:39:56.0000Z
---------------------------------------
    Ring opening angle B (deg):  -78.71537
Position angle of pole P (deg):   56.03599
 Observer-planet distance (km):    2766.486534 x 10^6
       Light travel time (sec):    9228.005777
```

2.4.4.2 Square-well model fits to individual ring profiles

The ring orbit model used to determine the occultation geometry and the ring orbital elements is based on a non-linear least squares fit to the set of estimated midtimes of individual ring profiles from a large set of occultations. In most cases, Uranus stellar ring occultation profiles are diffraction-limited, smoothed by the finite angular diameter of the occulted star, and affected by time constants associated with the recording electronics and/or chopping of the telescope secondary. At the same time, Voyager RSS occultations show most of the Uranian rings to be intrinsically sharp-edged (Gresh et al. 1989). Following past practice and for simplicity and consistency, we determine the midtimes of individual ring profiles using a diffraction-based square-well model (Elliot et al. 1984) that accounts for stellar and instrumental smoothing, as well as the instrumental response over the wavelength range of the filter used for the observations.

For users interested in the details of the individual square-well fits that underly the ring orbit model, we include a suite of files in the `data/ring_models/` directory that document these fits. For illustration, we describe the following files for the ring 4 egress event:

```
u17b_saao_188cm_2220nm_ring_four_egress_sqw.xml
u17b_saao_188cm_2220nm_ring_four_egress_sqw.pdf
u17b_saao_188cm_2220nm_ring_four_egress_sqw_p.tab
u17b_saao_188cm_2220nm_ring_four_egress_sqw_i.tab
u17b_saao_188cm_2220nm_ring_four_egress_sqw_s.tab
u17b_saao_188cm_2220nm_ring_four_egress_sqw_h.tab
u17b_saao_188cm_2220nm_ring_four_egress_sqw_c.tab
u17b_saao_188cm_2220nm_ring_four_egress_sqw.txt
```

The `*.xml` file contains a detailed description of each of the other files. Here, we provide a brief summary of the key points. Figure 18 (`u17b_saao_188cm_2220nm_ring_four_egress_sqw.pdf`) shows the observations of this individual Uranus ring occultation profile and the best-fitting diffraction square-well (sqw) model. In the description below, we also describe briefly the contents of the associated `*{p,i,s,h,c}.tab` files listed above. (For additional details about each of these files, see the `*.xml` file.)

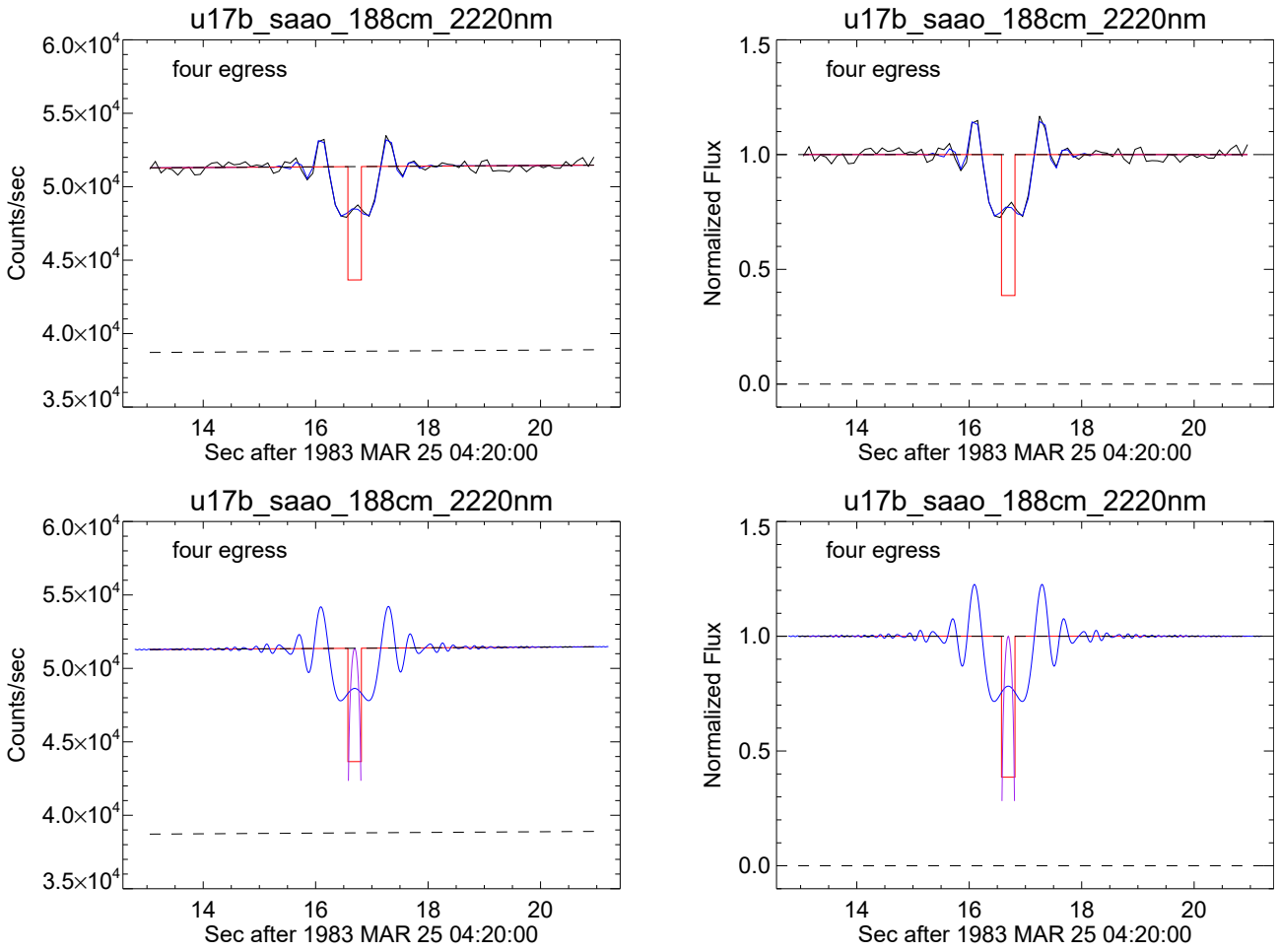

Fig. 18: Square-well model fit to the egress ring 4 profile of the occultation of Uranus star u17b observed from SAAO. See text for details. (`u17b_saao_188cm_2220nm_ring_four_egress_sqw.pdf`)

Upper left panel: Comparison of observed count rate (black) as a function of time (lower x axis), the best-fitting diffraction square well model (blue), and the corresponding square well itself (red). The full and zero stellar intensity levels are shown as dashed lines. The time-series data and the best-fitting model are included in the corresponding ring model `*p.tab` file (ex: `u17b_saao_188cm_2220nm_ring_four_egress_sqw_p.tab`).

Upper right panel: Same as upper left panel, but normalized to units of the flux of the unocculted star, so that the upper free-space stellar signal is 1.0 and 0.0 represents a complete loss of the stellar signal.

Lower left panel: The model point-source diffraction pattern (blue) for the square well itself (red), averaged over the filter bandpass and (possibly) at a higher time resolution than the observations themselves that are shown in the upper left panel. Especially for data sets with rather low time resolution, it is necessary to subdivide the observed time per bit (dt) into a higher-resolution "mesh." The number of mesh points (m) is always an odd integer. Then, when computing the best-fitting square well model to the actual data, the (possibly) higher-resolution model profile is summed over m points. Frequently, this summing converts a smooth and continuous diffraction pattern into a jagged pattern, reflecting the fact that the integration time dt is often longer than the time scale of variation of the diffraction pattern of the ring. The time-series model at the subdivided time resolution dt/m is included in `u17b_saao_188cm_2220nm_ring_four_egress_sqw_i.tab`.

Also included in the lower left panel is a curve representing the occultation star convolution kernel (the strip-brightness distribution of the star), shown as a purple curve centered at the mid-point of the geometric square well model. The time-series stellar convolution kernel is contained in `u17b_saao_188cm_2220nm_ring_four_egress_sqw_s.tab`.

For observations with an instrumental time constant included in the square-well diffraction model, the corresponding time constant convolution kernel is included in the lower panel plots as a green line, and in `u17b_saao_188cm_2220nm_ring_four_egress_sqw_h.tab`. (For the u17b occultation, there was no instrumental time constant, and thus no green line is visible in this figure. See Fig. 19 for an example of an event with a substantial time constant.)

When both a finite star (i.e., not a point source) and a non-zero instrumental time constant are included in the square-well model, the corresponding joint convolution kernel from these two separate sources of model smoothing is shown as an orange curve, and included in `u17b_saao_188cm_2220nm_ring_four_egress_sqw_c.tab`. This is not present for the u17b occultation, but is shown in See Fig. 19 for an event with a substantial time constant.

Lower right panel: Same as lower left panel, but normalized to units of the flux of the unocculted star, so that the upper free-space baseline is 1.0 and 0.0 represents a complete loss of the stellar signal.

Details of the diffraction square-well model fitted to the observations of an individual Uranus ring, for the given occultation event, are included in a text file. The fit results are contained in `u17b_saao_188cm_2220nm_ring_four_egress_sqw.txt` for our representative example. The first part of the file describes the IDL program that performed the fit of the square-well (sqw) model to the data. The occultation event, observatory, telescope, instrument, ring, and occultation direction are defined.

`DATA FILE_INFORMATION` documents the source data file and the specific subset of data to be fitted in this sqw model.

`EVENT INFORMATION` provides additional information about the specific ring event and event geometry.

SQUARE WELL MODEL INFORMATION specifies the number of mesh points m into which each observed time bin is subsampled to provide higher time resolution for the calculation of the square well diffraction pattern, before then coadding the subsampled model to the time resolution of the data being fitted.

SQUARE WELL MODEL FIT RESULTS contain the results of the non-linear least-squares fit of the sqw model to the data, including post-fit residuals, the initial and final parameter values, and their errors, calculated assuming that all data points have equal weight. Parameters that are fitted have an asterisk (*) preceding the corresponding initial value. The correlation matrix is also shown, with obvious two-letter abbreviations for the fitted variable names:

```
  Parameter       Initial Value     Final Value         Std. Dev.
-------------------------------------------------------------------
MID_TIME(s)    *    19457.693738    19457.693738          0.004728
MID_TIME(UTC)  *   04:20:16.6937   04:20:16.6937          0.004728
WIDTH(s)       *        0.240018        0.240018          0.016834
WIDTH(km)      *        1.103109        1.103109          0.077370
V_PERP(km/s)           4.504984        4.504984
STAR_CTS(/s)          12566.348470    12566.348470
BASE_CTS(/s)   *    51368.887965    51368.887965         31.999446
FRACTRANS      *        0.386062        0.386062          0.028218
STARDIAM(s)            0.233075        0.233075
STARDIAM(km)           1.049997        1.049997
SLOPE          *       23.445525       23.445525         13.151042
EQ_WIDTH(s)            0.147356        0.147356
EQ_WIDTH(km)           0.664132        0.664132
EQ_DEPTH(s)            0.228439        0.228439
EQ_DEPTH(km)           1.029570        1.029570
LIMB_DARKEN            0.000000        0.000000
TIME_CON(s)            0.000000        0.000000
TIME_CON(km)           0.000000        0.000000
R_DOT(km/s)            4.595936        4.595936
SIN_B                  0.980644        0.980644

Correlation matrix

       MT    WI    BC    FT    SL
MT   1.00 -0.00  0.00 -0.00  0.02
WI  -0.00  1.00  0.23  0.84 -0.03
BC   0.00  0.23  1.00  0.09 -0.14
FT  -0.00  0.84  0.09  1.00 -0.01
SL   0.02 -0.03 -0.14 -0.01  1.00
```

Note that the underlying model is performed in the time domain, but for convenience the corresponding length dimensions for the square-well width, star diameter, equivalent width, and equivalent depth are also shown. See Elliot et al. 1984 for further details.

As noted above, some occultation observations (particularly those observed in the chopping mode) have instrumental time constants that significantly affect the recorded signal. Figure 19 shows the α ring egress profile for the occultation of star u137 observed from the IRTF. Note the substantial smoothing of the point-source diffraction model and the time displacement of the observations relative to the fitted square well model shown in red. The

convolution kernel of the time response function is shown in green, and the joint convolution kernel combining the stellar disk and instrumental smoothing is shown in orange.

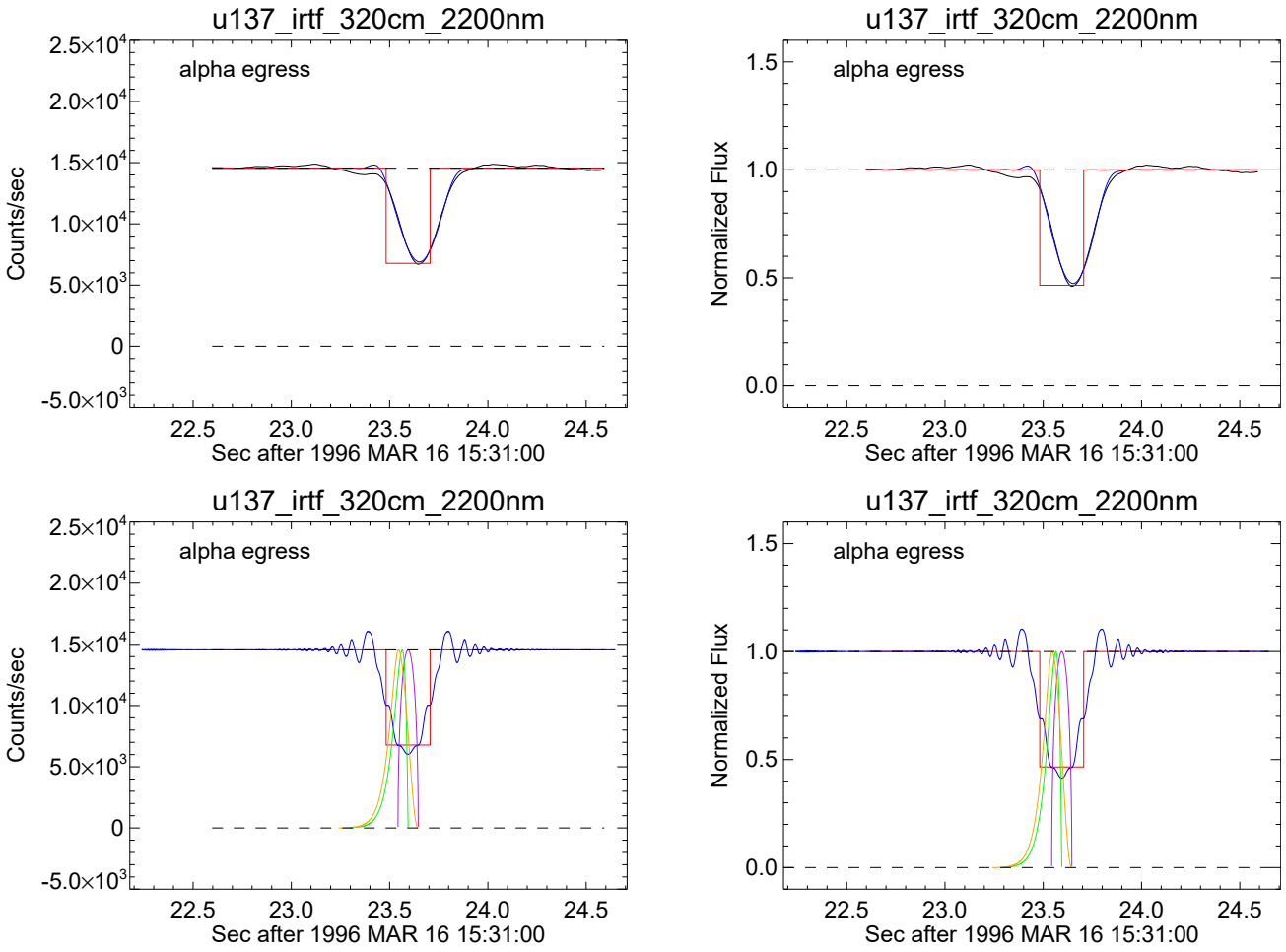

Fig. 19: Square-well model fit to the egress α ring profile of the occultation of Uranus star u137 observed from the IRTF on March 16, 1966. See text for details.

2.4.4.3 Table of ring event times and associated geometry

For every observation bundle, a ring-by-ring summary table is provided that contains information about the derived ring profile width, optical depth, and orbital geometry for all ring events (both those observed and those predicted but not seen in the data). For many users, this will be the single most useful table for a given occultation, meriting a detailed

description here.

For our sample bundle, the files are
`u17b_saao_188cm_2220nm_fitted_ring_event_times.{tab,xml}`.

Keyword variables include:

- `fresnel_scale` – The average Fresnel scale $F = \sqrt{\lambda D/2}$ for the occultation, where λ is the central wavelength and D is the mean distance from observer to ring plane
- `projected_star_diameter` – Projected angular diameter of occulted star, from observer to occulting object, in km. For all square-well models in the PDS archive, a uniform disk is assumed for the star (i.e., no limb darkening is included).
- `sigma_projected_star_diameter` – Uncertainty (1-sigma) in projected_star_diameter, in km
- `fractional_error_star_counts` – Fractional error (1-sigma) in starcounts used for square-well model fit. No units – non-dimensional value.
- `time_constant_type` – Type of instrumental time constant assumed in square-well model: one of three values: 'none' - No instrumental time constant, in which case time_constant and sigma_time_constant are both zero; 'single pole' - single pole filter with impulse response given by $h(t) = (t/t_c^2)\exp(-t/t_c)$ for $t > 0, 0$ for $t < 0$, where t_c is the time constant. See Eq. 9 Elliot et al. (1984) Astron. J. 1587-1603; 'double pole' - double pole filter.
- `time_constant` – Instrumental time constant of the detector, in seconds. See Eq. 9 Elliot et al. (1984) Astron. J. 1587-1603
- `sigma_time_constant` – Uncertainty in `time_contant`, in seconds.

Column entries for each ring include:

- `Ring` – Name of the ring.
- `Direction` – Indicates whether this timing is for ingress or egress.
- `Fitted UTC(Earth)` – Fitted midtime (at the earthbased observer) of square-well model fit to the occultation ring profile, using the model described in Elliot et al. (1984).
- `sigma (Fitted midtime)` – Estimated uncertainty in Fitted UTC(Earth), obtained by adding in quadrature the formal error from the least-squares square-well fit and the estimated contributions from the uncertainties in the projected diameter at Uranus of the occulted star, in the full stellar signal at the time of the ring event, and in the instrumental time constant (if non-zero).

- `Fractional transmission` – Fractional transmission of fitted square-well model, f_0 in Elliot et al. (1984), Eq. 1.

- `sigma (Fractional transmission)` – Estimated uncertainty in Fractional transmission, obtained by adding in quadrature the formal error from the least-squares square-well fit and the estimated contributions from the uncertainties in the projected diameter at Uranus of the occulted star, in the full stellar signal at the time of the ring event, and in the instrumental time constant (if non-zero).

- `Equivalent width` – The product of the fraction of light absorbed and/or scattered by the ring and the width of the ring (E in Elliot et al. (1984), Eq. 5) from the square-well fit to the ring occultation profile.

- `sigma (Equivalent width)` – Estimated uncertainty in Equivalent width (km), obtained by adding in quadrature the formal error from the least-squares square-well fit and the estimated contributions from the uncertainties in the projected diameter at Uranus of the occulted star, in the full stellar signal at the time of the ring event, and in the instrumental time constant (if non-zero).

- `Equivalent depth` – The square-well model fit parameter A defined in Elliot et al. (1984), Eq. 6, – a measure of the abundance of ring material, independent of the viewing geometry.

- `sigma (Equivalent depth)` – Estimated uncertainty in Equivalent depth (km), obtained by adding in quadrature the formal error from the least-squares square-well fit and the estimated contributions from the uncertainties in the projected diameter at Uranus of the occulted star, in the full stellar signal at the time of the ring event, and in the instrumental time constant (if non-zero).

- `Width` – The square-well model fit parameter W defined in Elliot et al. (1984), Eq. 4, - the width of the of ring.

- `sigma (Width)` – Estimated uncertainty in Width depth (km), obtained by adding in quadrature the formal error from the least-squares square-well fit and the estimated contributions from the uncertainties in the projected diameter at Uranus of the occulted star, in the full stellar signal at the time of the ring event, and in the instrumental time constant (if non-zero).

The table includes a Quality Index QI – a subjective assessment of the quality of each observed/predicted ring occultation. Possible values are:

0 Not observable – observations at the predicted occultation event time for this ring were either not recorded (for example, the star was below the horizon) or the data were too noisy to provide useful results (for example, during sunrise). [The egress ring 6 event in Fig. 14 is an example.]

1 High-SNR profile with sharp edges matched by square-well model fit [Fig. 18 is an example].

2 Moderate-SNR profile with well-defined midtime from square-well model fit but possible systematic deviations of observed ring profile from model fit. (The α and β ring profiles in Fig. 14 are examples.)

3 Low-SNR profile with clear ring detection but less-reliable ring width and or mid-time due to noise or substantial convolution by star diameter and/or instrumental time constant.

4 Unreliable detection – some hint of a ring occultation, fitted by square-well model, but 50% chance that it is just noise.

5 No detection – High-SNR signal level but no evidence of a ring occultation. Usually applies to the λ ring, which is known to be azimuthally incomplete. (The ingress λ ring region in Fig. 14 is an example.)

Examples of ring profiles with QI= 3 and 4 are shown in Fig. 20.

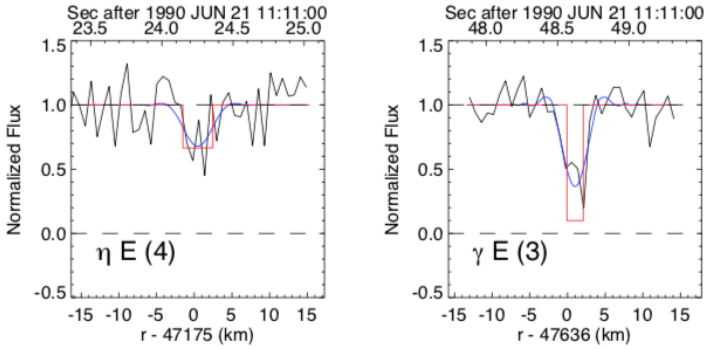

Fig. 20: Examples of ring profiles with QI of 3 (right) and 4 (left), from the 1990 June 21 occultation of U65 observed from the IRTF. The γ egress profile at right shows a clear but noisy detection, warranting a QI of 3. The η ring profile at left is marginal, and earns a QI of only 4, although its fitted midpoint is very close to the expected location based our our comprehensive ring orbit model.

In addition, the following column entries are extracted from the ring orbit fit contained in the `uranus_occ_support` bundle:

- `ringfit_UTC_corr(Earth)` – Observed ring event time (on Earth), corrected for any station offset time. For a ring event that was not observed (Quality Index= 0 or 5), the value given is the predicted value. *Note that these values may differ slightly from the* `Fitted UTC(Earth)` *values because the ring orbit fit used to compute the geometry of the latest square well model fits necessarily used earlier versions of the square-well model fits.*

- `ringfit_Radius` – The ring plane radius sampled by the occultation ray received at ringfit_UTC_corr. For a ring event that was not observed (Quality Index= 0 or 5), the value given is the predicted value.
- `ringfit_ET(RIP)` – Ephemeris time in seconds past J2000 of the moment the occultation ray penetrated the ring plane. For a ring event that was not observed (Quality Index= 0 or 5), the value given is the predicted value.
- `ringfit_Rdot` – Radial velocity of the occultation ray, measured in the ring plane in km/sec. For a ring event that was not observed (Quality Index= 0 or 5), the value given is the predicted value.
- `ringfit_Vperp_c` – Apparent velocity of star perpendicular to the edge of the ring in the sky plane, assuming a circular ring model, in km/sec.
- `ringfit_Vperp_e` – Apparent velocity of star perpendicular to the edge of the ring in the sky plane, assuming an eccentric ring model, in km/sec.
- `ringfit_Longitude` – Inertial longitude of ring intercept point in degrees. For a ring event that was not observed (Quality Index= 0 or 5), the value given is the predicted value.
- `ringfit_Anomaly` – True anomaly of the ring intercept point, given by the difference between the inertial longitude of the ring intercept point, ringfit_Longitude, and the longitude of periapse of the ring, precessed from the periapse longitude at epoch to the time at which the occultation ray penetrated the ring plane at Uranus. For a ring event that was not observed (Quality Index= 0 or 5), the value given is the predicted value.
- `ringfit_sin(B)` – Sine of the inclination of the ring plane relative to the observer. For a ring event that was not observed (Quality Index= 0 or 5), the value given is the predicted value.

2.5 The `context/` directory

The `context` directory contains two short files that are used by the PDS to cross-reference information about the observatory, telescope, and instrument used for the observations in a given observation bundle.

2.6 The `xml_schema/` directory

The `xml_schema/` directory is used by the PDS to identify the XML schema products of the archive bundle. The contents are unlikely to be of interest to the typical user.

3 The structure and contents of the uranus_occ_support bundle

The uranus_occ_support bundle contains information that applies to all occultation observation bundles. The directory structure is shown below in Fig. 21:

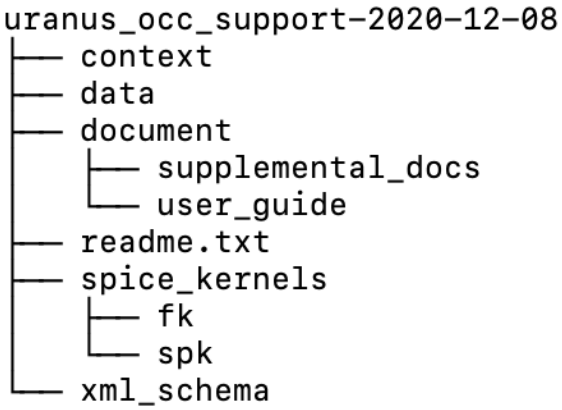

Fig. 21: Directory structure of uranus_occ_support bundle.

Briefly, the top-level directories contain:

- context/ Used internally by PDS.
- data/ Tabular data of occultation observations and individual ring events.
- document/ PDS documentation of the observation bundle.
- readme.txt A text file directing the user to this *User Guide*.
- spice_kernels/ Specialized spice kernels not available from NAIF.
- xml_schema/ Used internally by PDS.

We describe each of these directories below, following a logical sequence for the user, rather than a strictly alphabetical order.

3.1 readme.txt

The documentation for every observation bundle is consolidated into this *User Guide*, rather than residing in the document/ directory of each individual bundle. This single source of information will be updated as required, and we hope that users will benefit from the

introductory material in the guide that is applicable to every occultation bundle. The `readme.txt` file provides users with information about how to locate the current edition of this *User Guide* on the PDS.

3.2 The `document/` directory

The complete contents of this directory are listed in Fig. 22.

```
document
├── collection_document.csv
├── collection_document.xml
├── supplemental_docs
│   ├── rings-dictionary-attribute-definitions.txt
│   ├── rings-dictionary-attribute-definitions.xml
│   ├── uranus_occultations_index.tab
│   ├── uranus_occultations_index.xml
│   ├── uranus_ringocc_bundles_quality_rating.csv
│   └── uranus_ringocc_bundles_quality_rating.xml
└── user_guide
    ├── UranusPoleExample1.py
    ├── UranusPoleExample2.py
    ├── create_uranus_ringframes_french_et_al_1988_v1.pro
    ├── earth_based_uranus_stellar_occultation_user_guide.pdf
    ├── earth_based_uranus_stellar_occultation_user_guide.xml
    ├── occgeom_example1.pro
    ├── occgeom_example1.py
    ├── occgeom_example2.pro
    ├── occgeom_example2.py
    ├── plot_epsilon_ring_example.pro
    ├── plot_epsilon_ring_example.py
    ├── plot_epsilon_ring_example_IDL.pdf
    ├── plot_epsilon_ring_example_python.pdf
    ├── ring_longitude_example.pro
    └── ring_longitude_example.py
```

Fig. 22: Contents of the `document/` directory of the `uranus_occ_support` bundle.

The `document/` directory contains two brief files (`collection_document.{csv,xml}`) used by the PDS to describe the directory contents, and two subdirectories: `supplemental_docs/` and `user_guide/`.

3.2.1 The `document/supplemental_docs/` directory

This directory contains `rings-dictionary-attribute-definitions.tab`, a text file (and its associated `*.xml` file) of `rings` namespace attribute definitions, including all attributes in any of the label files prefaced with `rings:`. The files `uranus_occultations_index.{tab,xml}` contain metadata for PDS internal use. The table supports all of the Uranus Earth-based

occultation data bundles. Each row in the table supports a single radial profile and contains values for all of the key attributes used in the individual labels. Finally, this directory contains `uranus_ringocc_bundles_quality_rating.csv` and its associated `*.xml` label file, described in Section 4; the table contents are displayed in Table 9.

3.2.2 The `document/user_guide/` directory.

This contains this *User Guide* (`earth_based_uranus_stellar_occultation_user_guide.pdf`) and its associated `*.xml` label file, and a collection of example computer codes in IDL (`*.pro`) and Python (`*.py`) and resulting figures (`*.pdf`) that illustrate the use of specialized spice kernels (see Section 3.4) useful for computing Uranus ring geometry. These codes are described in detail in Appendix B.

3.3 The `data/` directory

The `data/` directory contains details of the ring orbit fit used to determine the orbital elements of the Uranian rings and the direction of the planet's pole from a comprehensive set of ring occultation observations. The directory structure and contents are shown in Fig. 23.

```
data
├── collection_data.csv
├── collection_data.xml
├── uranus_occultation_ring_fit_rfrench_20201201.tab
├── uranus_occultation_ring_fit_rfrench_20201201.txt
├── uranus_occultation_ring_fit_rfrench_20201201.xml
├── uranus_occultation_ring_fit_rfrench_input_data_20201201.tab
├── uranus_occultation_ring_fit_rfrench_input_events_20201201.tab
├── uranus_occultation_ring_fit_rfrench_input_observatories_20201201.tab
└── uranus_occultation_ring_fit_rfrench_input_stars_20201201.csv
```

Fig. 23: Contents of the `data/`directory of the `uranus_occ_support` bundle.

The `collection_data.{csv,xml}` files contain information used by the PDS system and are unlikely to be of interest to the typical user. The other files in the directory provide detailed information about the results the ring orbit fit or fits used to determine the geometry for all of the observation observation bundles in the Uranus ring occultation archive, as described below.

3.3.1 Ring orbit fit `rfrench_20201201` results

This section documents a ring orbit fit used to define the geometry of the Uranus ring and planet system underlying the results in the Uranus ring occultation observation bundles. The

fit was performed on 2020 Dec 1 and solved for the Uranus pole direction and the orbital elements of the rings, using the best occultation data available at the time. The planet pole direction is consistent with that of Jacobson 2014, who used a subset of the ring data (no γ or δ ring observations, and no Earthbased observations past July 11, 1992) included in our fit. (Updated versions of this fit may be provided from time to time, in which case they will be included in this `data/` directory as well.) The underlying algorithm for the fit is based on the well-tested IDL-based RINGFIT code used for determining the orbits of Saturn's rings (see Appendix A of French et al. 1993 and French et al. 2017 for details).

For reference, key inputs and outputs of the ring orbit fit are tabulated here. Table 2 contains the Uranus gravity parameters (used to calculate selected ring apsidal precession and nodal regression rates) and the planet's pole direction, Table 3 contains the coordinates of the occultation stars, Table 4 contains the geocentric coordinates of the groundbased telescopes used for the observations, Table 5 contains the time offsets applied to selected observations, Table 6 lists the SPICE kernels used for the fit, and Tables 7 and 8 contain the fitted ring orbital elements and ring normal modes, respectively. The individual ring semimajor axes agree with those of Jacobson 2014 to better than 0.5 km. All uncertainties are formal errors from the least squares fit, and do not take into account any systematic errors in the Voyager 2 trajectory, for example.

Take particular note of the epoch adopted for the orbital elements: UTC 1987 Jan 1 12:00:00. All previous published orbit fits use UTC 1977 Mar 10 20:00 UTC, but for a data set extending over decades, the correlations between angular rates and angles at epoch are greatly reduced by choosing an epoch approximately centered on the span of data being fitted.

Table 2: Uranus Gravity Parameters and Pole

Parameter	Value
$GM_{\rm Uranus}$ (km^3 s^{-2})	5793951.322
J_2[a]	3.510651×10^{-3}
J_4	-3.426361×10^{-5}
J_6	2.575121×10^{-7}
J_8	-2.876352×10^{-9}
J_{10}	3.495265×10^{-11}
J_{12}	$-4.499047 \times 10^{-13}$
J_{14}	6.038845×10^{-15}
α (deg)	77.311143 ± 0.000295
δ (deg)	15.172188 ± 0.000637

[a] The reference radius for the Uranus zonal harmonics is 25559 km.

I

The ring orbital elements derived from the fit are stored in a pair of PDS-readable table and label files: `uranus_occultation_ring_fit_rfrench_20201201.{tab,xml}`. Below, we extract descriptions and column definitions from the `*.xml` file (see the file itself for the complete contents of lines that have run off the page here).

```
This file contains the Uranus ring orbit model uranus_occultation_ring_fit_rfrench_20201201, based on
```

Table 3: Star Catalog Positions and Corrections

Star[a]	Catalog	Catalog RA (deg)	Catalog Dec (deg)	$\Delta\alpha \cos\delta$ (mas)	$\Delta\delta$ (mas)
U0	Hipparcos	219.54921290	−14.95473933	7.2894 ± 0.0143	-5.9489 ± 0.0276
U2	UCAC3	222.88056650	−16.03505700	-71.4800 ± 0.0594	70.6332 ± 1.5346
U5	UCAC2	223.35270950	−16.15356590	580.9142 ± 0.0171	-762.4547 ± 0.0198
U9	UCAC2	225.69257180	−16.88735590	-231.5229 ± 0.0308	-21.4399 ± 0.1328
U11	UCAC2	233.40997800	−18.90128950	-294.0489 ± 0.0271	27.1466 ± 0.0155
U12	UCAC2	229.54172530	−17.99479950	-197.0254 ± 0.0148	125.5688 ± 0.0469
U13	Hipparcos	237.10643560	−19.77402446	-3.1582 ± 0.0106	22.4703 ± 0.0319
U14	Hipparcos	242.14934740	−20.80743248	8.8145 ± 0.0081	-21.8549 ± 0.0232
U15	UCAC2	241.79331860	−20.74504340	120.3940 ± 0.0101	23.8196 ± 0.0301
U16	UCAC2	240.36678420	−20.48854530	1.5822 ± 0.0106	97.2459 ± 0.0236
U17	Hipparcos	247.63035990	−21.74199001	-35.8883 ± 0.0132	4.2931 ± 0.0216
U23	UCAC2	256.37848620	−22.87389030	97.8938 ± 0.0093	33.5835 ± 0.0125
U25	UCAC2	255.59000530	−22.80714590	64.0478 ± 0.0072	-291.8040 ± 0.0111
U28	UCAC2	261.49121500	−23.29306250	105.2868 ± 0.0105	3.5187 ± 0.0192
U34	UCAC2	266.09631680	−23.51762450	193.4087 ± 0.0157	236.1736 ± 0.1946
U36	UCAC4	266.62468120	−23.53889700	17.7831 ± 0.0108	75.4239 ± 0.0200
U1052	UCAC2	270.68744680	−23.64381530	-212.8897 ± 0.0311	-50.5611 ± 0.0132
U65	UCAC3	278.78923770	−23.52082560	12.5645 ± 0.0143	25.7170 ± 0.0178
U83	UCAC2	283.39508950	−23.25030480	-46.3858 ± 0.0147	15.9926 ± 0.0170
U84	UCAC2	283.26958000	−23.26173840	29.7982 ± 0.0220	-10.4845 ± 0.0115
U102A	UCAC2	287.52555270	−22.89765390	3.8207 ± 0.0134	33.8940 ± 0.0762
U102B	UCAC2	287.52555270	−22.89765390	-17.5753 ± 0.0000	55.0272 ± 0.0000
U103	UCAC2	287.39833590	−22.91141370	-6.6893 ± 0.0294	13.1822 ± 0.0110
U9539	UCAC2	292.54515500	−22.30772340	51.4787 ± 0.0099	68.8412 ± 0.0604
U134	UCAC2	299.02695120	−21.33800060	-13.5846 ± 0.0823	-28.4806 ± 0.2969
U137	UCAC3	305.94609740	−19.90650640	29.1605 ± 0.0200	49.4624 ± 0.1496
U138	UCAC2	306.77794560	−19.73023280	45.9821 ± 0.0190	0.2196 ± 0.0842
U144	UCAC2	307.35052090	−19.67061560	10.6506 ± 0.0528	-9.6759 ± 0.0969
U149	2MASS	311.58517900	−18.64293300	27.5223 ± 0.0152	-45.0370 ± 0.0584
U0201	UCAC2	330.11430530	−13.01352140	106.2185 ± 0.0334	52.9101 ± 0.0183
σ Sgr	Hipparcos	283.81631960	−26.29659428	0.0000	0.0000
β Per	Hipparcos	47.04220716	40.95565120	0.0000	0.0000

```
a non-linear least squares fit to ring occultation data. The algorithm for the non-linear
least squares fit to earthbased and spacecraft stellar occultations, and
radio science occultations, is documented in the following publication:
French, R. G. et al. (1993) "Geometry of the Saturn System from the 3 July 1989
Occultation of 28 Sgr and Voyager Observations" Icarus 103, 163-214.
The calculations generally follow the solar system barycenter vector approach described in
Appendix A.1.1. See also Appendix B for details of the calculations,
including a sample barycentric calculation for Saturn.

Note that the ring orbit model presented here differs from the French et al. (1993)
in several respects, as discussed in French, R. G. et al. (2010)
"Occultation Observations of Saturn's B Ring and Cassini Division", Astron. J.
 139:1649-1667 - see pp. 1650-1651 for details.

Keywords for *.xml file:
OrbitFit_ID                    = ringfit_v1.8.Ur017L-RF-V0204        / Orbit fit run ID
OrbitFit_YYYYMMDD              = 20201201                            / Date of orbit fit (YYYYMMDD)
GM_799                         =  5.7939513220000E+06                / GM of Uranus  km^3/s^2
J2                             =  3.5105610352900E-03                / Uranus gravitational harmonic coefficient 2
J4                             = -3.4263605093516E-05                / Uranus gravitational harmonic coefficient 4
J6                             =  2.5751209427419E-07                / Uranus gravitational harmonic coefficient 6
REFERENCE_RADIUS               =  2.5559000000000E+04                / Reference radius (km) for gravitational harmonic coeffic
EPOCH (UTC)                    = UTC Jan 01, 1987 12:00:00           / Epoch for the ring orbital elements
REFERENCE_FRAME                = J2000                               / Equinoctial reference frame for the ring orbital element
GM_701                         =  8.3500000000000E+01                / GM of Ariel km^3/s^2
GM_702                         =  8.5100000000000E+01                / GM of Umbriel km^3/s^2
```

Table 4: Geocentric Telescope Coordinates

Observatory	Tel.	Lat. (deg)	E. Lon. (deg)	X (km)	Y (km)	Z (km)	ρ (km)
Centro Astronomico Hispano-Aleman	123cm	37.038463	−2.546111	5081.718	−225.970	3838.490	6372.514
Cerro Tololo Inter-American Observatory	400cm	−30.002270	−70.805889	1815.109	−5214.008	−3187.793	6375.149
European Southern Observatory	360cm	−29.097215	−70.731694	1838.338	−5258.792	−3100.341	6375.460
IRTF	320cm	19.703718	−155.472200	−5464.341	−2493.446	2151.026	6379.907
Las Campanas Observatory	250cm	−28.840706	−70.702000	1845.617	−5270.846	−3075.346	6375.411
Lowell Observatory	180cm	34.915174	−111.535500	−1918.391	−4861.284	3647.848	6373.311
McDonald Observatory	270cm	30.502947	−104.021500	−1330.748	−5328.820	3235.692	6374.709
Mount Stromlo Observatory	190cm	−35.139179	149.007700	−4466.678	2683.034	−3667.365	6371.770
Observatoire du Pic du Midi et de Toulouse	200cm	42.744765	0.142300	4678.859	11.620	4324.313	6371.149
Observatorio del Teide	155cm	28.131963	−16.495833	5391.117	−1596.495	3006.188	6375.744
Palomar Observatory	508cm	33.177651	−116.862539	−2410.357	−4758.781	3487.762	6373.406
Siding Spring Observatory	390cm	−31.106585	149.066081	−4680.887	2805.218	−3292.789	6373.572
South African Astronomical Observatory	188cm	−32.205774	20.810700	5041.279	1916.080	−3396.995	6373.808
United Kingdom Infrared Telescope	320cm	19.706260	−155.476000	−5464.404	−2493.037	2151.286	6379.888

Table 5: Observatory Time Offsets

Event	Station	Offset (s)
U12	ESO	-0.0774 ± 0.0203
U12	Las Campanas	0.1307 ± 0.0288
U12	IRTF	0.0695 ± 0.0241
U14	ESO (1m)	-0.1020 ± 0.0085
U14	Las Campanas	0.0571 ± 0.0079
U14	Pic du Midi (1m)	3.6891 ± 0.0105
U14	Teide (ingress)	0.7331 ± 0.0140
U14	Teide (egress)	-0.0511 ± 0.0121
U14	ESO (2m)	0.3856 ± 0.0125
U36A	IRTF	9.4065 ± 0.4152
U36A	CTIO	-8.7463 ± 0.3307
u103	SAAO (egress)	0.0928 ± 0.0157
u103	CTIO	-0.0550 ± 0.0243
u134	HST	0.6921 ± 0.2401
u137	CAHA (ingress)	0.6358 ± 0.0098
u144	CAHA (egress)	0.4934 ± 0.0880
u144	DSS-43	0.5971 ± 0.3172
Vgr2 RSS	PPS	-0.0114 ± 0.0136
Vgr2 σ Sgr	Las Campanas (vis)	0.4142 ± 0.3072
Vgr2 β Per	Las Campanas (vis)	-0.0778 ± 0.0204

```
GM_703                          =  2.2690000000000E+02          / GM of Titania km^3/s^2
GM_704                          =  2.0530000000000E+02          / GM of Oberon km^3/s^2
GM_705                          =  4.3000000000000E+00          / GM of Miranda km^3/s^2
a_701                           =  1.9090000000000E+05          / semimajor axis of Ariel km
a_702                           =  2.6600000000000E+05          / semimajor axis of Umbriel km
a_703                           =  4.3630000000000E+05          / semimajor axis of Titania km
a_704                           =  5.8350000000000E+05          / semimajor axis of Oberon km
a_705                           =  1.2990000000000E+05          / semimajor axis of Miranda km
RA(pole)                        =  7.7311142789503E+01          / Right Ascension of Uranus Pole (J2000) - degrees
RA(pole) uncertainty            =  2.9482579245595E-04          / Uncertainty in Right Ascension of Uranus Pole (J2000) -
Dec(pole)                       =  1.5172187676545E+01          / Right Ascension of Uranus Pole (J2000) - degrees
Dec(pole) uncertainty           =  6.3677126332641E-04          / Uncertainty in Declination of Uranus Pole (J2000) - degr

Column header definitions for *.xml file:
 1 Ring name                                / Uranus ring name
 2 Semimajor axis                           / Semimajor axis in km
 3 Semimajor axis uncertainty               / Uncertainty in semimajor axis (km)
 4 Eccentricity                             / Eccentricity
 5 Eccentricity uncertainty                 / Uncertainty in eccentricity (-9.99d99 if eccentricity is a fixed value)
 6 Periapse longitude                       / Longitude of periapse at epoch, measured from the ascending node of the ring plar
 7 Periapse uncertainty                     / Uncertainty in periapse longitude in degrees (-9.99d99 if periapse longitude is a
 8 Periapse precession rate                 / Periapse precession rate (deg/day)
 9 Periapse precession rate uncertainty     / Uncertainty in periapse precession rate (-9.99d99 if periapse precession rate is
```

Table 6: Spice Kernels

kernel
vgr2.ura111.bsp
earthstns_itrf93_040916.bsp
earth_720101_031229.bpc
pg3f0000r.bsp
pg490000r.bsp
urkao_v1.bsp
naif0012.tls

```
10 Periapse precession rate method          / 0:fitted value 1:computed from Jn 2: computed from Jn, and five major Uranian sat
11 Inclination                              / Inclination (degrees)
12 Inclination uncertainty                  / Uncertainty in inclination in degrees (-9.99d99 if inclination is a fixed value)
13 Node longitude                           / Longitude of node at epoch, measured from the ascending node of the ring plane or
14 Node uncertainty                         / Uncertainty in node longitude in degrees (-9.99d99 if node longitude is a fixed v
15 Nodal regression rate                    / Nodal regression rate (deg/day)
16 Nodal regression rate uncertainty        / Uncertainty in nodal regression rate (-9.99d99 if nodal regression rate is a fixe
17 Nodal regression rate method             / 0:fitted value 1:computed from Jn 2: computed from Jn, and five major Uranian sat
18 Wavenumber                               / Wavenumber of normal mode (multiple modes possible per ring, -999 if no normal mo
19 Normal mode amplitude                    / Amplitude in km of normal mode (-9.99d99 if no normal mode for this ring)
20 Normal mode amplitude uncertainty        / Uncertainty in amplitude in km of normal mode (-9.99d99 if no normal mode for thi
21 Normal mode phase                        / Phase in degrees of normal mode at epoch (-9.99d99 if no normal mode for this rin
22 Normal mode phase uncertainty            / Uncertainty in degrees of normal mode phase (-9.99d99 if no normal mode for this
23 Normal mode pattern speed                / Pattern speed in degrees/day of normal mode (-9.99d99 if no normal mode for this
24 Normal mode pattern speed uncertainty    / Uncertainty in pattern speed in degrees/day of normal mode phase (-9.99d99 if no
25 Npts                                     / Number of fitted data points for this ring
26 RMS                                      / RMS residuals for this ring (km)
```

Although perhaps of less interest to the typical investigator, for users who would like to delve into in the details of the fit or who wish to write their own fitting codes and compare results with this fit, we provide an annotated version of the output file from the RINGFIT run (file `uranus_occultation_ring_fit_rfrench_20201201.txt`), described in more detail in Appendix A.

3.3.2 Input files for ring orbit fit `rfrench_20201201`

In addition to the files describe above, the `data/` directory contains a complete set of fitted ring event times for every ring occultation used in the orbit fit, as well as other auxiliary information. The contents of these machine-readable files are described in detail in `uranus_occultation_ring_fit_rfrench_20201201.xml`. The filenames and brief description are listed below:

- `uranus_occultation_ring_fit_rfrench_input_data_20201201.tab`: A table of individual ring occultation event times.

Table 7: Uranus Ring Orbital Elements

Element[a]	6	5	4	α
a (km)	41837.319 ± 0.123	42235.094 ± 0.118	42571.302 ± 0.117	44718.670 ± 0.112
$e(\times 1000)$	1.0169 ± 0.0026	1.9006 ± 0.0024	1.0643 ± 0.0024	0.7596 ± 0.0019
ae (km)	42.546 ± 0.109	80.273 ± 0.102	45.307 ± 0.103	33.968 ± 0.084
ϖ (deg)	60.016 ± 0.159	23.831 ± 0.066	77.332 ± 0.121	244.575 ± 0.140
i (deg)	0.06069 ± 0.00036	0.05581 ± 0.00029	0.03225 ± 0.00029	0.01503 ± 0.00026
$a \sin i$ (km)	44.318 ± 0.262	41.138 ± 0.217	23.959 ± 0.215	11.731 ± 0.200
$a \sin i$ (km)	212.786 ± 0.344	90.628 ± 0.323	156.502 ± 0.826	166.938 ± 1.183
$\dot{\varpi}$ (deg d^{-1})	2.76196 ± 0.00008	2.67159 ± 0.00003	2.59795 ± 0.00007	2.18544 ± 0.00007
$\dot{\Omega}$ (deg d^{-1})	-2.75640 ± 0.00014	-2.66632 ± 0.00012	-2.59310 ± 0.00030	-2.18104 ± 0.00038
$\dot{\varpi}$ (deg yr^{-1})	1008.8045 ± 0.0281	975.7973 ± 0.0122	948.9006 ± 0.0245	798.2332 ± 0.0258
$\dot{\Omega}$ (deg yr^{-1})	-1006.7756 ± 0.0511	-973.8727 ± 0.0453	-947.1306 ± 0.1103	-796.6267 ± 0.1403
N	48	65	63	81
rms (km)	0.302	0.247	0.296	0.295
Element[a]	β	η	γ	δ
a (km)	45661.249 ± 0.111	47176.230 ± 0.112	47626.488 ± 0.115	48300.447 ± 0.106
$e(\times 1000)$	0.4412 ± 0.0019	0.0034 ± 0.0021	0.1119 ± 0.0019	0.0060 ± 0.0020
ae (km)	20.148 ± 0.089	0.158 ± 0.098	5.331 ± 0.090	0.288 ± 0.095
ϖ (deg)	302.744 ± 0.275	340.231 ± 32.424	295.827 ± 0.992	125.882 ± 15.125
i (deg)	0.00464 ± 0.00018	0.00060 ± 0.00027	0.00030 ± 0.00026	0.00045 ± 0.00024
$a \sin i$ (km)	3.701 ± 0.146	0.498 ± 0.219	0.253 ± 0.218	0.375 ± 0.203
$a \sin i$ (km)	245.876 ± 5.629	4.006 ± 26.253	114.553 ± 47.759	116.400 ± 31.860
$\dot{\varpi}$ (deg d^{-1})	2.03088 ± 0.00012	1.81073	1.75342 ± 0.00052	1.71066 ± 0.00697
$\dot{\Omega}$ (deg d^{-1})	-2.02881 ± 0.00136	-1.80792	-1.74864	-1.64306 ± 0.00921
$\dot{\varpi}$ (deg yr^{-1})	741.7799 ± 0.0425	661.3701	640.4363 ± 0.1885	624.8203 ± 2.5450
$\dot{\Omega}$ (deg yr^{-1})	-741.0213 ± 0.4967	-660.3431	-638.6898	-600.1283 ± 3.3646
N	79	64	86	86
rms (km)	0.297	0.377	0.476	0.431
Element	λ	ϵ		
a (km)	50026.009	51149.465 ± 0.100		
$e(\times 1000)$	0.0000	7.9345 ± 0.0015		
ae (km)	0.000	405.844 ± 0.077		
ϖ (deg)	0.000	60.132 ± 0.011		
i (deg)	0.00000	0.00019 ± 0.00019		
$a \sin i$ (km)	0.000	0.169 ± 0.172		
Ω (deg)	0.000	298.506 ± 56.900		
$\dot{\varpi}$ (deg d^{-1})	1.47363	1.36327 ± 0.00001		
$\dot{\Omega}$ (deg d^{-1})	-1.47160	-1.36147		
$\dot{\varpi}$ (deg yr^{-1})	538.2443	497.9327 ± 0.0022		
$\dot{\Omega}$ (deg yr^{-1})	-537.5015	-497.2759		
N	14	90		
rms (km)	3.159	0.559		

[a] The epoch for the longitudes is 1987 Jan 1 12:00:00 (UTC).
[b] For reference, the fit ID is ringfit_v1.8.Ur017L-RF-V0201.

- `uranus_occultation_ring_fit_rfrench_input_events_20201201.tab`: A table of occultations (similar to occultation bundles) used for the Uranus ring orbit fit.
- `uranus_occultation_ring_fit_rfrench_input_observatories_20201201.tab`: A table of observatories and topocentric coordinates used for the Uranus ring orbit fit.
- `uranus_occultation_ring_fit_rfrench_input_stars_20201201.tab`: A table of star names and coordinates used for the Uranus ring orbit fit.

3.4 The `spice_kernels/` directory

NASA's Navigation and Ancillary Information Facility (NAIF) provides the "SPICE" observation geometry information system to assist scientists in planning and interpreting scientific observations from space-based instruments.

The `spice_kernels/` directory contains spice kernels used for this archive that are not publicly available on the JPL NAIF website. The directory structure and contents are shown below in Figure 24.

Table 8: Uranus Ring Normal Modes

Ring	m	ae (km)	ϕ (deg)[a]	Ω_m (deg d^{-1})
η	3	0.661 ± 0.091	26.487 ± 2.606	776.58268 ± 0.00149
γ	-2	0.629 ± 0.096	214.127 ± 3.918	1720.12500 ± 0.00176
γ	-1	1.653 ± 0.085	63.864 ± 3.018	2292.90577 ± 0.00155
γ	0	5.428 ± 0.093	26.385 ± 0.894	1145.57616 ± 0.00046
γ	6	0.725 ± 0.080	47.243 ± 1.214	956.41900 ± 0.00056
δ	2	3.162 ± 0.092	245.523 ± 0.765	562.51595 ± 0.00035

[a] The epoch for the longitude is 1987 Jan 1 12:00 (UTC)

```
spice_kernels/
├── collection_spice_kernels.csv
├── collection_spice_kernels.xml
├── fk
│   ├── uranus_ringframes_french_et_al_1988_v1.tf
│   ├── uranus_ringframes_french_et_al_1988_v1.xml
│   ├── uranus_ringframes_rfrench20201201_v1.tf
│   └── uranus_ringframes_rfrench20201201_v1.xml
└── spk
    ├── urkao_v1.bsp
    └── urkao_v1.xml
```

Fig. 24: Directory structure of the `spice_kernels/` directory of the `uranus_occ_support` bundle.

The `spice_kernels/` directory contains two brief files (`collection_spice_kernels.{csv,xml}`) that are used by PDS to cross-reference the contents of the directory, and two subdirectories, described below.

3.4.1 The `spice_kernels/fk/` directory

The `spice_kernels/fk/` directory contains two *frame kernels*[4] and their associated `*.xml` label files that enable users to compute the orientation of the Uranus equator and the ten classical Uranian rings at any given time, based on two Uranus ring orbit models:

- `uranus_ringframes_french_et_al_1988_v1.tf` – frame kernel containing the Uranus ring geometry from an early French et al. (1988) model, originally in the B1950 reference frame, but easily converted to J2000 using the SPICE toolkit.
- `uranus_ringframes_rfrench20201201_v1.tf` – frame kernel containing the Uranus ring orbit fit used for this archive described in Section 3.3.1.

Examples illustrating the use of these frame kernels are included in the `document/` directory (Section 3.2) and described in detail in Appendix B.

[4] Visit `https://naif.jpl.nasa.gov/pub/naif/toolkit_docs/Tutorials/pdf/individual_docs/` for more information about SPICE reference frames.

3.4.2 The `spice_kernels/spk/` directory

The `spice_kernels/spk/` directory contains any specialized SP-Kernel files[5] used for the ring orbit fit in Section 3.3.1 that are not available from NAIF. Currently, there is just one such kernel (with its accompanying label file):

- `urkao_v1.{bsp,xml}` – the flight path of the Kuiper Airborne Observatory during the discovery observations of the Uranian rings on March 20, 1977 (Elliot et al., 1977). Details concerning this kernel are provided in Appendix C.

3.5 The `context/` directory

The `context` directory contains two short files that are used by the PDS to cross-reference information contained in the support bundle. They are unlikely to be of interest to the typical user.

3.6 The `xml_schema/` directory

The `xml_schema/` directory is used by the PDS to identify the XML schema products of the archive bundle. The contents are unlikely to be of interest to the typical user.

4 Summary information about observation bundles

This section includes key summary information about the observation bundles in the Uranus ring occultation archive. Table 9 (provided as part of the support bundle in the `document/` folder in the file `uranus_ringocc_bundles_quality_rating.csv`) provides a convenient summary of the entire set of ring occultation bundles, identifying which rings were detected in each observation, the quality index QI for each observed or predicted ring event (defined in Section 2.4.4.3), and the average value for the occultation of the smoothing effects of the Fresnel scale $F = \sqrt{\lambda D/2}$, the projected star size $d*$, and the instrumental time constant τ_c (expressed in km as $\tau_c/v_\perp$, where $v_\perp$ is the velocity of the occultation perpendicular to the ring edge projected in the sky plane). These quantities are useful for assessing the magnitude of possible systematic errors in the fitted ring widths. In particular, for observation bundles for which the smoothing scales are several km or more, the square-well-fitted ring widths for narrow rings such as rings 6, 5, 4, and η might well be systematically high. Finally, the table includes a summary ranking for each observation bundle as a whole, determined from

[5] An SP-Kernel is the ephemeris (a.k.a. trajectory) of a solar system body, a space vehicle, or any other physical object.

the rounded average value of the QIs for the rings for which data were recorded, excluding the λ ring. The event is ranked as Good (G) if the rounded average is 1 or 2, Fair (F) if the result is 3, and Poor (P) if the result is 4.

Table 9: Occultation Bundle Quality Indices and Rank

	F	$d*$	$\tau_c/v_{\perp c}$	QI(ingress)										QI(egress)								
Bundle ID	km	km	km	6	5	4	α	β	η	γ	δ	λ	ϵ	6	5	4	α	β	η	γ	δ	λ	ϵ	Rank
u0_kao_91cm	0.99	7.50	0.00	3	3	3	2	2	4	2	2	5	2	3	3	4	2	2	4	2	2	5	2	F
u2_teide_155cm	1.13	3.37	0.00	0	0	0	0	0	0	3	3	0	3	0	0	0	0	0	0	0	0	0	0	F
u5_lco_250cm	1.71	0.60	1.49	3	3	3	3	3	3	3	3	0	3	0	3	3	3	3	3	3	3	0	3	F
u9_lco_250cm	1.71	0.40	1.83	0	0	0	3	3	3	3	3	0	3	0	0	4	3	3	0	3	3	0	3	F
u11_ctio_400cm	1.73	0.75	0.05	0	0	0	3	3	5	5	4	5	2	0	0	0	3	3	5	2	2	4	2	F
u12_ctio_400cm	1.76	1.60	0.42	5	3	5	5	5	3	3	5	5	1	2	2	2	2	2	2	2	2	5	1	F
u12_eso_360cm	1.76	1.60	0.40	2	2	2	2	2	2	2	2	5	5	2	2	2	2	2	2	2	2	5	1	G
u12_lco_250cm	1.76	1.60	0.00	4	3	4	3	3	3	3	3	0	3	1	1	1	1	1	1	1	1	5	1	G
u13_sso_390cm	1.72	2.35	0.00	3	3	3	2	2	3	3	3	5	2	3	3	3	2	2	3	3	3	5	2	F
u14_ctio_150cm	1.72	4.75	2.56	4	3	3	2	2	5	2	2	5	2	3	3	3	2	2	5	2	2	5	2	F
u14_ctio_400cm	1.09	4.75	0.00	3	3	3	2	2	4	2	2	5	2	4	3	3	2	2	3	2	2	5	1	F
u14_eso_104cm	1.72	4.75	0.50	5	3	3	2	5	5	2	2	5	2	3	3	3	2	2	4	1	1	5	1	F
u14_lco_100cm	1.09	4.75	0.00	5	5	5	3	2	5	3	3	5	2	5	5	5	2	3	5	2	2	5	2	P
u14_lco_250cm	1.72	4.75	0.67	5	3	3	2	2	5	2	2	5	2	3	3	3	2	2	3	2	2	5	2	F
u14_opmt_200cm	1.72	4.75	0.00	5	3	3	2	2	5	2	3	5	2	5	5	5	3	5	5	3	3	5	2	P
u14_opmt_106cm	1.09	4.75	0.00	5	4	3	3	3	3	5	5	5	2	0	0	0	0	0	0	0	0	0	0	P
u14_teide_155cm	1.09	4.75	0.00	5	3	3	2	2	4	2	2	5	2	4	4	4	3	3	5	3	3	5	2	F
u15_mso_190cm	1.72	3.10	0.93	3	2	2	2	2	2	2	2	5	2	2	2	2	2	2	2	2	2	5	2	G
u16_palomar_508cm	1.72	1.20	0.00	1	1	1	2	2	1	1	2	5	2	1	1	1	1	1	1	3	2	5	1	G
u17b_saao_188cm	1.75	1.05	0.00	1	1	1	1	1	1	1	1	5	1	5	1	1	1	2	5	5	5	5	5	G
u23_ctio_400cm	1.73	1.50	0.40	1	1	1	1	1	1	1	1	5	1	1	1	1	1	1	1	1	1	4	1	G
u23_mcdonald_270cm	1.73	1.50	0.57	0	0	0	0	0	0	0	0	0	0	4	2	2	2	2	3	2	2	2	3	G
u23_teide_155cm	1.73	1.50	0.07	5	5	5	4	5	5	3	4	5	3	0	0	0	0	0	0	0	0	0	0	P
u25_ctio_400cm	1.73	3.70	0.00	1	1	1	1	1	1	1	1	5	1	1	1	1	1	1	1	1	1	5	1	G
u25_mcdonald_270cm	1.73	3.70	0.00	1	1	1	1	1	1	1	1	5	1	1	1	1	1	1	1	1	1	5	1	G
u25_palomar_508cm	1.73	3.70	0.00	1	1	1	1	1	1	1	1	5	1	1	1	1	1	1	1	1	1	5	1	G
u28_irtf_320cm	1.74	1.50	0.58	1	1	1	1	1	1	1	1	4	5	1	1	2	1	1	1	1	1	5	1	G
u34_irtf_320cm	1.79	0.50	0.00	3	2	3	4	4	4	4	3	5	3	3	2	2	2	2	3	2	2	5	1	F
u36_ctio_400cm	1.76	0.65	0.00	0	0	0	0	0	0	0	0	0	0	1	1	1	1	2	4	3	3	5	3	G
u36_irtf_320cm	1.77	0.65	0.00	0	0	0	5	2	1	1	1	5	2	0	0	0	0	0	3	1	2	5	2	G
u36_sso_230cm	1.76	0.65	0.00	0	0	0	0	0	0	0	0	0	0	0	0	0	0	0	0	0	3	5	3	F
u36_sso_390cm	1.76	0.65	0.00	0	0	0	0	0	0	0	0	0	0	0	0	0	0	0	2	1	2	5	2	G
u36_maunakea_380cm	1.77	0.65	0.00	0	0	0	5	3	1	4	1	0	0	0	0	0	0	0	5	1	2	5	3	F
u1052_irtf_320cm	1.74	0.87	0.00	0	0	0	0	1	1	1	1	5	1	0	0	0	0	1	1	1	1	5	1	G
u65_irtf_320cm	1.74	3.00	0.00	5	3	3	3	5	3	3	2	5	3	5	2	3	2	2	4	3	2	5	1	F
u83_irtf_320cm	1.74	1.15	0.00	1	1	1	1	1	1	1	2	5	1	1	1	1	1	1	1	1	1	5	1	G
u84_irtf_320cm	1.74	0.90	0.00	1	1	1	1	1	1	1	1	5	1	1	1	1	1	1	1	1	1	5	1	G
u102a_irtf_320cm	1.75	0.55	2.85	5	4	4	3	5	5	5	5	5	5	3	3	5	3	3	5	5	3	5	3	P
u102b_irtf_320cm	1.75	0.45	2.85	5	5	3	3	3	5	5	5	5	5	5	5	5	3	3	5	5	5	5	3	P
u103_eso_220cm	1.75	0.86	0.58	2	2	3	2	2	4	2	2	3	1	5	3	3	3	3	5	5	3	5	2	F
u103_palomar_508cm	1.75	0.86	0.07	0	0	0	1	1	1	1	1	5	1	0	0	0	1	2	2	1	1	5	1	G
u9539_ctio_400cm	1.75	0.30	0.00	3	2	2	2	2	3	2	2	5	1	4	2	2	2	3	2	2	2	5	1	G
u134_saao_188cm	1.78	1.75	0.00	1	1	1	1	1	1	1	1	5	1	1	1	1	1	1	1	1	1	4	1	G
u137_hst_fos	0.91	2.50	0.00	0	0	0	0	0	0	0	0	0	0	5	5	5	3	3	5	4	3	5	3	P
u137_irtf_320cm	1.83	2.50	0.73	1	1	1	1	1	1	1	2	5	1	1	1	1	1	1	2	1	1	5	1	G
u138_hst_fos	0.90	2.50	0.00	0	0	0	0	0	0	0	0	0	1	1	1	1	2	1	1	1	2	3	0	G
u138_palomar_508cm	1.81	2.50	0.20	0	0	0	0	0	0	0	0	0	0	1	1	1	1	1	1	1	1	5	1	G
u144_caha_123cm	1.78	1.50	0.00	0	0	0	3	3	5	3	3	5	2	0	0	0	3	3	5	3	3	5	3	F
u144_saao_188cm	1.79	1.50	0.00	5	5	5	3	3	5	3	3	5	3	0	0	0	0	0	0	0	0	0	0	P
u149_lowell_180cm	1.15	1.20	0.00	5	5	5	3	4	5	3	3	5	2	5	5	5	5	5	5	5	5	5	3	P
u149_irtf_320cm	1.81	1.20	0.00	0	0	0	0	0	0	0	0	0	0	6	3	3	3	3	3	3	3	5	5	P
u0201_palomar_508cm	1.77	0.30	0.16	0	0	0	2	2	3	3	3	5	2	0	0	0	2	2	3	2	3	5	2	G

Acknowledgements

This work was supported by NASA PDART grant NNX15AJ60G: "Restoration and Submission of Uranus Ring Occultation Observations to the Planetary Data System." Hearty thanks to Amanda Bosh and Michael Person, who generously provided access to MIT's digital archive of Uranus occultation data. We are grateful to our many colleagues who have planned, participated in, and analyzed these observations, and to generations of Wellesley College students who helped make this archive possible.

Appendices

A Selected output from the RINGFIT orbital fit to the rings

We reproduce here selected sections of the RINGFIT results file `uranus_occultation_ring_fit_rfrench_20201201.txt` that is contained in the `data/` directory of the `uranus_occ_support` bundle described in Section 3.3. (In some cases, the text shown here runs off the side of the page; view the actual results file to see the complete text.)

```
%%% This file docouments the Uranus ring orbit fit model entitled
%%%      uranus_occultation_ring_fit_rfrench_20201201
%%%
%%% All annotations are preceded by %%%
%%%
%%% This is an annotated version of the output file produced by the IDL
%%% program ringfit_infile_v1.8.pro. The algorithm for the non-linear
%%% least squares fit to earthbased and spacecraft stellar occultations, and
%%% radio science occultations, is documented in the following publication:
%%% French, R. G. et al. (1993) "Geometry of the Saturn System from the 3 July 1989
%%% Occultation of 28 Sgr and Voyager Observations" Icarus 103, 163-214.
%%% The calculations generally follow the solar system barycenter vector approach described in
%%% Appendix A.1.1. See also Appendix B for details of the calculations,
%%% including a sample barycentric calculation for Saturn.
%%%
%%% Note that the geometrical model presented here differs from the French et al. (1993)
%%% in several respects, as discussed in French, R. G. et al. (2010)
%%% "Occultation Observations of Saturn's B Ring and Cassini Division", Astron. J.
%%%  139:1649-1667 - see pp. 1650-1651 for details.
%%%
%%% Detailed intermediate calculations are included for a representative Earth-based ring occultation observation
%%% Detailed intermediate calculations are included for a representative spacecraft-based stellar occultation observation
%%% Detailed intermediate calculations are included for a representative radio science occultation observation
%%%
ringfit_infile_v1.8.pro run on Tue Dec  1 23:44:27 2020 by rfrench@maxwell.fios-router.home
....
%%% This section summarizes the number of parameters to be fitted, specifies the
%%% finite differences used for numerical partial derivatives in the non-linear
%%% least-squares fit, and indicates whether general relativistic bending is
%%% taken into account, and if so, whether the J2 term is included.
%%% Note that, although the code includes planet pole precession, it does not
%%% affect the results if the pole precession rates are set to zero, which is
%%% the case for all Uranus ring fits.
%%%
%%% This section also defines the Epoch for all ring orbital elements.
%%%
%%% All calculations are performed in the J2000 inertial frame.
%%%
%%% This section contains the results of the least-squares fit. If the fit is unweighted,
%%% then USE_SIGMA_KM = 0, and the scaled parameter errors Sigma(scld) are appropriate.
%%% If   USE_SIGMA_KM = 1, then the fit is a weighted fit, and the unscaled parameter errors
%%% Sigma(unscl) should be used.
%%%
USE_SIGMA_KM = 0, unweighted fit, so use Sigma(scld) (pcerror)

                    Parameter       Initial         Final    Final-Init  Sigma(unscl)   Sigma(scld)   Final/Sigma  |Diff|/Sigma
```

```
-------------------------------------------------------------------------------------------------------------------------------
                     RP_(deg)     77.311143     77.311143      0.000000      0.000661      0.000295       262227.      0.000000
                     DP_(deg)     15.172188     15.172188      0.000000      0.001427      0.000637       23826.7      0.000000
       1   Ring_6    A_(km)     41837.31905   41837.31905       0.00000       0.27634       0.12328       339365.      0.000000
       2   Ring_5    A_(km)     42235.09430   42235.09430       0.00000       0.26365       0.11762       359081.      0.000000
       3   Ring_4    A_(km)     42571.30227   42571.30227       0.00000       0.26130       0.11657       365196.      0.000000
       4   Alpha     A_(km)     44718.67027   44718.67027       0.00000       0.25210       0.11247       397623.      0.000000
...
%%%
%%% This section lists statistics of the fit: ring by ring, sorted by event, and sorted by
%%% spacecraft stellar occultation, radio science (RSS) observations, and occultation star.
%%%
                   Ring-by-ring Statistics

Ring        # wt'd pts    unwtd-rms (km)      wtd-rms (sigma)    Semimajor Axis
-------------------------------------------------------------------------------
1   Ring_6       48           0.301952             0.301952        41837.3190
2   Ring_5       65           0.246707             0.246707        42235.0943
3   Ring_4       63           0.296163             0.296163        42571.3023
4   Alpha        81           0.294908             0.294908        44718.6703
5   Beta         79           0.296651             0.296651        45661.2492
6   Eta          64           0.376697             0.376697        47176.2304
7   Gamma        86           0.475822             0.475822        47626.4880
8   Delta        86           0.430850             0.430850        48300.4466
10  Epsilon      90           0.559106             0.559106        51149.4654

Total # weighted pts: 662...
%%%
%%% This section lists ring-by-ring results for Earth-based stellar occulation data.
%%% The results are sorted by Event ID, which uniquely identifies an occultation, and by
%%% Observatory, indicated by the column "OBS". Each Event ID begins with a listing of
%%% information about the occulted star, giving the catalog position, the parallax and
%%% proper-motion-corrected position, and both catalog and parallax/proper motion-corrected
%%% positions also corrected for star offsets dRA and dDE defined previously. NOTE THAT
%%% the code computes the parallax and proper motion individually for each ring event at
%%% the actual observed time for each ring feature; these summary star positions are for
%%% reference but differ very slightly from the actual star positions used for each point
%%% by virtue of the difference between the listed epoch and the actual observing ring time.
%%%
%%%
%%% The individual Earth-based observations begin here. Column definitions follow:
%%%  i             - Data point index, increasing monotonically. Note that, because of
%%%                  sorting of the output, the order of the output may not correspond
%%%                  to the order of the input data.
%%%  Occul         - YYYY-MM-DD of the occultation event (to within a few days).
%%%  Ring          - Name of the uranian ring.
%%%  Obs           - Observatory code - typically a 3-letter code.
%%%  I/E           - (I)ngress or (E)gress.
%%%  Wt.           - Data point weight - always 1.0.
%%%  UTC(corr.)    - Observed ring event time (on earth), corrected for any station offset time.
%%%  UTC(model)    - The predicted observed ring event time, based on final ring orbit model.
%%%  DT(obs-mod)   - Difference between the corrected observed time and the model time (sec).
%%%  UTC(uncorr.) - The input observed ring event time, uncorrected for station offset time.
%%%  R (obs.)      - The ring plane radius sampled by the occultation ray received at UTC(corr.).
%%%  R (model)     - The model ring plane radius sampled by the occultation ray received at UTC(corr.),
%%%                  computed based on the calculated true anomaly at the observed ring intercept point.
%%%  DR(obs-mod)   - Difference between the observed and model radius, in km.
%%%  Delta         - Distance between sky plane and ring plane along occultation ray (<0 means ring
%%%                  intercept point is closer to observer than the sky plane), in km.
%%%  Ulon          - Inertial longitude of ring intercept point, defined previously, in degrees.
%%%  Delta/c       - Light travel time from sky plane to ring plane, in seconds,
%%%  V-perp-c      - Apparent velocity of star perpendicular to the edge of the ring in the sky plane,
%%%                  assuming a circular ring model, in km/sec.
%%%  V-perp_e      - Apparent velocity of star perpendicular to the edge of the ring in the sky plane,
```

```
%%%                 assuming an eccentric ring model, in km/sec.
%%%  R-dot        - Radial velocity of the occultation ray, measured in the ring plane in km/sec.
%%%  Anomaly      - True anomaly of the ring intercept point, given by the difference between the
%%%                 inertial longitude of the ring intercept point, Ulon, and the longitude of
%%%                 periapse of the ring, precessed from the periapse longitude at epoch to the
%%%                 time at which the occultation ray penetrated the ring plane at Uranus.
%%%  Sin B        - Sine of the inclination of the ring plane relative to the observer.
%%%  Rlon-dot     - Transverse velocity of the occultation ray (in the direction of increasing
%%%                 longitude of the ring), measured in the ring plane, in km/sec.
%%%
%%% Additional detailed geometrical information is included below for the
%%% first delta ring observation, which includes the calculation of an m=2
%%% normal mode. These results should be useful for users wishing to compare
%%% their calculations of ring occultation geometry with the results of RINGFIT.
%%%

Event ID    1: Earth-based stellar occultation U0  1977-03-10 of Star No. 12  U0  Parallax and proper motion computed at each ri
/Volumes/dione_raid2/Research/RINGFIT/stars/data/ustarsALLd.v3.merged.sortedA.csv Hipparcos 71567
J2000 Catalog Star Position at epoch 1991 APR 02 13:30:00.00 : 14h 38m 11.811096000s -14d 57m 17.061588000s 219.549212900000015
J2000 Parallax/PM  Position at epoch 1977 MAR 10 00:00:00.00 : 14h 38m 11.862240295s -14d 57m 16.890292924s 219.549426001229676
J2000 P/PM+dRA/dDE Position at epoch 1977 MAR 10 00:00:00.00 : 14h 38m 11.862743290s -14d 57m 16.896241785s 219.549428097041528
J2000 Cat.+dRA/dDE Position at epoch 1991 APR 02 13:30:00.00 : 14h 38m 11.811598995s -14d 57m 17.067536861s 219.549214995812292

  i      Occul      Obs             UTC(corr.)          R (obs.)      Delta     V-perp-c Anomaly
         Ring       I/E             UTC(model)          R (model)      Ulon     V-perp_e  Sin B
                    Wt.             DT(obs-mod)         DR(obs-mod)   Delta/c     R-dot  Rlon-dot
                                    UTC(uncorr.)
-------------------------------------------------------------------------------------------------
  47  1977-03-10    KAS      1977 MAR 10 20:11:46.5426   51553.7576  -23952.1  -11.08985  179.239
     10  Epsilon    I        1977 MAR 10 20:11:46.4242   51555.2734    33.751  -11.09025 -0.80470
                    1.000                    0.1184      -1.5157   -0.0799  -12.80557   6.9361
                             1977 MAR 10 20:11:46.5426

  48  1977-03-10    KAS      1977 MAR 10 20:16:02.7975   48303.6433  -21768.9  -10.95021  280.591
     8   Delta      I        1977 MAR 10 20:16:02.8525   48302.9536    35.862  -10.95019 -0.80471
                    1.000                   -0.0550       0.6897   -0.0726  -12.55057   7.4180
                             1977 MAR 10 20:16:02.7975
%%%   Detailed intermediate results for the Delta ring observation above:
%%%   Refer to Fig. A1, French et al. (1993) Icarus, 103, 163-214, and text
%%%   for definitions of quantities listed below.
%%%   (All distances are in km, velocities in km/sec, and time is in seconds.)
%%%      Uncorrected observed time (t0):          1977 MAR 10 20:16:02.797500
%%%      ET - UTC (sec):                               48.18552206814611
%%%      R_EO(t0):                                   -3943.95749102        -1043.33961644        -4902.71889305
%%%      Rdot_EO(t0):                                 0.21368163696844     -0.46908403424226     -0.07155364678403
%%%      R_E(t0):                                  -146413723.45278105     22000724.80130254      9534588.96482056
%%%      Rdot_E(t0):                                 -5.41517912374310    -27.05009690613461    -11.73078298285219
%%%      R_S(ti):                                 -2144317704.76815534  -1627873077.37443089   -682587278.22581458
%%%      Rdot_S(ti):                                  4.27732344737725     -5.08564771620784     -2.28811438910359
%%%      Star source catalog and ID:              Hipparcos 71567
%%%      Catalog RA,Dec of star:                      219.54921289999999    -14.95473933000000
%%%      Star epoch:                              JD 2448349.0625
%%%      Star epoch (ET sec):                        -276128941.81434351
%%%      parallax (mas):                                    1.77000000
%%%      proper motion RA/Dec (mas/yr):                   -52.61000000          -12.21000000
```

As noted, detailed intermediate calculations are included for representative Earth- and spacecraft-based stellar occultations and a radio science occultation. For example, here are the intermediate results for the δ ring ingress event observed from the Kuiper Airborne Observatory (KAO) during the discovery observations of the rings:

```
%%%      nhat(star)(corrected for pm, parallax):        -0.74495940463009     -0.61517723841202     -0.25805513130518
%%%      \Delta_1:                                    2681944693.24169827
%%%      nhat(pole)                                      0.21200672249011      0.94156982893160      0.26172391343688
%%%      longitude of periapse at time ti:            -104.80228255709690
%%%      longitude of node at time ti:                 104.80244506295202
%%%   Normal mode parameters for this ring event. See Nicholson et al. (2014)
%%%   "Noncircular features in Saturn's rings II: The C ring" Icarus 231, 373-396
%%%   Eqs. 5 and 6. Variable names are as follows:
%%%       da(km)   - radial amplitude of the normal mode of given wavenumber m (A_m in Eq. 5)
%%%     Lon(deg)   - longitude at epoch of one of the m radial minima (\delta_m in Eq. 6)
%%%     Lod(d/d)   - pattern speed of normal mode in deg/day (Omega_p in Eq. 6; see also Eq. 7)
%%%     m theta    - m * theta, where theta is defined in Eq. 6; see also Eq. 5
%%%    dr (mode)   - local radial distortion of the mode -- see Eq. 5.
%%%      Normal mode m=2:
%%%        da(km):                                      3.16218750796573
%%%        Lon(deg):                                  245.52255689676579
%%%        Lod(d/d):                                  562.51595138984521
%%%        m theta (deg):                             144.04958582855761
%%%      dr (mode) - local radial distortion:           2.55987104984279
```

Here is the detailed output for a representative spacecraft stellar occultation:

```
%%%
%%% Spacecraft stellar occultation results begin here. The stellar coordinates are as
%%% previously described for Earth-based observations, except that parallax is computed
%%% from the spacecraft position, not from the Earth.
%%%
Event ID   41: Voyager 2 stellar occultation VGR2 SSgr 1986-01-24 of Star No. 8 SSgr at epoch UTC 1986 Jan 24
/Volumes/dione_raid2/Research/RINGFIT/stars/data/ustarsALLd.v2.merged.sortedA.csv Hipparcos 92855
J2000 Catalog Star Position : 18h 55m 15.916704000s -26d 17m 47.739408000s 283.816319599999986 -26.296594280000001
J2000 Parallax/PM  Position : 18h 55m 15.919652520s -26d 17m 47.470724987s 283.816331885498300 -26.296519645829648
J2000 + dRA/dDE    Position : 18h 55m 15.919652520s -26d 17m 47.470724987s 283.816331885498300 -26.296519645829648

Ring         Side    SCET(obs.corr)         R (obs.)      Delta    V-perp-c Anomaly
Instr.               SCET (model)           R (model)      Ulon    V-perp-e  Sin B
Weight               DT(obs-mod)           DR(obs-mod)   Delta/c     R-dot  Rlon-dot
                     SCET(obs_uncorr)
-------------------------------------------------------------------------------
10  Epsilon   I 1986 JAN 24 05:15:54.2342   50871.1214  734634.3   -0.99051  313.037
   PPS          1986 JAN 24 05:15:54.5697   50870.7771   266.549   -0.97502 -0.89027
   1.000                          -0.3355       0.3443   2.45048   -1.02625   2.8901
                1986 JAN 24 05:15:53.8200
%%%   Detailed intermediate results for the Epsilon ring observation above:
%%%   Refer to Fig. A1, French et al. (1993) Icarus, 103, 163-214, and text
%%%   for definitions of quantities listed below.
%%%   (All distances are in km, velocities in km/sec, and time is in seconds.)
%%%      Uncorrected SCET observed time (t0):      1986 JAN 24 05:15:53.820000
%%%      Corrected SCET time:                      1986 JAN 24 05:15:54.2342
%%%      ET - UTC (sec):                               55.18459057816327
%%%      R_E0(t0):                                            0.00000000            0.00000000            0.00000000
%%%      Rdot_E0(t0):                                  0.00000000000000      0.00000000000000      0.00000000000000
%%%      R_E(t0):                                   -549591182.09125376  -2572817445.90378666  -1119051960.71511626
%%%      Rdot_E(t0):                                   7.21613717528297    -15.28551295764167     -7.16751766190884
%%%      R_S(ti):                                   -549439805.13795936  -2573469297.76834774  -1119328409.74474788
%%%      Rdot_S(ti):                                   6.63204976727579     -1.45521716548996     -0.73149137565176
%%%      Star source catalog and ID:               Hipparcos 92855
%%%      Catalog RA,Dec of star:                       283.81631959999999    -26.29659428000000
%%%      Star epoch:                               JD 2448349.0625
%%%      Star epoch (ET sec):                       -276128941.81434351
%%%      parallax (mas):                                      14.54000000
%%%      proper motion RA/Dec (mas/yr):                       13.87000000          -52.65000000
%%%      nhat(star)(corrected for pm, parallax):       0.21409658891065     -0.87057384738130     -0.44301673430305
```

```
%%%      \Delta_1:                                          734634.31836612
%%%      nhat(pole)                                        0.21199792746546      0.94157333259599      0.26171843285185
%%%
```

And finally, here is the output for a representative RSS occultation event:

```
                    ****** RSS OCCULTATION OBSERVATIONS ******

%%%
%%% Radio Science occultation results begin here. Column definitions follow:
%%% The individual Earth-based observations begin here. Column definitions follow:
%%%  Ring         - Index number (1 to 10 from ring 6 to epsilon), and name of the uranian ring.
%%%  Instr.       - Spacecraft instrument making the measurement (ex: Voyager PPS or UVS)
%%%  Weight       - Data point weight - always 1.0.
%%%  Side         - (I)ngress or (E)gress.
%%%  UTC(obs.corr)- Observed ring event time (ERT= Earth Received Time), corrected for any station offset time.
%%%  UTC(model)   - The predicted observed ring time (ERT), based on final ring orbit model.
%%%  DT(obs-mod)  - Difference between the corrected observed time and the model time (sec).
%%%  UTC(uncorr.) - The observed ring time (ERT), uncorrected for any station offset time.
%%%  SCET (corr.) - Calculated SCET (SpaceCraft Event Time) (at spacecraft) of the transmission
%%%                 of the ray received UTC(obs.corr), corrected for any station offset time.
%%%  SCET (model) - Model value of SCET (SpaceCraft Event Time) (at spacecraft) of the transmission
%%%                 of the ray received UTC(obs.corr), corrected for any station offset time.
%%%  Travel Time  - HH:MM:SS.SSSS of light travel time between UTC(obs.corr) and SCET (corr.).
%%%  R (obs.)     - The ring plane radius sampled by the occultation ray received at UTC(corr.).
%%%  R (model)    - The model ring plane radius sampled by the occultation ray received at UTC(corr.),
%%%                 computed based on the calculated true anomaly at the observed ring intercept point.
%%%  DR(obs-mod)  - Difference between the observed and model radius, in km.
%%%  Delta        - Distance between spacecraft and ring plane along occultation ray (always >0),
%%%  Ulon         - Inertial longitude of ring intercept point, defined previously, in degrees.
%%%  Delta/c      - Light travel time between spacecraft and ring plane, in seconds,
%%%  V-perp-c     - Apparent velocity of star perpendicular to the edge of the ring in the sky plane,
%%%                 assuming a circular ring model, in km/sec.
%%%  V-perp_e     - Apparent velocity of star perpendicular to the edge of the ring in the sky plane,
%%%                 assuming an eccentric ring model, in km/sec.
%%%  R-dot        - Radial velocity of the occultation ray, measured in the ring plane in km/sec.
%%%  Anomaly      - True anomaly of the ring intercept point, given by the difference between the
%%%                 inertial longitude of the ring intercept point, Ulon, and the longitude of
%%%                 periapse of the ring, precessed from the periapse longitude at epoch to the
%%%                 time at which the occultation ray penetrated the ring plane at Uranus.
%%%  Sin B        - Sine of the inclination of the ring plane relative to the observer.
%%%  Rlon-dot     - Transverse velocity of the occultation ray (in the direction of increasing
%%%                 longitude of the ring), measured in the ring plane, in km/sec.
%%%
%%% Additional detailed geometrical information is included below for the
%%% first RSS delta ring observation, which includes the calculation of an m=2
%%% normal mode. These results should be useful for users wishing to compare
%%% their calculations of ring occultation geometry with the results of RINGFIT.
%%%
-------------------------------------
Event ID   40: Voyager 2 RSS occultation VGR2 RSS  1986-01-24

Ring        Side        UTC(obs.corr)             SCET (corr.)        R (obs.)    Delta   V-perp_c   Anomaly
DSN         Band        UTC(model)                SCET (model)        R (model)   Ulon     V-perp-e  Sin B
Weight                  DT(obs-mod)               Travel Time        DR(obs-mod)  Delta/c    R-dot  Rlon-dot
                        UTC(uncorr.)
-------------------------------------------------------------------------------------------------------------
1   Ring_6    I 1986 JAN 24 22:46:41.2206  1986 JAN 24 20:01:50.5240   41871.7027 155596.6  -8.10241  144.435
DSS-43          1986 JAN 24 22:46:41.1946  1986 JAN 24 20:01:50.4979   41871.9138  340.785  -8.10070  0.98910
 1.000                           0.0261              2:44:50.7080      -0.2112  0.51901  -8.10245  -2.8909
                1986 JAN 24 22:46:41.2320
```

```
  ...
8   Delta     I 1986 JAN 24 22:33:31.8796  1986 JAN 24 19:48:41.1683   48301.4010 144318.1  -8.17672   82.111
DSS-43          1986 JAN 24 22:33:31.8645  1986 JAN 24 19:48:41.1532   48301.5248  343.502  -8.17671  0.98909
 1.000                              0.0151               2:44:50.7226      -0.1237  0.48139  -8.17680  -2.5061
                1986 JAN 24 22:33:31.8910
%%%   Detailed intermediate results for the Delta ring observation above:
%%%   Refer to Fig. A1, French et al. (1993) Icarus, 103, 163-214, and text
%%%   for definitions of quantities listed below.
%%%   (All distances are in km, velocities in km/sec, and time is in seconds.)
%%%      Uncorrected observed time earth received time:           1986 JAN 24 22:33:31.891000
%%%      Corrected observed time earth received time:             1986 JAN 24 22:33:31.8796
%%%      ET - UTC (sec):                                               55.18461002071152
%%%      DSN-centered spacecraft pos,vel when ray received:         -464591851.74407053  -2685560656.13861036  -1167945231.8814
%%%                                                                   37.28835888054799     -0.54102897352525      0.3225720187
%%%   (^^^^^ corrected for light travel time ^^^)
%%%   source code for above:
%%%   ;              target     obs time                          obs  pos'n vec
%%%   cspice_spkezr, spacecraft, ETsec, frame_heliocentric, 'CN', DSN, state_ref0, LTime
%%%      Uranus-centered S/C pos,vel when ray emitted:                 -67002.12673786      -117035.14868807       -70084.4178
%%%                                                                    6.08769583035971    -14.93289204134465     -5.7643798201
%%%   (^^^^^ uncorrected for light travel time ^^^)
%%%   source code for above:
%%%   ET_SC = ETsec - LTime ; the time the ray was emitted from the S/C
%%%   ; state_ref: instantaneous planet-centered S/C state vector at time ray was emitted
%%%   cspice_spkezr, spacecraft, ET_SC, frame_heliocentric,'NONE', planet, state_ref,LTime_sc_planet
%%%      SSB planet pos,vel when ray emitted:                     -549092485.34124517  -2573545486.55556154  -1119366708.3628
%%%                                                                  6.63208741076307     -1.45443842948248     -0.7311055479
%%%   (^^^^^ uncorrected for light travel time ^^^ -- SSB is Solar Sytem Barycenter)
%%%   source code for above:
%%%   ; instantaneous planet state vector
%%%   cspice_spkezr, planet, ET_SC, frame_heliocentric,'NONE','SSB', state_sat_ssb,LTime_sat_ssb
%%%      \Delta_1:                                                    144318.11373399
%%%      nhat(pole)                                                  0.21200548109227      0.94157254229629      0.2617151573
%%%   Normal mode parameters for this ring event. See Nicholson et al. (2014)
%%%   "Noncircular features in Saturn's rings II: The C ring" Icarus 231, 373-396
%%%   Eqs. 5 and 6. Variable names are as follows:
%%%       da(km)   - radial amplitude of the normal mode of given wavenumber m (A_m in Eq. 5)
%%%     Lon(deg)   - longitude at epoch of one of the m radial minima (\delta_m in Eq. 6)
%%%     Lod(d/d)   - pattern speed of normal mode in deg/day (Omega_p in Eq. 6; see also Eq. 7)
%%%     m theta    - m * theta, where theta is defined in Eq. 6; see also Eq. 5
%%%    dr (mode)   - local radial distortion of the mode -- see Eq. 5.
%%%      Normal mode m=2:
%%%        da(km):                                                     3.16218750796573
%%%        Lon(deg):                                                 245.52255689676579
%%%        Lod(d/d):                                                 562.51595138984521
%%%        m theta (deg):                                            110.69803011725890
%%%      dr (mode) - local radial distortion:                          1.11765203419874
```

B Using frame kernels to compute ring geometry

The Uranus ring occultation observation bundles contain detailed information about the geometry of individual observations, based on the best available ring orbit solution available at the time of submission. For many users, this information will be sufficient, but with the eventual improvement in the determination of the direction of the Uranus pole and ring orbital elements, some users may wish to recompute the mapping between observed

time and the absolute radius scale of a given ring. Others may wish to compute the event geometry on their own: it is often useful to be able to determine the longitudes of periapse and of the ascending node of a ring at any given time, or to compute the true anomaly of a particular ring intercept point during an occultation. However, such geometric calculations are complicated by the rapid apsidal precession and nodal regression of the rings.

To make these calculations more accessible to the general user, we have produced two SPICE *frame kernels* that incorporate the Uranus pole direction and the ring orbital elements. Together with the NAIF toolkit, a Uranus ring frame kernel makes it easy to compute such quantities as the instantaneous ring plane pole, the inertial longitude of a given ring plane point, and the apparent view of an elliptical ring in the sky plane as viewed from the Earth.

The two Uranus ring frame kernels are provided in the `spice_kernels/fk/` directory, and in this Appendix we illustrate their use with the IDL and Python codes provided in the `document/` directory.

B.1 Determining the pole direction of a ring plane at a given time

We begin with a simple example of computing the direction of the ring plane pole at a given time for one of the inclined Uranian rings. First, we use the `uranus_ringframes_French_et_al_1988.tf` frame kernel, which is based on the Uranus ring orbit solution of French et al. 1988. The kernel itself is a human-readable text file that defines the following reference frames for the Uranus equator and the ten classical rings:

```
URANUS_EQUATORIAL
URING_6
URING_5
URING_4
URING_ALPHA
URING_BETA
URING_ETA
URING_GAMMA
URING_DELTA
URING_LAMBDA
URING_EPSILON
```

The kernel file contains extensive documentation about the format and orbital elements used to construct the file. Here is part of that documentation:

```
\begintext

   The ring frames are implemented using the Euler family of the
   parameterized dynamic frame class.

   The epoch of the elements is
   UTC Mar 10, 1977 20:00:00
```

```
The corresponding TDB date is
1977 MAR 10 20:00:48.185522 TDB

The Euler angle sequence for the ring frames is

[ arg of periapse ]  [ inclination ]   [ longitude of node ]
                  3               1                       3

The specific constants for the orientation of the rings are:

   Ring      peri(deg)  peri_dot  inc(deg) node(deg)  node_dot
   ------------------------------------------------------------
  Ring 6     242.80000  2.76187    0.06160  12.12000  -2.75641
  Ring 5     170.31000  2.67151    0.05360 286.57000  -2.66633
  Ring 4     127.28000  2.59807    0.03230  89.26000  -2.59311
  Alpha      333.24000  2.18530    0.01520  63.08000  -2.18152
  Beta       224.88000  2.03084    0.00510 310.05000  -2.02747
  Eta        228.10000  1.81080    0.00110 188.73000  -1.80798
  Gamma      132.10000  1.75128    0.00150 251.30000  -1.74861
  Delta      216.70000  1.66702    0.00110 260.70000  -1.66455
  Lambda       0.00000  1.47384    0.00000   0.00000  -1.47180
  Epsilon    214.97000  1.36325    0.00020 246.60000  -1.36145

Euler frames require the inverse of this sequence, since the
mapping from the Euler frame to its base frame is what's defined.
The required sequence is:

[ -longitude of node ]  [ -inclination ]  [ -arg of periapse ]
                     3                1                      3

Note that in the frame definitions below, the angular rates are
scaled from degrees/day to degrees/second, as required by the
SPICE frames system.
```

To validate and illustrate the use of the frame kernel, we include the IDL source file `create_uranus_ringframes_tf_French_et_al_1988.pro` that was used to produce the kernel. As part of its output, it produces a table of instantaneous B1950 ring pole directions for the Voyager 2 Uranus RSS ring occultations, which we compare here to the same quantities calculated by Gresh et al. 1989.

```
Comparison with Gresh et al. 1989 Icarus 78, 131 -- Table II

Ring Frame      I/E Ring Intercept Time (UTC) pi0(deg) Omega0(deg) RA(deg) Dec(deg)
-------------------------------------------------------------------------------
URING_6          I  1986 Jan 24 20:01:51.081   196.778    75.833   76.6588  15.0966
URING_5          I  1986 Jan 24 20:00:57.680   191.348   282.326   76.5427  15.1003
URING_4          I  1986 Jan 24 20:00:26.589   270.225   322.396   76.5765  15.0861
URING_ALPHA      I  1986 Jan 24 19:55:58.385   217.990   190.584   76.5940  15.1266
URING_BETA       I  1986 Jan 24 19:54:07.459   328.839   217.012   76.5937  15.1158
URING_ETA        I  1986 Jan 24 19:50:59.318   338.692    87.258   76.5980  15.1116
URING_GAMMA      I  1986 Jan 24 19:50:04.813    49.723   342.331   76.5964  15.1103
URING_DELTA      I  1986 Jan 24 19:48:41.478   221.153   264.255   76.5958  15.1118
URING_EPSILON    I  1986 Jan 24 19:43:36.672   314.620   152.786   76.5970  15.1119
URING_6          E  1986 Jan 24 22:33:33.858   197.069    75.543   76.6587  15.0963
```

```
URING_5          E  1986 Jan 24 22:34:17.110   191.633   282.042   76.5426  15.1005
URING_4          E  1986 Jan 24 22:35:06.301   270.504   322.118   76.5764  15.0862
URING_ALPHA      E  1986 Jan 24 22:39:26.294   218.238   190.337   76.5941  15.1267
URING_BETA       E  1986 Jan 24 22:41:26.104   329.075   216.776   76.5937  15.1158
URING_ETA        E  1986 Jan 24 22:44:28.220   338.910    87.040   76.5980  15.1116
URING_GAMMA      E  1986 Jan 24 22:45:22.825    49.936   342.118   76.5964  15.1103
URING_DELTA      E  1986 Jan 24 22:46:43.642   221.359   264.049   76.5958  15.1118
URING_EPSILON    E  1986 Jan 24 22:52:50.317   314.799   152.608   76.5970  15.1119
-------------------------------------------------------------------------------
```

Figure 25 shows the results from Table II of Gresh et al. 1989 for comparison. The results agree at the level expected from roundoff of the input pole direction and orbital elements.

TABLE II

ELEMENTS OF KEPLERIAN RING ORBITS USED IN PROCESSING[a]

Ring	a (km)	$e \times 10^3$	i (deg)	Ingress				Egress			
				ω_0 (deg)	Ω_0 (deg)	α_r[b] (deg)	δ_r[b] (deg)	ω_0 (deg)	Ω_0 (deg)	α_r (deg)	δ_r (deg)
6	41,837.15	1.013	0.0616	196.774	75.623	76.6587	15.0964	197.065	75.332	76.6586	15.0961
5	42,234.82	1.899	0.0536	191.348	282.126	76.5426	15.1004	191.632	281.843	76.5426	15.1007
4	42,570.91	1.059	0.0323	270.224	322.212	76.5764	15.0862	270.503	321.934	76.5763	15.0863
α	44,718.45	0.761	0.0152	217.990	190.454	76.5940	15.1266	218.238	190.207	76.5941	15.1267
β	45,661.03	0.442	0.0051	328.839	216.902	76.5937	15.1158	329.075	216.666	76.5937	15.1158
η	47,175.91	(0.004)	0.0011	338.878	87.169	76.5980	15.1116	339.096	86.951	76.5980	15.1116
γ	47,626.87	0.109	0.0015	49.722	342.747	76.5964	15.1103	49.935	342.534	76.5964	15.1103
δ	48,300.12	0.004	0.0011	221.325	264.175	76.5958	15.1118	221.531	263.969	76.5958	15.1118
ε	51,149.32	7.936	0.0002	314.620	152.739	76.5970	15.1119	314.799	152.560	76.5970	15.1119

[a] Adapted from Table XIV of French *et al.* (1988). (a, e, ω_0, i, Ω_0 denote, respectively, semimajor axis, eccentricity, longitude of periapse, inclination, and longitude of ascending node). Both ω_0 and Ω_0 are adjusted to correspond to the event times given in Table I, and are measured relative to the ascending node of the ring on the Earth's mean equator of 1950.0.

[b] Because of varying inclination of individual rings, profile reconstruction with accurate radial scale requires specification of a different ring plane normal (or pole) for each ring. α_r and δ_r denote right ascension and declination of individual poles used in processing.

Fig. 25: Table II of Gresh et al. 1989.

Using a frame kernel, it is easy to express the ring plane pole in any desired reference frame. The short IDL code fragment below, from the end of `create_uranus_ringframes_tf_French_et_al_1988.pro`, uses the frame kernel file and the `icy` implementation of the NAIF toolkit[6] to determine the pole direction of the ring 6 orbit plane at the time of the Voyager 2 Uranus ring 6 ingress occultation in both the B1950 and the J2000 reference frames:

```
cspice_furnsh,['naif0012.tls','uranus_ringframes_French_et_al_1988.tf']
cspice_str2et,'UTC 1986 Jan 24 20:01:51.081',ETsec_ring6_ingress
ring_pole       = [0.d0,0.d0,1.d0]

cspice_pxform,'URING_6','B1950',ETsec_ring6_ingress,rotate
cspice_mxv,rotate,ring_pole,pole_B1950
```

[6] https://naif.jpl.nasa.gov/pub/naif/toolkit_docs/IDL/index.html

```
cspice_recrad,pole_B1950,len,RA,DE
RAdeg           = RA * cspice_dpr()
DEdeg           = DE * cspice_dpr()
print,'B1950 pole direction for Voyager 2 RSS ring 6 ingress:'
print,RAdeg,DEdeg,format='("RA = ",F7.4," Dec = ",F7.4," deg")'

cspice_pxform,'URING_6','J2000',ETsec_ring6_ingress,rotate
cspice_mxv,rotate,ring_pole,pole_J2000
cspice_recrad,pole_J2000,len,RA,DE
RAdeg           = RA * cspice_dpr()
DEdeg           = DE * cspice_dpr()
print,'J2000 pole direction for Voyager 2 RSS ring 6 ingress:'
print,RAdeg,DEdeg,format='("RA = ",F7.4," Dec = ",F7.4," deg")'

end
```

The results are shown below:

```
B1950 pole direction for Voyager 2 RSS ring 6 ingress:
RA = 76.6588 Dec = 15.0966 deg
J2000 pole direction for Voyager 2 RSS ring 6 ingress:
RA = 77.3726 Dec = 15.1592 deg
```

For Python users, we include the equivalent code in Python 3.9 in the file `UranusPoleExample1.py`, using the SpiceyPy[7] implementation of the NAIF toolkit:

```
bash-3.2$ cat UranusPoleExample1.py
# UranusPoleExample1.py

import spiceypy as spice

spice.furnsh(['naif0012.tls','uranus_ringframes_French_et_al_1988.tf'])
ETsec_ring6_ingress = spice.str2et('UTC 1986 Jan 24 20:01:51.081')
ring_pole = [0.0, 0.0, 1.0]

rotate = spice.pxform('URING_6','B1950',ETsec_ring6_ingress)
pole_B1950 = spice.mxv(rotate,ring_pole)
len,RA,DE = spice.recrad(pole_B1950)
RAdeg = RA * spice.dpr()
DEdeg = DE * spice.dpr()
print('B1950 pole direction for Voyager 2 RSS ring 6 ingress:')
print("RA = ",'{:07.4f}'.format(RAdeg)," Dec = ",'{:07.4f}'.format(DEdeg))

rotate = spice.pxform('URING_6','J2000',ETsec_ring6_ingress)
pole_J2000 = spice.mxv(rotate,ring_pole)
len,RA,DE = spice.recrad(pole_J2000)
RAdeg = RA * spice.dpr()
DEdeg = DE * spice.dpr()
print('J2000 pole direction for Voyager 2 RSS ring 6 ingress:')
print("RA = ",'{:07.4f}'.format(RAdeg)," Dec = ",'{:07.4f}'.format(DEdeg))
```

[7] https://github.com/AndrewAnnex/SpiceyPy

The results from the Python routine are shown below:

```
bash-3.2$ python3.9 UranusPoleExample.py
B1950 pole direction for Voyager 2 RSS ring 6 ingress:
RA =  76.6588  Dec =  15.0966
J2000 pole direction for Voyager 2 RSS ring 6 ingress:
RA =  77.3726  Dec =  15.1592
```

We can compare these results to those that use `uranus_ringframes_rfrench20201201.tf`, a frame kernel based on the more recent Uranus ring orbit fit documented in the `geometry/` directory. When substituted for `uranus_ringframes_French_et_al_1988.tf` in the Python code above (as is done in the Python file `UranusPoleExample2.py`), the results differ very slightly because of the improved Uranus pole direction and ring 6 orbit:

```
bash-3.2$ python3.9 UranusPoleExample2.py
B1950 pole direction for Voyager 2 RSS ring 6 ingress:
RA =  76.6579  Dec =  15.0935
J2000 pole direction for Voyager 2 RSS ring 6 ingress:
RA =  77.3718  Dec =  15.1560
```

B.2 Confirming the definition of the origin of inertial longitude

In this example, we use the `URANUS_EQUATORIAL` frame to confirm that the origin of inertial longitude in the Uranus equatorial plane is the ascending node of the intersection of the Uranus equator and the J2000 Earth equator. We do this by comparing the direction of a unit vector with zero longitude in the equatorial plane with the cross-product of the Earth's J2000 pole direction and the Uranus pole direction. The IDL version is contained in `UranusLongitudeExample.pro`:

```
; UranusLongitudeExample.pro
;
; Confirm that the intersection of the ascending node of the
; Uranus equator and the Earth's J2000 equator define the
; origin of longitude in the Uranus ring frame kernel.
;
; Revisions:
; 2019 Dec 21 - rfrench - original version

cspice_furnsh,['naif0012.tls','uranus_ringframes_rfrench20201201.tf']

cspice_str2et,'TDB 2000 Jan 1 12:00:00.000',ETepoch

; Determine J2000 coordinates of origin of longitude in URANUS_EQUATORIAL
; frame

zero_longitude       = [1.d0,0.d0,0.d0]
pole      = [0.d0,0.d0,1.d0]
cspice_pxform,'URANUS_EQUATORIAL','J2000',ETepoch,rotate
```

```
cspice_mxv,rotate,zero_longitude,zero_longitude_J2000
cspice_mxv,rotate,pole,UranusPole_J2000

; compute the intersection of the Earth's equator and Uranus equator from
; the cross-product of the Earth's J2000 pole and Uranus pole

cspice_vcrss, pole,UranusPole_J2000,intersection

; normalize the intersection vector to unity, for direct comparison
; between two vectors

intersection /= cspice_vnorm(intersection)

; compute angular separation between the two independent calculations

print,'J2000 zero of longitude from URANUS_EQUATORIAL frame:'
print,zero_longitude_J2000,format='(3F)'

print,'J2000 zero of longitude from cross-product of poles:'
print,intersection,format='(3F)'

print,'Angular difference between independent calculations of'
print,'direction of origin of longitude in Uranus equator:'
print,cspice_vsep(intersection,zero_longitude_J2000) * cspice_dpr(),' degrees'

end
```

Here are the results of the IDL code:

```
IDL> .run UranusLongitudeExample.pro
J2000 zero of longitude from URANUS_EQUATORIAL frame:
      -0.9755772808276375       0.2196564798337461       0.0000000000000000
J2000 zero of longitude from cross-product of poles:
      -0.9755772808276374       0.2196564798337461       0.0000000000000000
Angular difference between independent calculations of
direction of origin of longitude in Uranus equator:
   6.5568814e-15 degrees
```

The Python version is contained in `UranusLongitudeExample.py`:

```
# UranusLongitudeExample.py
import spiceypy as spice

spice.furnsh(['naif0012.tls','uranus_ringframes_rfrench20201201.tf'])
ETepoch  = spice.str2et('TDB 2000 Jan 1 12:00:00.000')
zero_longitude = [1.0,0.0,0.0]
pole = [0.0, 0.0, 1.0]

rotate = spice.pxform('URANUS_EQUATORIAL','J2000',ETepoch)
zero_longitude_J2000 = spice.mxv(rotate,zero_longitude)
UranusPole_J2000 = spice.mxv(rotate,pole)

intersection = spice.vcrss(pole, UranusPole_J2000)
intersection /= spice.vnorm(intersection)
```

```
print('J2000 zero of longitude from URANUS_EQUATORIAL frame:')
print('{:20.15f}'.format(zero_longitude_J2000[0]))
print('{:20.15f}'.format(zero_longitude_J2000[1]))
print('{:20.15f}'.format(zero_longitude_J2000[2]))

print('J2000 zero of longitude from cross-product of poles:')
print('{:20.15f}'.format(intersection[0]))
print('{:20.15f}'.format(intersection[1]))
print('{:20.15f}'.format(intersection[2]))

print('Angular difference between independent calculations of')
print('direction of origin of longitude in Uranus equator:')
print('{:20.15f}'.format(spice.vsep(intersection,zero_longitude_J2000) * spice.dpr()),' degrees')
```

The Python results agree with the IDL results:

```
bash-3.2$ python3.9 UranusLongitudeExample.py
J2000 zero of longitude from URANUS_EQUATORIAL frame:
  -0.975577280827638
   0.219656479833746
   0.000000000000000
J2000 zero of longitude from cross-product of poles:
  -0.975577280827637
   0.219656479833746
   0.000000000000000
Angular difference between independent calculations of
direction of origin of longitude in Uranus equator:
   0.000000000000007  degrees
```

B.3 Computing the skyplane view of the epsilon ring

As a more complex example of the use of a Uranus rings frame kernel, we compute the orientation of the ϵ ring at a specific time and produce a simple plot of the outline of Uranus and the ϵ ring as observed from Earth, marking the periapse location of the ring. (For simplicity, we assume that Uranus is spherical and we mark only the pole location, and omit lines of latitude and longitude.)

The IDL version of the code is `plot_epsilon_ring_example.pro` (listed below) and it produces Fig. 26.

```
; plot_epsilon_ring_example.pro
;
; Illustrate use of uranus_ring_frames *tf frame kernel
; to plot epsilon ring as seen from Earth

; !!!  Modify this line to point to your local kernels directory !!!

kernels_dir = '../../../../kernels/'
kernels = kernels_dir + [ $
```

```
        'ura111.bsp',$
        'uranus_ringframes_rfrench20201201_v1.tf',$
        'naif0012.tls']
cspice_furnsh,kernels

; specify a time at which to calculate the orientation of the epsilon ring

UTCstr  = '2020 Jan 25 12:00:00'
cspice_str2et,UTCstr,ETsec

Re      = 25559.d0 ; Equatorial radius of Uranus

; construct a transformation from Earth equatorial to sky plane frames

cspice_spkezr,'Uranus',ETsec,'J2000','CN','Earth',state,ltime
cspice_recrad,state[0:2],dist,ra,dec

cspice_rotate, dec, 2, mm_temp1
cspice_rotate, -ra, 3, mm_temp2
cspice_mxm, mm_temp2,mm_temp1, mm_SKY2EEQ
cspice_pxform,'URANUS_EQUATORIAL','J2000',ETsec,mm_UR2EEQ

; Uranus pole direction in J2000 coordinates

nhat_pole       = reform(mm_UR2EEQ[2,*])
nhat_pole       *= Re ; scale by radius of planet

; compute sky plane coordinates of pole

cspice_mtxv,mm_SKY2EEQ,nhat_pole,pole_sky

; compute epsilon ring sky plane coordinates

a_km_ring       = 51149.d0
ae_km_ring      = 406.d0
e_ring          = ae_km_ring/a_km_ring
ntheta          = 360L*50L
theta           = dindgen(ntheta)* cspice_rpd()/50.d0
rvals           = a_km_ring * (1.d0 - e_ring^2)/(1.d0 + e_ring * cos(theta))
xvals           = rvals * cos(theta)
yvals           = rvals * sin(theta)
ff_km           = dblarr(ntheta)
gg_km           = dblarr(ntheta)
cspice_pxform,'URING_EPSILON','J2000',ETsec-ltime,mm_RPL2EEQ
cspice_mtxm,mm_SKY2EEQ,mm_RPL2EEQ, mm_RPL2SKY
for nn=0,ntheta-1 do begin
        vec_ring = [xvals[nn],yvals[nn],0.]
        cspice_mxv,mm_RPL2SKY, vec_ring,vec_sky
        ff_km[nn] = vec_sky[1]
        gg_km[nn] = vec_sky[2]
endfor

; plot the results

set_plot,'PS'
ps_figure       = 'plot_epsilon_ring_example_IDL.ps'
device,file     = ps_figure,xsize=7,ysize=7,yoffset=0.5,/inch
!P.font = 0
```

```
title   = 'Epsilon ring from Earth '+UTCstr
xtitle  = 'East (km)'
ytitle  = 'North (km)'
xrange  = -3.0*[-1,1]*re
yrange  =  3.0*[-1,1]*re

; draw outline of circular planet on sky

xx      = cos(theta)
yy      = sin(theta)
x       = Re * xx
y       = Re * yy
plot,/iso,x,y,xrange=xrange,yrange=yrange,/xstyle,/ystyle,$
        title = title,xtitle=xtitle,ytitle=ytitle

; mark the visible pole location

if pole_sky[0] lt 0.d0 then $
        plots,pole_sky[1],pole_sky[2],psym=4 $
else $
        plots,-pole_sky[1],-pole_sky[2],psym=4

; draw epsilon ring and periapse location

oplot,ff_km,gg_km
plots,ff_km[0],gg_km[0],psym=1,symsize=3 ; mark periapse

device,/close
print,'Saved plot as '+ps_figure
end
```

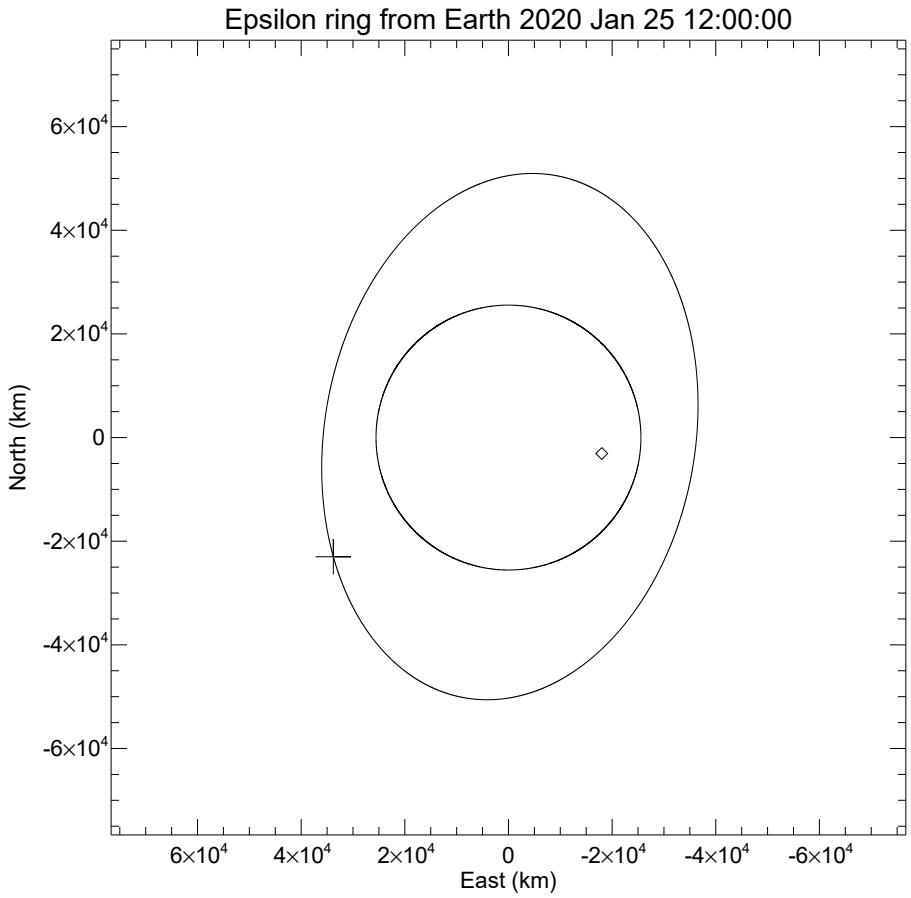

Fig. 26: Sky plane view of Uranus and the ϵ ring as observed from Earth on 2020 Jan 25 12:00 UTC. The visible Uranus pole is marked by a diamond and the + symbol marks the location of the periapse of the ϵ ring at the time of observation.

The Python version of the code is `plot_epsilon_example.py` (listed below) and it produces Fig. 27.

```
# plot_epsilon_ring_example.py
#
# Illustrate use of uranus_ring_frames *tf frame kernel
# to plot epsilon ring as seen from Earth

import matplotlib.pyplot as plt
import numpy as np
import spiceypy as spice

# !!!  Modify this line to point to your local kernels directory !!!

kernels_dir = '../../../../kernels/'

kernels = ['ura111.bsp',
        'uranus_ringframes_rfrench20201201_v1.tf',
        'naif0012.tls']

kernels_list=[kernels_dir + k for k in kernels]
spice.furnsh(kernels_list)

UTCstr  = '2020 Jan 25 12:00:00'
ETsec = spice.str2et(UTCstr)

Re      = 25559.0 # Equatorial radius of Uranus

# construct a transformation from Earth equatorial to sky plane frames

state,ltime = spice.spkezr('Uranus',ETsec,'J2000','CN','Earth')
dist,ra,dec = spice.recrad(state[0:3])

mm_temp1    = spice.rotate(dec,2)
mm_temp2    = spice.rotate(-ra,3)
mm_SKY2EEQ  = spice.mxm(mm_temp2,mm_temp1)
mm_UR2EEQ   = spice.pxform('URANUS_EQUATORIAL','J2000',ETsec)

# Uranus pole direction in J2000 coordinates

nhat_pole   = mm_UR2EEQ[0:3,2]
nhat_pole  *= Re # scale by radius of planet
nhat_pole   = np.array(nhat_pole)

# compute sky plane coordinates of pole

pole_sky    = spice.mtxv(mm_SKY2EEQ,nhat_pole)

# compute epsilon ring sky plane coordinates

a_km_ring       = 51149.
ae_km_ring      = 406.
e_ring          = ae_km_ring/a_km_ring
ntheta          = 360*50
theta           = np.radians(np.arange(ntheta)/50.)
rvals           = a_km_ring * (1.0 - e_ring**2)/(1.0 + e_ring * np.cos(theta))
xvals           = rvals * np.cos(theta)
yvals           = rvals * np.sin(theta)
```

```
mm_RPL2EEQ      = spice.pxform('URING_EPSILON','J2000',ETsec-ltime)
mm_RPL2SKY      = spice.mtxm(mm_SKY2EEQ,mm_RPL2EEQ)

ntheta
ff_km           = np.zeros(ntheta)
gg_km           = np.zeros(ntheta)
zvals           = np.zeros(ntheta)
for nn in range(ntheta):
        vec_ring  = np.array([xvals[nn],yvals[nn],0])
        vec_sky   = spice.mxv(mm_RPL2SKY,vec_ring)
        ff_km[nn] = vec_sky[1]
        gg_km[nn] = vec_sky[2]

# plot the results

plt.xlabel('East (km)')
plt.ylabel('North (km)')
plt.title('Epsilon ring from Earth '+UTCstr)
plt.axis('equal')
plt.axis([3*Re,-3*Re,-3*Re,3*Re])

# draw outline of circular planet on sky

xx      = np.cos(theta)
yy      = np.sin(theta)
x       = Re * xx
y       = Re * yy

plt.plot(x,y)

# mark the visible pole location

if pole_sky[0] < 0:
        plt.plot(pole_sky[1],pole_sky[2],"o")
else:
        plt.plot(-pole_sky[1],-pole_sky[2],"o")

# draw epsilon ring and periapse location

plt.plot(ff_km,gg_km)
plt.plot(ff_km[0],gg_km[0],marker='+',markersize=10)

plt.tight_layout()
pdf_figure = 'plot_epsilon_ring_example_python.pdf'
plt.savefig(pdf_figure)
print('Saved plot as '+pdf_figure)
plt.show()
```

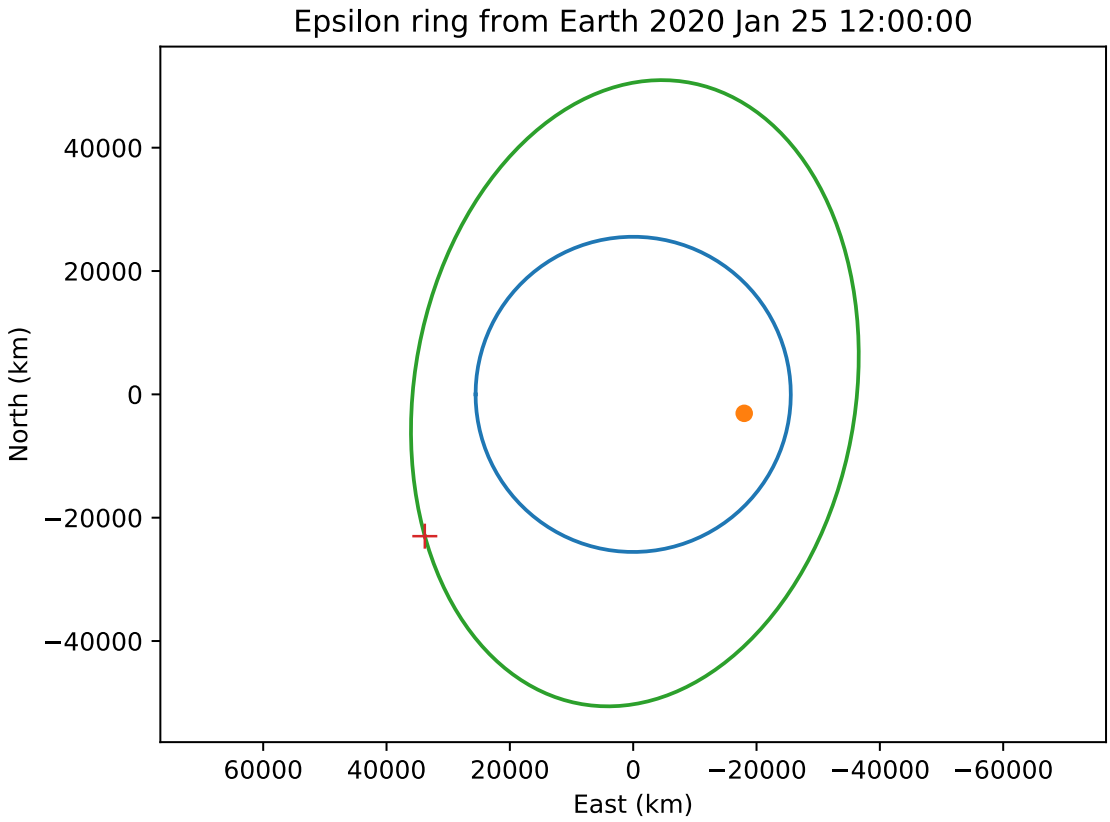

Fig. 27: Sky plane view of Uranus (blue circle) and the ϵ ring (green ellipse) as observed from Earth on 2020 Jan 25 12:00 UTC. The visible Uranus pole is marked by the orange dot and the + symbol marks the location of the periapse of the ϵ ring at the time of observation.

As an independent verification of these results, we include Fig. 28, produced using the Planet Viewer tool at the PDS Ring-Moon Systems node.[8] The computed periapse location of the ϵ ring matches the IDL and Python results.

[8] `https://pds-rings.seti.org/tools/viewer2_ura.html`

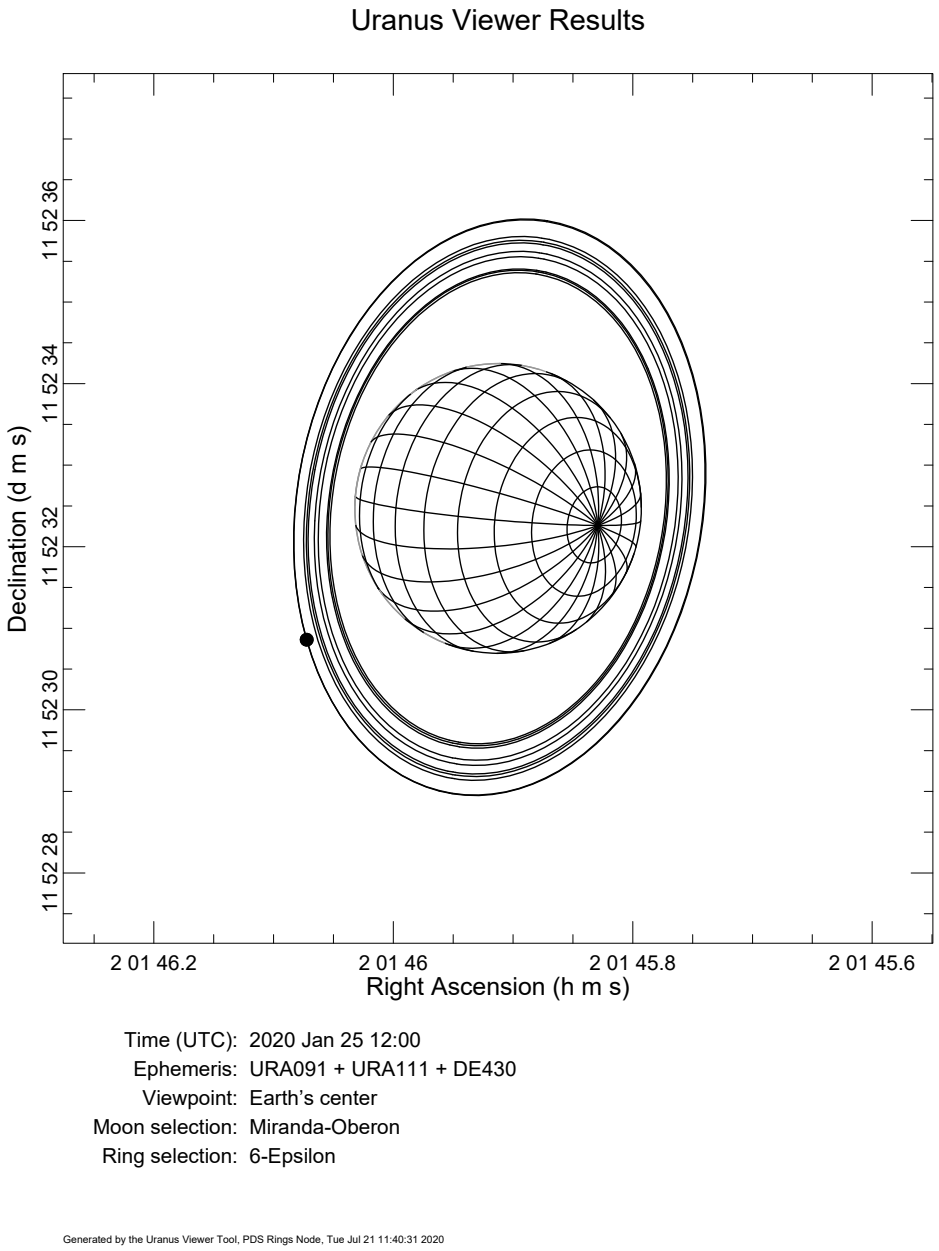

Fig. 28: Sky plane view of Uranus and the ten classical rings as observed from Earth on 2020 Jan 25 12:00 UTC. The periapse of the ϵ ring at the time of observation is marked by a black dot on the outer ring, at the same position angle as in Figs. 26 and 27.

B.4 Computing the ring longitude as a broken angle

The longitude of a point in the ring plane is measured in the direction of orbital motion along the planet's invariable plane (in this case, the Uranus equatorial plane), and thence along the ring plane; the origin of longitude (the prime meridian) is the ascending node of the planet's invariable plane on the Earth's mean equator in the inertial frame of interest (usually J2000, but for comparison with historical results, as shown above, B1950 is sometimes used.) The inclinations of the Uranian rings are so small that the difference between this broken-angle definition and the simpler longitude of the projection of the point in the ring plane into the Uranus equator can almost always be neglected. Nevertheless, it is sometimes useful to compute the longitude rigorously.

The `document/` directory of the support bundle contains IDL and Python source codes that illustrate several approaches to calculating the ring longitude. In these examples, we calculate the longitude of periapse of each of the ten rings at 1997 March 10 20:00:00 UTC.

The preface to the IDL program `ring_longitude_example.pro` is shown below:

```
; ring_longitude_example.pro
;
; Revisions:
;       2020 Jul 21 - rfrench@wellesley.edu - original version
;       2020 Dec 05 - rfrench@wellesley.edu - updated tf kernel
;
; Illustrate several methods of computing the longitude of
; periapse of a ring, both by explicit computations and
; using matrix transformations based on two different
; uranus_ring_frames *tf frame kernels:
;
;       1) uranus_ringframes_french_et_al_1988_v1.tf
;          French et al. (1988) Icarus 73, 349 Table XIV
;          Orbital elements in the B1950 frame.
;       2) uranus_ringframes_french20201201_v1.tf
;          based on a ring orbit fit performed on
;          2020 Dec 1 and used as the basis for
;          computing the geometry of Uranus ring occultations
;          submitted to NASA's Planetary Data System
;          in 2020 by Richard G. French, Wellesley College.
;          This kernel is in the J2000 frame
;
; The frame kernels are text files and they contain sufficiently
; detailed information to enable users to construct their own for
; any ring orbit model and Uranus pole direction.
;
; In this example program:

; The periapse longitude is calculated in the J2000 frame
; using each kernel for the ten classical Uranian rings, for
; a single event time.
; ######################################################################
```

The ring frame kernel is specified in the outer loop, and the inner loop then steps through all

ten rings to compute the longitude of periapse using a variety of methods.[9] To illustrate the results, we show below the two calculations for the ring 6 (the most inclined of the Uranian rings), first using the frame kernel for the Uranus ring orbit solution of French et al. 1988.

```
Uranus frame kernel: uranus_ringframes_french_et_al_1988_v1.tf
This is in the B1950 inertial frame
Pole direction (B1950) :        76.596900       15.111700
Pole direction (J2000) :        77.310823       15.174546
URING_6
Epoch of orbital elements (UTC) : 1977 MAR 10 20:00:00.00000
Node and node rate:        12.120000      -2.7564105
Inclination (deg) :     0.061600000
Apse and apse rate:        242.80000       2.7618676
Compare the three different calculations of the node longitude at the event time:
  36.5408974750753
  36.5408974750762
  36.5408974750762
argument of periapse at the event time =        221.70218
Compare the two different calculations of the periapse longitude at the event time,
and the approximate result obtained by projecting the periapse line in the ring plane
into the equatorial plane.
 258.2430750501080
 258.2430750501080
 258.2430586027863
```

For comparison, the results using the newer ring kernel are shown below:

```
Uranus frame kernel: uranus_ringframes_rfrench20201201_v1.tf
This is in the J2000 inertial frame
Pole direction (J2000) :        77.311143       15.172188
URING_6
Epoch of orbital elements (UTC) : 1987 JAN 01 12:00:00.00000
Node and node rate:        212.78591      -2.7564015
Inclination (deg) :     0.060692494
Apse and apse rate:        60.015614       2.7619562
Compare the three different calculations of the node longitude at the event time:
  35.2968854930787
  35.2968854930793
  35.2968854930793
argument of periapse at the event time =        222.87851
Compare the two different calculations of the periapse longitude at the event time,
and the approximate result obtained by projecting the periapse line in the ring plane
into the equatorial plane.
 258.1753985627183
 258.1753985627183
 258.1753825341249
```

[9] See the source codes for details about the various approaches used for the calculations.

The Python code `ring_longitude_example.py` produces virtually identical results:

```
bash-3.2$ python3.9 ring_longitude_example.py
Uranus frame kernel:  uranus_ringframes_french_et_al_1988_v1.tf
This is in the B1950 inertial frame
Pole direction (B1950) :  76.5969 15.111699999999999
Pole direction (J2000) :  77.31082299700378 15.174546376751062
URING_6
Epoch of orbital elements (UTC) : 1977 MAR 10 20:00:00.00000
Node and node rate:  12.12 -2.756410493618673
Inclination (deg) : 0.0616
Apse and apse rate:  242.8 2.76186757392544
Compare the three different calculations of the node longitude at the event time:
36.540897475075326
36.540897475076235
36.540897475076235
argument of periapse at the event time =  221.7021775750327
Compare the two different calculations of the periapse longitude at the event time,
and the approximate result obtained by projecting the periapse line in the ring plane
into the equatorial plane.
258.243075050108
258.243075050108
258.24305860278633
```

Using the newer frame kernel:

```
Uranus frame kernel:  uranus_ringframes_rfrench20201201_v1.tf
This is in the J2000 inertial frame
Pole direction (J2000) :  77.3111427895027 15.172187676544723
URING_6
Epoch of orbital elements (UTC) : 1987 JAN 01 12:00:00.00000
Node and node rate:  212.785905011383 -2.756401503801938
Inclination (deg) : 0.060692493924569095
Apse and apse rate:  60.015613930862 2.761956170049721
Compare the three different calculations of the node longitude at the event time:
35.29688549307866
35.29688549307929
35.29688549307929
argument of periapse at the event time =  222.87851306963967
Compare the two different calculations of the periapse longitude at the event time,
and the approximate result obtained by projecting the periapse line in the ring plane
into the equatorial plane.
258.1753985627183
258.1753985627183
258.1753825341249
```

B.5 Computing the ring intercept point for a stellar occultation

In this section, we describe complete IDL and Python codes to compute the circumstances of two actual ring occultation events. In each case, we determine the location of the observer, apply corrections to the direction of the occulted star and (in one case) a fitted offset time for the start time of a given occultation observation, and solve for the ring intercept radius, longitude, and mean anomaly (longitude relative to periapse). We also solve for the model radius of the ring point, taking account of any normal modes for the ring that are included in the ring orbit model. As certification of the validity of the results, we compare the final values to the ring orbit fit results. In both cases, the computed ring intercept radii agree with the ring orbit fit results to within 20 cm, confirming the accuracy and utility of the ring frame kernel produced using the ring orbit fit results.

The algorithm for calculating the occultation geometry is based on the heliocentric geometric model documented in Appendix A of French et al. 1993 and modified very slightly by French et al. 2017. Users interested in the details of the calculations should view the source code side-by-side with these references at hand.

The first example is the ingress δ ring occultation of star U14 observed on 1982 Apr 22 from the OPMT (Observatoire du Pic du Midi et de Toulouse) 2-meter telescope. For this event, we have applied the fitted elements for the $m = 2$ normal mode when computing the model radius for the ring event. We also illustrate two different methods for computing the geocentric position of the observer, one using a specially-constructed site kernel that we have used for our orbit fits, and the second a more traditional approach showing the conversion from geodetic coordinates to geocentric rectilinear coordinates using the ITRF earth rotation model.

The IDL program `occgeom_example1.pro` produces the following results – see the source code for details of the various computation methods.

```
IDL> .run occgeom_example1.pro
Results of occgeom_example1.pro

PDART bundleID: uranus_ringocc_u14_opmt_200cm
Occultation of star u14 by the delta ring during the 22 Apr 1982 occultation
as observed from OMPT at 1982 APR 22 01:37:00.9786

Comparison of results from this calculation and ring orbit fit:

Ring plane intercept radius       = 48295.92514134160592
compared to ring orbit fit result = 48295.92514482405386

sinB of ring plane                =    -0.96376069931359
compared to ring orbit fit result =    -0.96376069931409

Confirm that ring intercept vector has nearly zero z-element in ring plane:
R_SI_ringplane =        39564.876      -27696.877   7.2568218e-07

model radius   = 48297.15285620259965 compared to 48297.15352867436013
```

```
ring longitude =    36.18019697920170 compared to    36.18019697548471
ring anomaly   =   325.00655694643535 compared to   325.00648390211916

Pole directions:
Uranus pole (J2000) =        77.31114278950268       15.17218767654473
From orbit model    =        77.31114278950268       15.17218767654473
ring pole (J2000)   =        77.31152129173510       15.17193314469322

Comparison of geocentric position calculated two ways:
Explicit calculation =     4678.858375      11.620907    4324.312734
Using a site kernel  =     4678.860868      11.620913    4324.315038
```

The second example is the ingress ring 6 occultation of star U0 observed from the KAO (Kuiper Airborne Observatory) during the discovery observations of 10 March 1977. In this case, we made use of the special kernel file described in Appendix C that incorporates the flight path of the KAO during the observations. The results of the Python code `occgeom_example2.py` are shown below

```
bash-3.2$ python3.9 occgeom_example2.py
Results of occgeom_example2.py

PDART bundleID:  uranus_occ_u0_kao_91cm
Occultation of star u0 by ring 6 during 1977 March 10 occultation
as observed from the Kuiper Airborne Observatory
at 1977 MAR 10 20:24:48.2297

Comparison of results from this calulation and ring orbit fit:

Ring plane intercept radius       =  41877.63050519712
compared to ring orbit fit result =  41877.63033057637

sinB of ring plane                =  -0.8045319672612397
compared to ring orbit fit result =  -0.8045319672611818

Confirm that ring intercept vector has nearly zero z-element in ring plane:
R_SI_ringplane =  [-3.91950606e+04  1.47473103e+04 -1.15700459e-07]

model radius   =  41877.134617476215  compared to  41877.13461724056
ring longitude =  41.22768982845844   compared to  41.22770289837172
ring anomaly   =  159.38097468506226  compared to  159.3809737855939

Pole directions:
Uranus pole (J2000)     =  77.31114278950268 15.172187676544727
From ring orbit fit     =  77.31114278950268 15.17218767654473
ring plane pole (J2000) =  77.32319027517893 15.112619726004423
```

The IDL version gives similar results:

```
IDL> .run occgeom_example2.pro
Results of occgeom_example2.pro

PDART bundleID: uranus_occ_u0_kao_91cm
```

```
Occultation of star u0 by ring 6 during 1977 March 10 occultation
as observed from the Kuiper Airborne Observatory
at 1977 MAR 10 20:24:48.2297

Comparison of results from this calculation and ring orbit fit:

Ring plane intercept radius = 41877.63050519712124
compared to R_obs           = 41877.63033057637222

sinB of ring plane                =    -0.80453196726124
compared to ring orbit fit result =    -0.80453196726118

Confirm that ring intercept vector has nearly zero z-element in ring plane:
R_SI_ringplane =       -39195.061       14747.310  -1.1570046e-07

model radius   = 41877.13461747621477 compared to 41877.13461724056106
ring longitude =    41.22768982845844 compared to    41.22770289837172
ring anomaly   =   159.38097468506226 compared to   159.38097378559391

Pole directions:
Uranus pole (J2000)     =        77.31114278950268       15.17218767654473
From orbit model        =        77.31114278950268       15.17218767654473
ring plane pole (J2000) =        77.32319027517893       15.11261972600442
```

C Custom spk kernel for the KAO

The `spice_kernels/spk/` directory contains `urkao_v1.bsp`, the flight path of the Kuiper Airborne Observatory (KAO) during discovery observations of the Uranian rings from the occultation of star U0 on the 1977 March 10 (Elliot et al., 1977). This kernel is used in the second example program described in Appendix B.5. The body ID and period covered by the spice kernel can be found using the NAIF utility program `brief`:

```
 brief urkao_v1.bsp
 ...
 Summary for: urkao_v1.bsp

Body: 399600
      Start of Interval (ET)              End of Interval (ET)
      ----------------------------        ----------------------------
      1977 MAR 10 20:01:50.185            1977 MAR 10 22:26:20.185
```

In this spice kernel, the body ID of the KAO is set to 399600, and the following SPICE toolkit calls in IDL demonstrate how to determine the topocentric position of the aircraft at a given time in UTC:

```
UTCstr  = '1977 March 10 21:00:00'
cspice_furnsh,'/data/RS_share/kernels/'+['naif0012.tls','urkao_v1.bsp','pck00008.tpc']
cspice_STR2ET,UTCstr,ETsec
```

```
cspice_spkezp,399600L,ETsec,'IAU_EARTH','NONE',399,posEarth,ltime
cspice_recrad,posEarth,range,lon_radians,lat_radians
print,'Position of KAO at '+UTCstr+':'
print,'longitude,latitude (deg) = ',lon_radians*cspice_dpr(),lat_radians*cspice_dpr()
```

The result is:

```
Position of KAO at 1977 March 10 21:00:00:
longitude,latitude (deg) =        90.873469      -51.524377
```

Over the interval spanned by the spice kernel, the extracted KAO flight path is shown in Fig. 29:

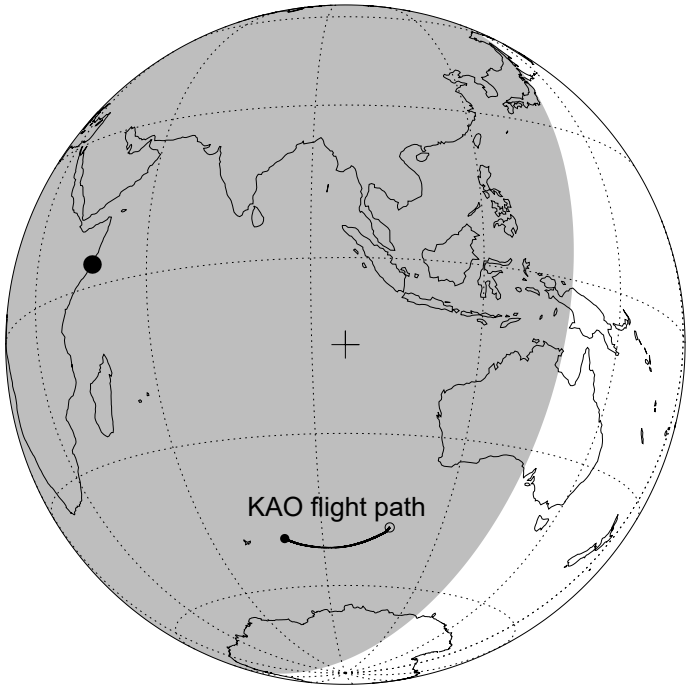

Fig. 29: Flight path of the KAO during the 1977 March 10 discovery observations of the Uranian rings, beginning a the filled circle and ending at the open circle. The large dark circle marks the antisolar point on Earth, and the + symbol marks the sub-Uranus point on Earth at mid-occultation time.

References

Elliot, J. L., Dunham, E. and Mink, D. (1977). The rings of Uranus. *Nature* **267**(5609), 328–330.

Elliot, J. L., French, R. G., Meech, K. J. and Elias, J. H. (1984). Structure of the Uranian rings. I - Square-well model and particle-size constraints. *Astron. J.* **89**, 1587–1603.

Elliot, J. L., Glass, I. S., French, R. G. and Kangas, J. A. (1987). The occultation of KME 17 by Uranus and its rings. *Icarus* **71**(1), 91–102.

French, R. G., Elliot, J. L., French, L. M., Kangas, J. A., Meech, K. J., Ressler, M. E., Buie, M. W., Frogel, J. A., Holberg, J. B., Fuensalida, J. J. and Joy, M. (1988). Uranian ring orbits from earth-based and Voyager occultation observations. *Icarus* **73**(2), 349–378.

French, R. G., McGhee-French, C. A., Lonergan, K., Sepersky, T., Jacobson, R. A., Nicholson, P. D., Hedman, M. M., Marouf, E. A. and Colwell, J. E. (2017). Noncircular features in Saturn's rings IV: Absolute radius scale and Saturn's pole direction. *Icarus* **290**, 14–45.

French, R., Nicholson, P., Cooke, M., Elliot, J., Matthews, K., Perkovic, O., Tollestrup, E., Harvey, P., Chanover, N., Clark, M., Dunham, E., Forrest, W., Harrington, J., Pipher, J., Brahic, A., Grenier, I., Roques, F. and Arndt, M. (1993). Geometry of the Saturn system from the 3 July 1989 occultation of 28 Sgr and Voyager observations. *Icarus* **103**, 163–214.

Gresh, D. L., Marouf, E. A., Tyler, G. L., Rosen, P. A. and Simpson, R. A. (1989). Voyager radio occultation by Uranus' rings I. Observational results. *Icarus* **78**(1), 131–168.

Jacobson, R. A. (2014). The orbits of the Uranian satellites and rings, the gravity field of the Uranian system, and the orientation of the pole of Uranus. *Astron. J.* **148**(5), 76.

Nicholson, P. D., Pater, I. D., French, R. G. and Showalter, M. R. (2018). *The Rings of Uranus*. Cambridge Planetary Science. Cambridge University Press. pp. 93–111.